Novel Algorithms for Rotor Angle Security Assessment in Power Systems

by

Darshana Prasad Wadduwage

A thesis submitted to the Faculty of Graduate Studies of

The University of Manitoba

in partial fulfillment of the requirements of the degree of

DOCTOR OF PHILOSOPHY

Department of Electrical and Computer Engineering

University of Manitoba

Winnipeg

To my wife Sumudu and sons Rivinu and Kavinu

Acknowledgement

First, I offer my sincere gratitude to my advisor, Professor Udaya Annakkage for his continuous support in numerous ways throughout the research. Further, I am thankful to my co-advisor, Professor Christine Wu. It was an honor for me to work with both of them. I am also thankful to Dr. Krish Narendra at ERLPhase Power Technologies Ltd. and Professor R. Tulasiram for their valuable feedback provided during the research discussions. Further, the assistances given to me by the staff of the Department of Electrical and Computer Engineering, specially Mr. Erwin Dirks and Ms. Amy Dario are highly acknowledged.

A special thank goes to my loving wife, Sumudu who always encouraged me to successfully complete my studies. Further, I am thankful to my mother and late father. Their blessings were always with me.

Furthermore, I am thankful to University of Moratuwa, Sri Lanka where I am employed as a lecturer, for granting me study leave to complete this thesis. Finally, I greatly appreciate the financial support given to me by the Natural Sciences and Engineering Research Council of Canada (NSERC), University of Manitoba Graduate Fellowship, MITAC accelerate program and the ERLPhase Power Technologies Ltd.

D. Prasad Wadduwage

December 2015

Stanley Pauley Center

University of Manitoba

Winnipeg, MB, Canada

Abstract

This thesis proposes two novel algorithms to analyze whether the power system loses synchronism subsequent to credible contingencies. The two algorithms are based on the concept of Lyapunov exponents (LEs) and the Prony analysis respectively.

The concept of LEs is a theoretically sound technique to study the system stability of nonlinear dynamic systems. The LEs measure the exponential rates of divergence or convergence of trajectories in the state space. Considering the higher computational burden associated with the convergence of the true LEs, a modified algorithm is proposed to study the transient stability of the post-fault power system. It is shown that the finite-time LEs calculated by the modified algorithm accurately predicts the said stability.

If the power system is transient stable, the rotor angle trajectories of the post-fault system exponentially decay with time. The damping ratios of the dominant oscillatory modes present in these power swings provide the indication on the oscillatory stability. The improved Prony algorithm presented in the thesis can be used to identify the oscillatory stability of the power system subsequent to a contingency.

It is shown that that these new algorithms can be used in two applications in power systems, online dynamic security assessment and online oscillations monitoring. The proposed algorithm for rotor angle security assessment first uses the LEs-based algorithm to identify the transient stability. The stable cases are then processed by the improved Prony algorithm. The proposed online oscillations monitoring algorithm uses an event-detection logic and a parallel filter bank before applying the improved Prony algorithm on the measured response to extract the dominant oscillatory modes and to determine their frequencies and damping ratios.

The suitability of the two algorithms for the aforementioned applications is inves-

tigated using different case studies. It is shown that the computational burdens of the two algorithms are acceptable for the online applications. Furthermore, the oscillations monitoring algorithm, extracts only the dominant modes present in the input signal, extracts both low-frequency inter-area modes and sub-synchronous modes, and performs well under noisy conditions. These features make it more appropriate for wide-area monitoring of power system oscillations using synchronized measurements.

Symbols

t	time
Δt	time step
x, u, y	state vector, input vector, output vector
Z	transformed state vector
A	state matrix
V	bus voltage vector
I	current injection vector
Y	network admittance matrix
P, Q	active power and reactive power
λ_i	i^{th} eigenvalue
$\sigma, j\omega$	real part and imaginary part of an eigenvalue
f, ζ	frequency and damping ratio of an oscillatory mode
P_m	per unit mechanical power input of a synchronous generator
P_e	per unit electrical power output of a synchronous generator
ω_0	synchronous speed
δ	generator rotor angle
$\Delta\omega$	speed deviation from synchronous speed
H, K_D	inertia constant and mechanical damping constant of a sync. gen.
E_B	infinite bus voltage
Λ_i	i^{th} Lyapunov exponent
ΔU	orthogonalized vector
ΔV	orthonormalized vector
T_C	fault clearing time
ϕ	right eigenvector

B	residue of an eigenvalue
p	order of the Prony model
N	number of samples inside a data window
z	discrete domain root
R_a	stator resistance
R_{1d}	direct-axis damper winding resistance
R_{1q}, R_{2q}	quadrature axes damper winding resistances
R_{fd}	field winding resistance
X_l	leakage reactance
$X_d, X_d^{'}, X_d^{''}$	direct axis reactance, transient reactance, sub-transient reactance
$X_q, X_q^{'}, X_q^{''}$	quadrature axis reactance, transient reactance, sub-transient reac.
e_d, e_q	direct and quadrature axis voltage
e_{fd}	field winding voltage
i_d, i_q	direct and quadrature axis current
ψ_{fd}	field winding flux
ψ_{1d}	direct axis damper winding flux
ψ_{1q}, ψ_{2q}	quadrature axis damper windings fluxes
I_R, I_I	real and imaginary axes currents
V_R, V_I	real and imaginary axes voltages

Acronyms

AESOPS	Analysis of Essentially Spontaneous Oscillations in Power Systems
AGC	Automatic Generation Control
AR	AutoRegressive
BCU	Boundary of stability-region-based Controlling Unstable eq. point
CWT	Continuous Wavelet Transform
DAE	Differential Algebraic Equation
DSA	Dynamic Security Assessment
EAC	Equal Area Criterion
EEAC	Extended Equal Area Criterion
EMD	Empirical Mode Decomposition
EMTP	Electro-Magnetic Transient program
ER	Energy Ratio
ERA	Eigen Realization Algorithm
FT	Fourier Transform
GEAC	Generalized Equal Area Criterion
GSR	Gram-Schmidt Reorthonormalization
HHT	Hilbert-Huang Transform
IMF	Intrinsic Mode Function
LE	Lyapunov Exponents
LLE	Largest Lyapunov Exponent
MAM	Modified Arnoldi Method
MP	Matrix Pencil
NERC	North American Electric Reliability Corporation
NETS	New England Test System

NYPS	New York Power System
OMIB	One Machine Infinite Bus
PEBS	Potential Energy Boundary Surface
PMU	Phasor Measurement Unit
SCADA	Supervisory Control And Data Acquisition
SIME	SIngle Machine Equivalent
SNR	Signal-to-Noise Ratio
SSAT	Small Signal Analysis Tool
STFT	Short Time Fourier Transform
SVD	Singular Value Decomposition
TDS	Time Domain Simulation
TSAT	Transient Security Assessment Tool
UEP	Unstable Equilibrium Point
WAMS	Wide Area Measurement System

Table of Contents

List of Figures

List of Tables

Chapter 1

Introduction

Reliability is a major concern of an electrical power utility in order to ensure adequate electricity supply to consumers. Every power utility has standards to express its reliability. For example, North American Electric Reliability Corporation (NERC) establishes such standards for United States, Canada and the northern portion of Baja California in Mexico. NERC defines two fundamental concepts mentioned below for the reliability of a bulk-power system [1]:

Adequacy: The ability of the electric system to supply the aggregate electric power and energy requirements of the electricity consumers at all times, taking into account scheduled and reasonably expected unscheduled outages of system components.

Operating reliability: The ability of the electric system to withstand sudden disturbances such as electric short circuits or unanticipated loss of system components.

NERC further highlights the below mentioned characteristics, which are mandatory for a bulk-power system to achieve an adequate level of reliability.

1. The system is controlled to stay within acceptable limits during normal operation;

2. The system performs acceptable after credible contingencies;

3. The system limits the impact and scope of instability and cascading outages when they occur;

4. The system's facilities are protected from unacceptable damage by operating them within facility ratings;

5. The system's integrity can be restored promptly if it is lost;

6. The system has the ability to supply the aggregate electric power and energy requirements of the electricity consumers at all times, taking into account scheduled and reasonably expected unscheduled outages of system components.

A bulk-power system can experience imminent disturbances during its operation. It is clear from the above discussion that the security of the bulk-power system against such disturbances is important to achieve the overall goal of reliability of the system. This introductory chapter systematically addresses the need for security analysis in power systems giving due consideration to the overall goal of adequate level of reliability of the system.

1.1 Operating states of a power system

The six characteristics mentioned above in order to achieve the adequate level of reliability are related to the operating states of the power system. It is the usual practice in power system's security assessment literature to refer to the five operating states shown in Fig. 1.1, which was adopted from [2]. The five operating states shown in Fig. 1.1 are the extensions of the three operating states, normal, emergency and restorative, which were originally proposed in [3]. The letters **E** and **I** refer to

the equality and inequality constraints on the power system operation.[1] These five operating states are briefly summarized below:

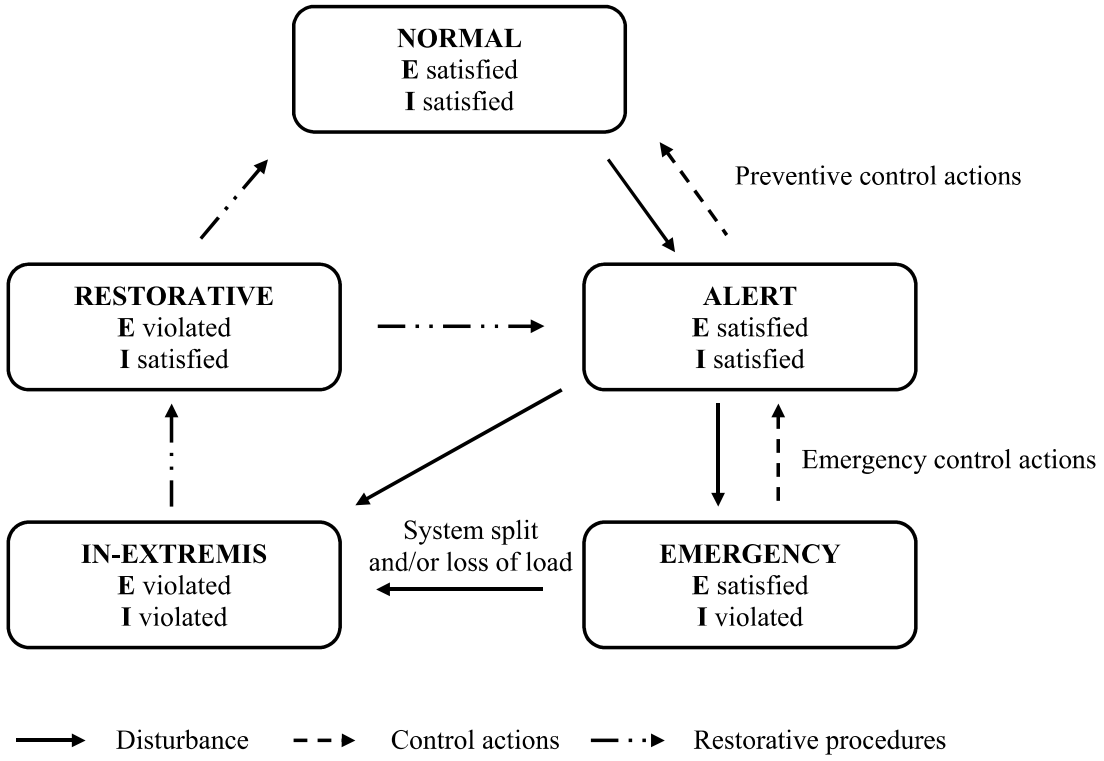

Figure 1.1: Operating states of a power system [2]

- Normal state

  When the power system is operating in *normal* state, the total load demand is adequately supplied by the generation and all variables are within their desired limits. Furthermore, the system has an adequate level of security to survive from the disturbances to which the system may be subjected. Therefore, the

[1]The equality constraints give the relationships between the total load and the generation, whereas the inequality constraints impose conditions on the power system variables. For example, the voltage of a bus bar in a transmission system (V) should be such that $0.95V_{rated} \leq V \leq 1.05V_{rated}$, where V_{rated} is the rated voltage.

power system is secure as long as it is operating in the normal state [2].

- Alert state

  The power system enters into an *alert* state when the security level falls below an acceptable level or when the probability of the disturbances increases. The total load demand is still supplied by the generation. However, now there is a higher possibility of entering into an emergency state subsequent to a disturbance if the preventive control actions are not timely taken to bring the system into the normal state [2].

- Emergency state

  The power system enters into the *emergency* state if it experiences a sufficiently severe disturbance before taking the appropriate preventive control actions. Now the inequality constraints are violated, but still the total load is supplied by the generation. The emergency control actions are required to bring the system at least into the alert state [2].

- In-extremis state

  Depending on the severity of the disturbance, the *in-extremis* state may be directly reached from the alert state or it may be due to the delay or failure in emergency control actions when the power system is in the emergency state. Now, a large portion of the consumers are without power. The emergency control actions must be initiated to avoid a system wide blackout [2].

- Restorative state

  If the wide scale blackout is prevented by the appropriate control actions, the next objective is to supply the electricity to the consumers gradually and re-

connect the system. It is said that the power system is now operating in a *restorative* state. Eventually, the result could be that the power system state is transferred to the alert state or the normal state [2].

It is understood from this discussion that the security level of a power system changes due to unexpected disturbances. The security analysis of the power system always related with determining whether the system reaches the new operating points without violating the constraints subsequent to a pre-determined set of credible fault scenarios [4]. Thus, the stability analysis of the operating points of the post-fault power system subsequent to credible fault scenarios is an integral component of the security analysis in power systems.

1.2 Power system stability analysis

The power system is a nonlinear dynamic system. Hence, the stability of an equilibrium point in a power system has similar dynamics to the stability of any nonlinear dynamic system. According to [4], the stability of a power system can be defined as follows:

'*Power system stability is the ability of an electric power system, for a given initial operating condition, to regain a state of operating equilibrium after being subjected to a physical disturbance, with most system variables bounded so that practically the entire system remains intact.*'

Thus, the stability of an equilibrium point in a power system depends on, i) the initial operating point, and ii) the type of the disturbance. It is important to highlight the below mentioned aspects in a scenario of power system stability analysis.

- It is the usual practice to treat that the power system is operating in a pre-disturbance equilibrium point prior to an occurrence of a disturbance.

- A disturbance in power systems perturbs the state variables resulting the trajectories to diverge or converge to the attractors. Hence, from theoretic viewpoint, this stability problem is a *system stability problem*, where the disturbance is on the initial conditions [5].

- If the post-fault system is stable subsequent to the disturbance, the trajectories converge to a stable attractor in the state space. This stable attractor is usually an equilibrium point which is *asymptotically stable*.

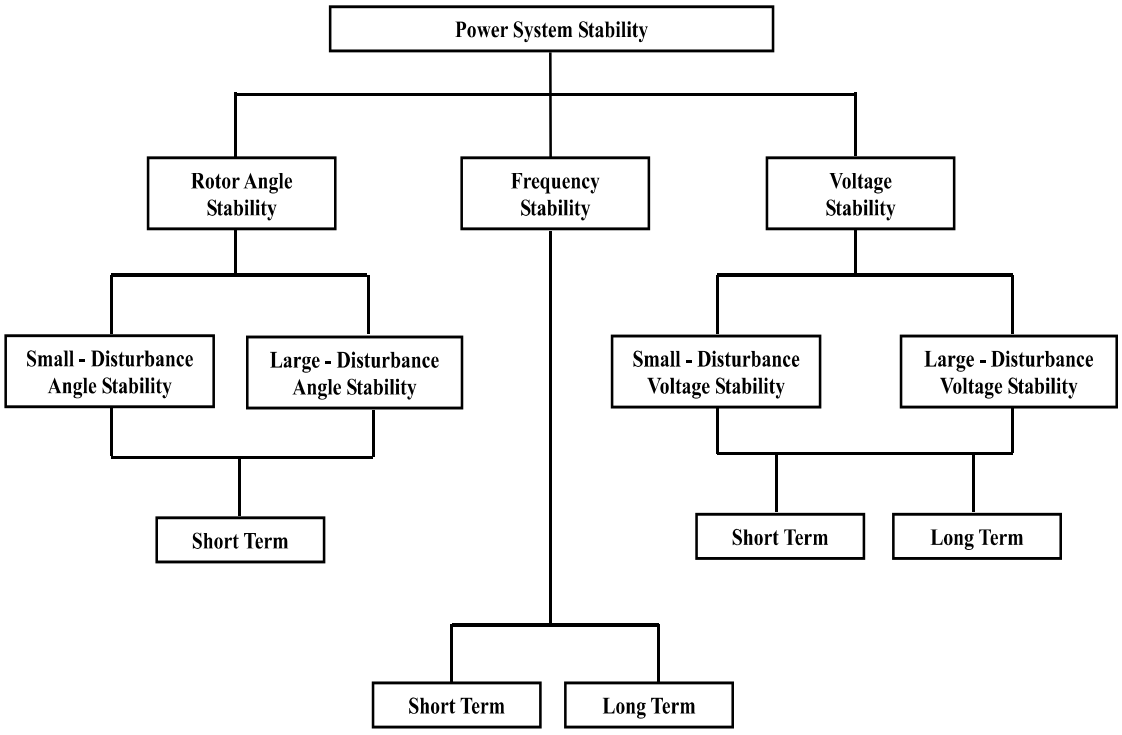

Figure 1.2: Classification of power system stability [4]

The power system stability is studied under different aspects as shown in Fig. 1.2, which was adopted from [4]. The basic objective of this classification is to study different forms of instabilities that a power system can undergo during its operation.

Nevertheless, the aforementioned key factors remain valid irrespective of the type of the stability problem. In Fig. 1.2, the rotor angle, voltage and frequency are the three main variables where the power system instability can be observed. It is the usual practice to use the method of linearization to study the system stability subsequent to a small-magnitude disturbance. However, the nonlinear effects of the power system need to be considered to study the system stability subsequent to a large-magnitude disturbance. The fast detection of a particular instability scenario before leading to a collapse in the power system is an important aspect to ensure the security of the system.

A power system operating state is classified as insecure due to rotor angle instability, voltage instability and/or frequency instability. This thesis focuses on the rotor angle stability problem. The resulting instability in this case may be an aperiodic increase in the rotor angles (transient instability) or a gradual increase in rotor angle oscillations over several seconds (oscillatory instability). The rotor angle stability problem is discussed in detail in Chapter 2.

1.3 Power system security analysis

The word security implies the freedom of risk or danger. In the context of power systems, the security is an instantaneous time-varying condition reflecting the robustness of the system to imminent disturbances [4]. The utilities continuously monitor the power system to check whether it is operating satisfactorily. If it is found that the system is operating in an insecure state, necessary actions need to be initiated to ensure the continuity of supply as much as possible. On the other hand, if the power system is in the normal state, the security of the power system can be assessed for a pre-determined list of credible fault scenarios. These three basic elements (security

monitoring, security assessment and control) are tied together as shown in Fig. 1.3 and are briefly described below:

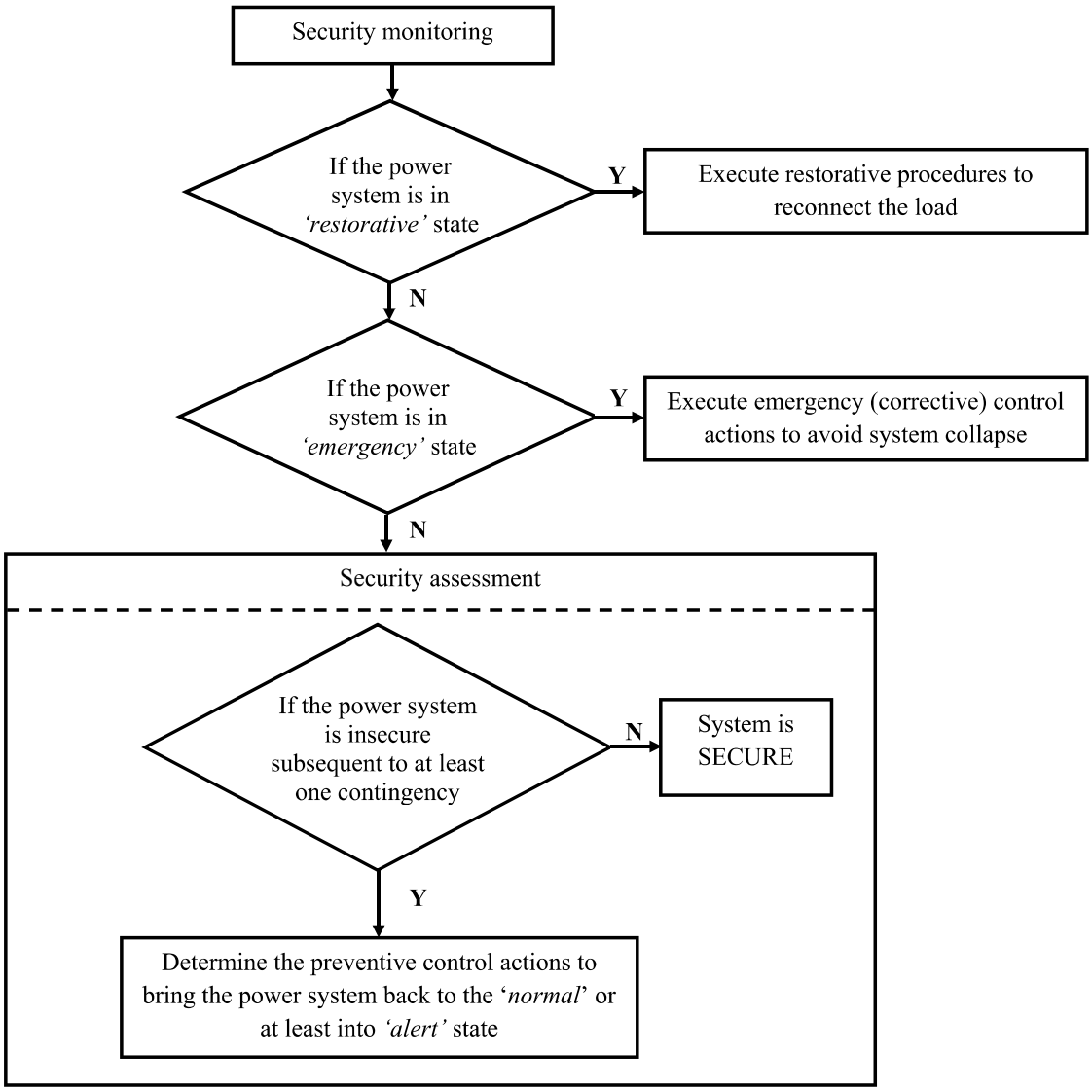

Figure 1.3: Basic steps in real-time security analysis

1.3.1 Power system real-time monitoring

Power systems are monitored in real-time in order to have the measurements of key parameters such as bus voltage magnitudes and angles, currents flowing through the

lines, power flowing through the lines, breaker status, etc. These measurements are sent to the control center via supervisory control and data acquisition (SCADA) systems or wide-area measurement systems (WAMS).

A SCADA system collects data from remote terminal units placed at generation, transmission and distribution stations and sends those to the control center [6]. On the other hand, a WAMS consists of phasor measurement units (PMUs) installed at widely dispersed locations of the power system. A PMU produces synchronized phasor, frequency and rate of change of frequency estimates from voltage and/or current signals [7]. The synchronized phasor provided by the PMU is a phasor with the angle referenced to an absolute GPS-driven time reference [7]. Thus, the synchrophasor data received from multiple PMUs can be directly compared since they are calculated with respect to a common reference. Further, these data are available at the control center at a higher rate compared to the traditional SCADA data. Thus, the trend in today's interconnected power systems is to install PMUs, thereby forming a WAMS.

As described in Section 1.2, a power system can be insecure due to three forms of instability problems. Thus, the data available from SCADA systems or WAMS need to be processed by appropriate algorithms in order to extract the useful information for the operator. If the power system is in a restorative state, then the load should be gradually reconnected. On the other hand, if the system is in an emergency state, which might lead to a system wide collapse, the operator must be alarmed to initiate appropriate control actions.

1.3.2 Power system security assessment

The main objective of the security assessment is to determine whether the power system is secure or not subsequent to a pre-determined list of disturbances, which

may be experienced by the system. Such an assessment is done when the power system is in the normal operating state. The security assessment of the power system has two steps; i) determining whether the equality and inequality constraints are satisfied at the new operating point reached after the fault scenario (***static security assessment***), and ii) determining whether the new operating point can be reached (***dynamic security assessment***).

The dynamic security assessment of the power system is usually done using a deterministic approach. That is, the stability of the post-fault power system with respect to rotor angle stability, voltage stability and the frequency stability explained in Section 1.2 is determined with respect to a pre-determined list of credible fault scenarios at frequent time intervals [8], [9]. These fault scenarios include outages such as loss of generating units or transmission components (transformers, transmission lines, etc), which are usually selected on the basis of their probabilities of occurrences. If it is found that the system is insecure for at least one fault scenario, the necessary preventive actions need to be determined as mentioned in Section 1.3.3.

1.3.3 Security enhancement

If the power system is insecure due to any reason, it should be brought back to the normal state using appropriate security enhancement procedures. These actions depend on the operating state of the power system.

Turbine governor control, generator voltage regulation, transformer tap changing, capacitor switching, etc are some of the direct control actions, which are being taken when the system is in the alert state. Furthermore, if the system is insecure for at least one fault scenarios in the list of credible fault scenarios, the preventive control actions must be initiated considering the probability of the occurrence of the event and

the economic factors. Hence, the preventive control actions without the optimization are poorly determined problems [3], [10]. Therefore, some of the preventive control actions are selected from a list of candidate solutions by minimizing an objective function, e.g. unit commitment, economic load dispatch, etc.

Emergency control actions are initiated subsequent to the actual occurrence of a disturbance in the system. Now, the main objective is to protect the system as early as possible. Fault clearing, out-of-step tripping, and generator shedding are some examples of emergency control actions.

1.4 Need for online security analysis in power systems

An electrical power system is usually designed well to achieve the overall goal of reliability in the system. It is mandatory that the bulk-power system is operated within the desired security limits on this regard.

Traditionally, the electrical power utilities were operating as stand-alone entities. However, with the restructuring happened in the electricity industry, the utilities not only electrify their consumers but also share the surplus energy between adjacent utilities. Such interconnections have the advantages of keeping lower electricity rates, providing/receiving the support to/from adjacent areas when there is an increase/decrease in load, etc. These energy economy translations have resulted in the operations of transmission systems closer to the security limits.

The security level of a bulk-power system is changing with time due to changes in load/generation, control actions, etc. Therefore, it is important to determine the security level of a power system subsequent to an anticipated list of disturbances during the normal operation. If emergency control actions are not timely taken subsequent to an actual occurrence of a disturbance, the power system may eventually collapse as

happened in 10th August, 1996 and 14th August, 2003 blackouts [11]. Therefore, it is important to analyse the power system in an online [2] environment to check whether the system is operating in a secure manner.

The focus of this thesis is to determine whether the power system is rotor angle stable subsequent to a fault scenario, which has gained a significant attention of power system engineers. In order to emphasise the importance of the said stability problem, consider Fig. 1.4, which shows the active power flow through a transmission line prior and during the blackout occurred on 10th of August, 1996 [11].

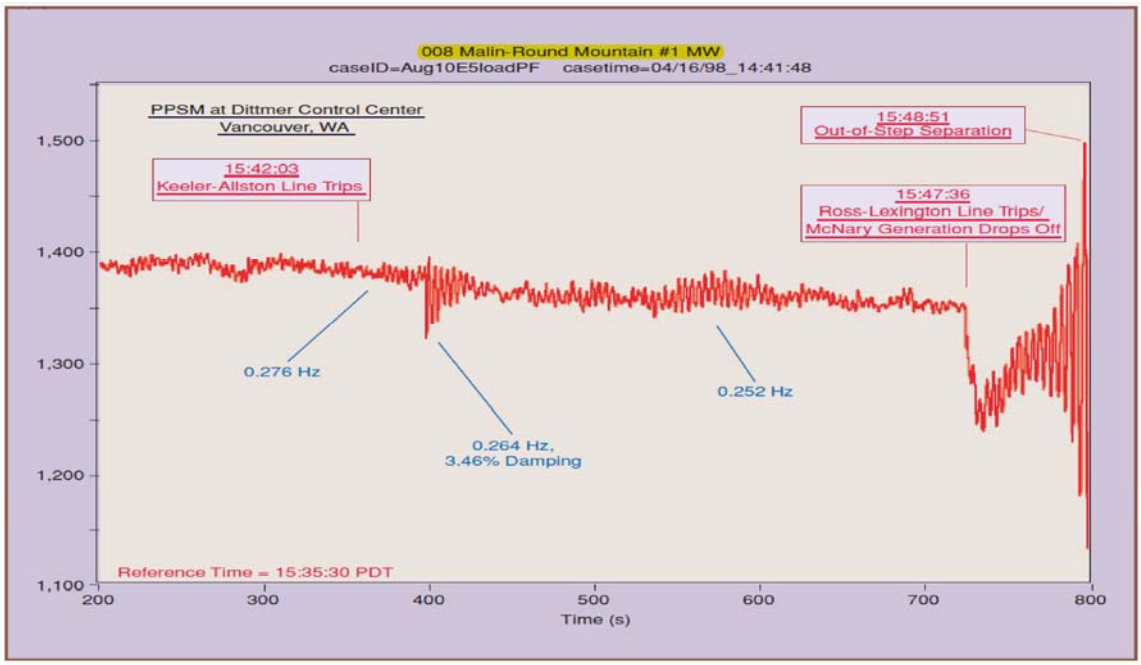

Figure 1.4: Active power flow along a major transmission line during 1996 blackout [11]

The key observations of this figure are;

[2] The term *real-time* means that "N"seconds of simulation actually takes "N"seconds in real-time such as real-time digital simulation. However, in actual environment, the implementation of real-time monitoring systems is limited by the computational capacity of the existing hardware. Thus, the term *online* is used in this thesis.

- Failure of the power system in this case was due to a slowly increasing rotor angle oscillation after time, $t = 700$ s (oscillatory stability problem).

- A poorly-damped low-frequency mode at frequency, 0.248 Hz and damping, 3.46% was excited by the first disturbance around $t = 400$ s. The system survived from this disturbance without losing synchronism. However, the power system entered to the alert state.

- A second disturbance occurred after $t = 700$ s, causing the damping of the low-frequency mode to become negative. The system eventually collapsed showing slowly increasing rotor angle oscillations.

Following two conclusions can be made based on these observations:

- If the system was continuously monitored for the excitation of poorly-damped modes subsequent to large-magnitude disturbances using an appropriate algorithm, the failure could have been avoided by alarming for necessary preventive actions.

- If a dynamic security assessment was done in appropriate time intervals including the first and the second disturbances, the failure could have been forecasted.

It is evident now that the accurate and fast decisions about the rotor angle stability of the power system are important to ensure the security of the power system. These were the main motivations behind the development of two novel algorithms proposed in this thesis for oscillations monitoring applications and dynamic security assessment studies.

1.5 Objectives of the research

The main goal of this research is to develop and evaluate the performances of novel algorithms for determining the rotor angle stability of the power system subsequent to large-magnitude disturbances. These algorithms can then be used for security assessment of the power system with respect to rotor angle stability in an online environment. Thus, the objectives of this study are to accurately determine the first-swing rotor angle stability, multi-swing rotor angle stability and the oscillatory stability within a computational time which is acceptable for online applications. The following approaches are proposed in this thesis to achieve the above objectives.

1. A novel algorithm based on the concept of Lyapunov exponents (LEs) is proposed to determine the large-disturbance rotor angle stability of the power system.

2. An improved Prony algorithm is proposed to determine the oscillatory stability. The proposed algorithm extracts only the dominant oscillatory modes present in the input signals and accurately determines their frequencies and damping ratios.

3. A hybrid algorithm including both the LEs-based algorithm and the improved Prony algorithm is proposed to be used in a dynamic security assessment program. The proposed hybrid algorithm accurately determines the security of the power system with respect to both transient and oscillatory rotor angle stability of the power system subsequent to a set of known disturbances.

4. An oscillation monitoring algorithm including the improved Prony algorithm is proposed to monitor the power system oscillations. The proposed oscillation

monitoring algorithm can extract low-frequency inter-area oscillations as well as sub-synchronous oscillations present in an input signal.

1.6 Thesis outline

The rest of this thesis is organized as mentioned below to achieve the aforementioned objectives.

Chapter 2 starts with an introduction to the fundamental concepts of the stability of a nonlinear dynamic system. Next, the derivation of the mathematical model of a power system based on the valid assumptions required to assess the rotor angle stability problem of the power system is presented. A comprehensive literature review to assess the said stability issue is presented at the end of this chapter highlighting their pros and cons.

Chapter 3 presents the novel algorithm based on the concept of LEs proposed in this thesis to assess the rotor angle stability problem. First, this chapter describes the concept of LEs and the procedure for deriving a spectrum of LEs using a mathematical model. Then the relationships between the largest Lyapunov exponents (LLEs) and the equilibrium points of the post-fault systems are established using a test power system. In order to reduce the significant computational burden associated with the conventional algorithm, a modified algorithm is proposed at the end of this chapter which can accurately determine the stability of the post-fault power system within an acceptable time.

Chapter 4 presents an improved Prony algorithm to extract the dominant oscillatory modes present in an input signal and to determine their frequencies and damping ratios. Initially, this chapter presents the theory of the Prony algorithm. Then the limitations of the conventional algorithm are highlighted and the proposed

improved algorithm is systematically derived. The suitability of the proposed algorithm for the intended application is presented at the end of the chapter using the simulation results obtained by the test power system models.

Chapter 5 presents a hybrid algorithm using the two algorithms presented in Chapter 3 and Chapter 4 to be used in a dynamic security assessment program. The performance of the proposed hybrid algorithm is evaluated using two test power system models.

Chapter 6 presents an oscillation monitoring algorithm using the improved Prony algorithm presented in Chapter 4 to monitor power system oscillations in an online environment. The proposed algorithm extracts only the dominant oscillatory modes present in an input signal. The suitability of the proposed algorithm for extracting low-frequency oscillations and sub-synchronous oscillations is presented in this chapter using a set of test power systems.

Chapter 7 presents the conclusions and the contributions of this research work.

Appendices explain the mathematical model of a test power system and the procedure for deriving a small-signal stability assessment program from the mathematical model.

Chapter 2

Rotor Angle Security Assessment in Power Systems

2.1 Introduction

From a mathematical point of view, a power system is a nonlinear, multivariable dynamic system. Thus, the definitions and theories of nonlinear dynamic systems are also applicable to a power system. However, certain assumptions are made to derive the dynamic model and hence to assess the stability of equilibrium points due to complex dynamics associated with different elements in power systems. Among different types of stability problems explained in Chapter 1, the rotor angle stability is the area of interest in this thesis. The rotor angle security assessment involves studying whether the equilibrium points of the post-fault systems are rotor angle stable if any of the fault scenarios from a pre-defined set of fault scenarios are happened at the current operating point. Thus, the rotor angle security assessment is a subset of the tasks associated with the dynamic security assessment (DSA) of power systems.

The goal of this chapter is to systematically address the rotor angle stability

problem in power systems. This accompanies the following objectives: i) review the theory of stability of nonlinear dynamic systems, ii) derive the power system dynamic model suitable to assess the rotor angle stability, iii) explain how to study the stability subsequent to different types of disturbances in power systems, and iv) review the literature on determining the rotor angle stability in power systems.

For detailed explainations of stability concepts presented in Section 2.2, readers can refer [5].

2.2 Stability concepts of dynamic systems

The term *Dynamic System* is a mathematical concept, where a set of known rules describes the behavior of the system in a geometrical space. In general, a set of first order ordinary differential equations shown in Eq. (2.1) models the dynamic behavior of such a system [5].

$$\begin{aligned} \dot{x_1} &= f_1(t, x_1, x_2, \cdots, x_m, u_1, u_2, \cdots, u_n) \\ \dot{x_2} &= f_2(t, x_1, x_2, \cdots, x_m, u_1, u_2, \cdots, u_n) \\ \vdots & \qquad\qquad \vdots \\ \dot{x_m} &= f_m(t, x_1, x_2, \cdots, x_m, u_1, u_2, \cdots, u_n) \end{aligned} \tag{2.1}$$

where, t represents the time and u_i is the i^{th} input to the system.

The variable, x_i is called the i^{th} *state* of the system and $\dot{x_i}$ is its time derivative. The hyper-plane formed by using all state variables as the coordinate axes is called the *state plane* or *phase plane*. Eq. (2.2) shows the compact form of Eq. (2.1) using vector notations $\mathbf{x}, \mathbf{u}$ and $\mathbf{f}(\mathbf{t}, \mathbf{x}, \mathbf{u})$.

$$\dot{\mathbf{x}} = \mathbf{f}(\mathbf{t}, \mathbf{x}, \mathbf{u}) \tag{2.2}$$

where,

$$\mathbf{x} = \begin{bmatrix} x_1 \\ x_2 \\ \vdots \\ x_m \end{bmatrix} \qquad \mathbf{u} = \begin{bmatrix} u_1 \\ u_2 \\ \vdots \\ u_n \end{bmatrix} \qquad \mathbf{f}(\mathbf{t}, \mathbf{x}, \mathbf{u}) = \begin{bmatrix} f_1(t, x, u) \\ f_2(t, x, u) \\ \vdots \\ f_m(t, x, u) \end{bmatrix}$$

There is another set of equations as shown in Eq. (2.3) for the dynamic system, where $\mathbf{y}$ is the output vector comprising all the outputs of the system. Eq. (2.2) and Eq. (2.3) together form the state space model of the dynamic system.

$$\mathbf{y} = \mathbf{h}(\mathbf{t}, \mathbf{x}, \mathbf{u}) \tag{2.3}$$

The input to the system ($\mathbf{u}$) can be represented as a function of time or the state vector or both. This representaion gives the unforced state equation: $\dot{\mathbf{x}} = \mathbf{f}(\mathbf{t}, \mathbf{x})$ of the dynamic system. The system is said to be *autonomous* if the function $\mathbf{f}$ does not depend on time, that is, $\dot{\mathbf{x}} = \mathbf{f}(\mathbf{x})$, and *nonautonomous* otherwise. The locus of a solution $\mathbf{x}(\mathbf{t})$ of the dynamic system in the state plane is known as a *trajectory*.

An equilibrium point of the dynamic system is a point in the state plane having the property that when the state of the system starting at that point remains at the same point for all future time. Stability of equilibrium points is very important, and is often characterized using the **Lyapunov Stability Theory** originally proposed by A. M. Lyapunov [12]. This theorem states that an equilibrium point at the origin[1] is

[1] an equilibrium point not at the origin can be shifted to the origin using a change of variables

stable if all solutions starting at nearby points stay nearby; otherwise, it is unstable. Mathematically, the conditions for equilibrium can be illustrated as follows:

For an autonomous system given by $\dot{\mathbf{x}} = \mathbf{f}(\mathbf{x})$, the equilibrium point $x = 0$ is:

- stable if, for each $\epsilon > 0$, there is $\delta = \delta(\epsilon) > 0$ such that:

  $||x(0)|| < \delta \Rightarrow ||x(t)|| < \epsilon, \forall t \geq 0$

- unstable if not stable

- asymptotically stable if it is stable and δ can be chosen such that:

  $||x(0)|| < \delta \Rightarrow \lim_{t\to\infty} x(t) \to 0$

- exponentially stable if it is stable and there are $\epsilon > 0, \delta > 0, \alpha > 0$ such that:

  $||x(0)|| < \delta \Rightarrow ||x(t)|| < \epsilon||x(0)||e^{-\alpha t}, \quad t \geq 0$

Lyapunov stability theory provides a sufficient condition for the stability of an equilibrium point at the origin in the state space. Each equilibrium point has a region of attraction known as the *stability region*. In the case of an asymptotically stable equilibrium point, all the trajectories starting from the states inside the stability region converge to the equilibrium point of the stability region. Further, this equilibrium point is gloablly asymptotically stable if the stability region covers the entire state space.

Local stability of a nonlinear system in the vicinity of an equilibrium point is determined using the method of linearization. The linearized set of equations of the autonomous system $\dot{\mathbf{x}} = \mathbf{f}(\mathbf{x})$ shown in Eq. (2.4) are derived using the Taylor series expansion at the equilibrium point and neglecting the higher order terms.

$$\dot{\Delta\mathbf{x}}(t) = A\Delta\mathbf{x}(t) \tag{2.4}$$

where A is the state matrix of size $(m \times m)$.

The eigenvalues of the matrix A are the values of the scalar parameter λ for which there exist non trivial solutions for $A\phi = \lambda\phi$, where ϕ is an $(m \times 1)$ vector. Thus, the eigenvalues of A are given by the solution of the equation: $det(A - \lambda I) = 0$.

The stability of the equilibrium point at the origin of the linear time invariant system given by Eq. (2.4) is completely characterized by the location of the eigenvalues of A. This equilibrium point is asymptotically stable only if all the eigenvalues of A have negative real parts. This method is valid only to analyze the stability of the nonlinear system around the equilibrium point since it approximates the behaviour of the nonlinear system around an equilibrium point.

2.3 Power system stability analysis

This section systematically derives the mathematical model of the power system to determine the rotor angle stability.

2.3.1 Illustration of a stability analysis scenario

A typical power system consists of many elements as shown in Fig. 2.1. The system is energized by a large number of synchronous generators. The dynamic behavior of this system can be represented using two sets of equations [13], [14]. In vector-matrix form, this representation looks like:

$$\dot{\mathbf{x}} = \mathbf{f}(\mathbf{x}, \mathbf{V}, \mathbf{u}) \tag{2.5}$$

$$0 = \mathbf{g}(\mathbf{x}, \mathbf{V}, \mathbf{u}) \tag{2.6}$$

where, $\mathbf{x}$ is a state vector, $\mathbf{V}$ is the bus voltage vector and $\mathbf{u}$ is a vector representing the inputs and other parameters which influence on the dynamic behavior of the system.

The two functions $\mathbf{f}$ and $\mathbf{g}$ do not depend on time, hence the Eq. (2.5) and Eq. (2.6) represent an autonomous system.

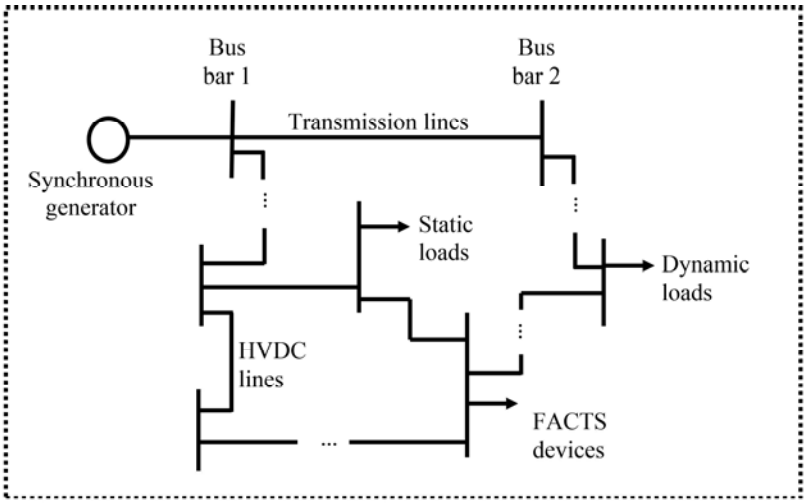

Figure 2.1: Structure of a typical power transmission system

The power system is operating in an equilibrium point under normal operating conditions. Rates of changes of the state variables at this operating point are equal to zero. The system can then subject a disturbance. These disturbances are categorized into two types as *event-type* and *norm-type*[4].

- An event-type disturbance is described by a fault scenario such as a three-phase fault in a transmission line near a bus bar and the fault is cleared by isolating the faulted line after a time period known as the *fault clearing time* by the protection devices. Such a scenario is also known as a *contingency*.

- A norm type disturbance is described by the size of the signal. The variations in the loads are considered as norm type disturbances.

The power system reaches a stable equilibrium point if the system still remains stable subsequent to a disturbance. The equilibrium point of the post-fault system may or may not be that of the pre-fault system depending on the type of the disturbance as well as whether there any structural changes have happened in the system. Furthermore, the type of the disturbance determines the method of analysis of the stability of the equilibrium points of the post-fault systems. In general, nonlinearities in the power system response need to be considered to assess the stability subsequent to an event-type disturbance. However, the system stability under the norm type disturbances can be studied using linear control theory.

Mathematical formulation of a stability analysis scenario

The overall state space representation of a given power system becomes more complex when the dynamic behavior of all the elements are modeled using a set of first order differential equations. Therefore, simplifying assumptions are made to accurately represent the power system to assess a given stability scenario [14]. These assumptions are:

1. Ignore the transients associated with the transmission network. Such transients decay rapidly.

   This assumption allows to represent the network in the node-admittance matrix form given below.

   $$\mathbf{I} = \mathbf{YV} \tag{2.7}$$

   where, $\mathbf{I}$ is the current injection vector, $\mathbf{V}$ is the bus voltage vector and $\mathbf{Y}$ is the network admittance matrix.

2. Ignore the transients associated with the stator windings of the synchronous

generators.

It is assumed that the flux linking the stator windings change instantly following a disturbance. Due to this simplification, only a fundamental frequency component is observed in the stator current waveforms.

3. Ignore the effect of speed variations associated with the stator voltages.

Assumptions 2 and 3 allow to represent the dynamic behavior of a synchronous generator using a set of first order differential and algebraic equation shown in Eq. (2.8) and Eq. (2.9) respectively.

$$\dot{\mathbf{x}_d} = \mathbf{f}_d(\mathbf{x}_d, \mathbf{u}_d, \mathbf{V}_d) \tag{2.8}$$

$$\mathbf{I}_d = \mathbf{g}_d(\mathbf{x}_d, \mathbf{V}_d) \tag{2.9}$$

where, $\mathbf{x}_d$ is the state vector, $\mathbf{u}_d$ is the input vector, $\mathbf{I}_d$ is the real and imaginary components of the current injected by the generator to the transmission network and $\mathbf{V}_d$ is the real and imaginary components of the voltage of the network bus to which the generator is connected.

The dynamic behavior of all the dynamic devices can be represented as in Eq. (2.8) and Eq. (2.9). The overall dynamic model of the power system shown in Eq. (2.10) and Eq. (2.11) is derived by combining the equations of the individual devices and the node-admittance matrix form given in Eq. (2.7). This is known as the differential and algebraic equation (DAE) representation of the power system.

$$\dot{\mathbf{x}} = \mathbf{f}(\mathbf{x}, \mathbf{u}, \mathbf{V}) \tag{2.10}$$

$$\mathbf{I}(\mathbf{x}, \mathbf{V}) = \mathbf{YV} \tag{2.11}$$

The input vector is assumed to be a known function of time. Thus, Eq. (2.10) is usually written excluding $\mathbf{u}$. The initial operating point is given by (x_0, V_0).

Voltage and current waveforms in power systems at steady state follow cyclic variations at the nominal system frequency. Subsequent to a disturbance, the mathematical representations shown in Eq. (2.10) and Eq. (2.11) cause amplitude and phase angle modulations of the voltage and current signals at low frequencies. These modulating frequencies correspond to the rotor angle oscillations in the power system. Such transients are known as *electromechanical transients*. Thus, the mathematical representation explained above is suitable to study the stability of electromechanical transients. Obviously, the aforementioned mathematical modeling is not suitable to study the effects of the stator transients and the network transients, hence electromagnetic transient programs (EMTPs) are used to study such transients in power systems [15].

Models used for stability analysis of electromechanical transients

A typical power system consists of synchronous generators, static loads, dynamic loads, HVDC links, FACTS devices, etc. These individual devices are modeled in different degrees of complexities for stability assessment studies of electromechanical transients. This section summarizes the models of such devices. A detailed derivation

of these models are given in [14].

Synchronous generators and the associated controls

A synchronous generator is driven by a prime mover and the field winding is energized via a dc source. The stator winding of the generator provides the useful electrical energy to the network. The associated controls of the generator includes the governor, exciter and the power system stabilizer. The prime mover governing system provides a means of controlling the power and the frequency. The purpose of the excitation system combined with the automatic voltage regulator is to control the field voltage so as to keep the generator terminal voltage within the desired limits. A power system stabilizer may be used with the excitation system to add damping to the generator rotor oscillations.

The simplest representation of the synchronous generator provides two state variables; a) rotor angle, and b) speed deviation of the generator from the synchronous speed. A more detailed representation uses six state variables including the above two and four more state variables to represent the dynamics of the flux in the field winding and the damper windings. The stator voltage is written using algebraic equations. Each pole in the transfer functions of the exciter, power system stabilizer and the turbine-governor system adds an additional state to the system representation. For example, a synchronous generator and the controls can be represented using 17 state variables including 6 for the generator, 5 for the excitation system, 3 for the power system stabilizer and 3 for the turbine-governor system. Appendix A provides the mathematical model of a synchronous generator and the associated controls of a 16 generator 68 bus test system used for stability assessment studies in this thesis.

Load models

A load can be represented using either a static load model or a dynamic load

model. A static load model does not provide state variables for the system representation. Active and reactive power consumptions of the static loads are represented as functions of the bus voltage magnitude and the frequency. For example, the polynomial model of the static load is given below:

$$P = P_0(a_1 v^{n_1} + a_2 v^{n_2} + a_3 v^{n_3})(1 + a_7 \Delta f) \quad (2.12)$$

$$Q = Q_0(a_4 v^{n_4} + a_5 v^{n_5} + a_6 v^{n_6})(1 + a_8 \Delta f) \quad (2.13)$$

Constant impedance, constant current and constant power load models are represented by substituting $n_1 = n_4 = 2, n_2 = n_5 = 1$ and $n_3 = n_6 = 0$ respectively. Δf is the frequency deviation which is used to represent the frequency sensitivity of the loads. These loads are treated as current injections at the respective node in the network equation.

The dynamic loads such as induction motors, synchronous motors, etc are represented using their dynamics. These add additional state variables to the system representation.

Other devices

HVDC links, FACTS devices, etc are also modeled using a set of differential and algebraic equations in the stability studies.

2.3.2 Power system stability analysis under event-type disturbances

An event-type disturbance is described by a specific fault scenario. Let the fault occurs at time, $t = 0$ and is cleared at $t = t_c$. The differential equations describing

the behavior of the system during different time intervals of the fault scenario can be written as follows:

$$\dot{\mathbf{x}} = \begin{cases} \mathbf{f_{pre}}(\mathbf{x}, \mathbf{V_{pre}}) & t < 0 \\ \mathbf{f_{during}}(\mathbf{x}, \mathbf{V_{during}}) & t < t_c \\ \mathbf{f_{post}}(\mathbf{x}, \mathbf{V_{post}}) & t > t_c \end{cases} \tag{2.14}$$

where, subscripts "pre", "during" and "post" refer the pre-fault, during-fault and post-fault periods respectively.

The three functions $\mathbf{f_{pre}}, \mathbf{f_{during}}$ and $\mathbf{f_{post}}$ are considered to be autonomous for the purpose of analysis. Further, the algebraic equations in Eq. (2.11) also change during different time intervals of the fault scenario.

Subsequent to an event-type disturbance, the interest is on the stability of the equilibrium point of the post-fault system given by $\mathbf{f_{post}} = 0$. If the post-fault system is stable, the state trajectories converge to this equilibrium point. Thus, the equilibrium point is asymptotically stable. For a given fault scenario, the stability of the equilibrium point depends on the values of the state variables at which the fault is cleared. Thus, change in the fault clearing time disturbs the initial conditions of the post-fault system dynamic equations.

2.3.3 Power system stability analysis under norm-type disturbances

A power system operating in an equilibrium point subjects to small magnitude disturbances such as changes in load power. The stability subsequent to these types of disturbances is known as the small-signal stability of the power system. The said

stability is studied using the method of linearization. The DAEs of the individual dynamic devices given in Eq. (2.8) and Eq. (2.9) are linearized around the equilibrium point to derive the following equations.

$$\Delta\dot{\mathbf{x}}_i = \mathbf{A}_i\Delta\mathbf{x}_i + \mathbf{B}_i\Delta\mathbf{u}_i + \mathbf{E}_i\Delta\mathbf{V}_i \tag{2.15}$$

$$\Delta\mathbf{I}_i = \mathbf{C}_i\Delta\mathbf{x}_i + \mathbf{D}_i\Delta\mathbf{V}_i \tag{2.16}$$

where, $\Delta\mathbf{x}_i$, $\Delta\mathbf{u}_i$, $\Delta\mathbf{I}_i$ and $\Delta\mathbf{V}_i$ represent the perturbed values of the i^{th} device state variables, control inputs, real and imaginary components of the injected current from the device to the network and the real and imaginary components of the network bus voltages respectively.

Eq. (2.17) and Eq. (2.18) are developed by combining the linearized form of the individual dynamic device equations.

$$\Delta\dot{\mathbf{x}} = \mathbf{A}_D\Delta\mathbf{x} + \mathbf{B}_D\Delta\mathbf{u} + \mathbf{E}_D\Delta\mathbf{V} \tag{2.17}$$

$$\Delta\mathbf{I} = \mathbf{C}_D\Delta\mathbf{x} + \mathbf{D}_D\Delta\mathbf{V} \tag{2.18}$$

These equations together with the linearized node-admittance matrix given by $\Delta\mathbf{I} = \mathbf{Y}\Delta\mathbf{V}$ form the linearized state space model of the power system shown in Eq. (2.20).

$$\Delta\dot{\mathbf{x}} = \{\mathbf{A}_D + \mathbf{E}_D(\mathbf{Y} - \mathbf{D}_D)^{-1}\mathbf{C}_D\}\Delta\mathbf{x} + \mathbf{B}_D\Delta\mathbf{u} \tag{2.19}$$

$$\Delta\dot{\mathbf{x}} = \mathbf{A}\Delta\mathbf{x} + \mathbf{B}\Delta\mathbf{u} \tag{2.20}$$

The locations of the eigenvalues of the matrix **A** in the state space determine the small-signal stability of the power system. If all the eigenvalues have negative real parts, the system has local stability about the equilibrium point. The complex eigenvalues of **A** always occur in conjugate pairs ($\sigma \pm j2\pi f$), where each pair corresponds to a single oscillatory mode. The mode exponentially decays with time as shown in Fig. 2.2 if the real part of the eigenvalue (σ) is negative. The damping ratio (ζ) of the oscillatory mode is defined as given in Eq. (2.21).

$$\zeta = \frac{-\sigma}{\sqrt{\sigma^2 + \omega^2}} \times 100\% \tag{2.21}$$

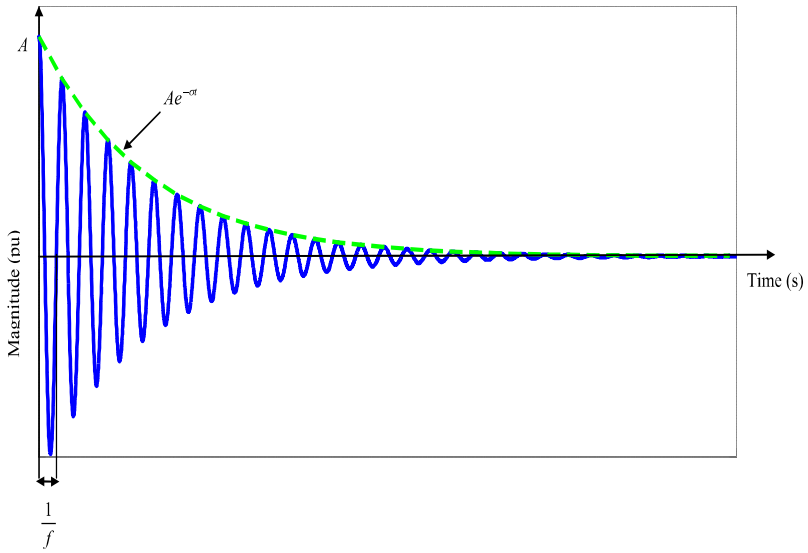

Figure 2.2: Illustration of an oscillatory mode

The decaying rate of the amplitude of the oscillation is determined by the damping ratio, that is, the amplitude of the oscillation decays to 37% of its initial amplitude in $\frac{1}{|\sigma|}$ s or $\frac{1}{2\pi\zeta}$ cycles of oscillation [14].

The procedure of determining the state space model using the mathematical model of a power system and identifying the electromechanical oscillatory modes are pre-

sented in Appendix C using a test power system.

In summary, subsequent to a disturbance, the power system can become rotor angle unstable showing aperiodic increase in rotor oscillations in the first swing due to insufficient synchronizing torque or slowly increasing rotor oscillations over several seconds due to insufficient damping torque. These two scenarios are referred to as *transient stability* problem and *oscillatory stability* problem respectively. In a large interconnected power system, the transient instability may occur beyond the first swing due to inter-area oscillations or nonlinear effects [4]. Such a scenario is referred to as a *multi-swing transient stability* problem.

2.4 Rotor angle security assessment: Literature review

The overall problem of rotor angle security assessment includes studying whether the equilibrium point of the post-fault system is both transient stable and oscillatory stable subsequent to a set of known contingencies. As explained above, the transient instability can be observed as a first-swing instability or as a multi-swing instability in a multi-machine power system. On the other hand, the oscillatory instability is due to insufficient damping of the rotor oscillations. Thus, accurate identification of the damping of the rotor angle oscillatory modes provides the useful information on the oscillatory stability of the post-fault system. Further, the damping ratio is a stability margin which indicates how close is the post-fault systems equilibrium point to oscillatory instability.

The focus of this thesis is online rotor angle security analysis in power systems. Thus, the related literature on rotor angle stability analysis is important to understand the pros and cons of the existing methods. Fig. 2.3 shows the classification of existing methods for transient and oscillatory rotor angle stability assessment in

power systems. These methods are briefly summarized in Section 2.5 and Section 2.6. The LEs-based algorithm and the improved Prony algorithm proposed in this thesis can be used in a DSA program. The improved Prony algorithm can be used for online oscillation monitoring purposes. Thus, the pros and cons of each method shown in Fig. 2.3 are illustrated giving due consideration to their applicability into aforementioned two applications.

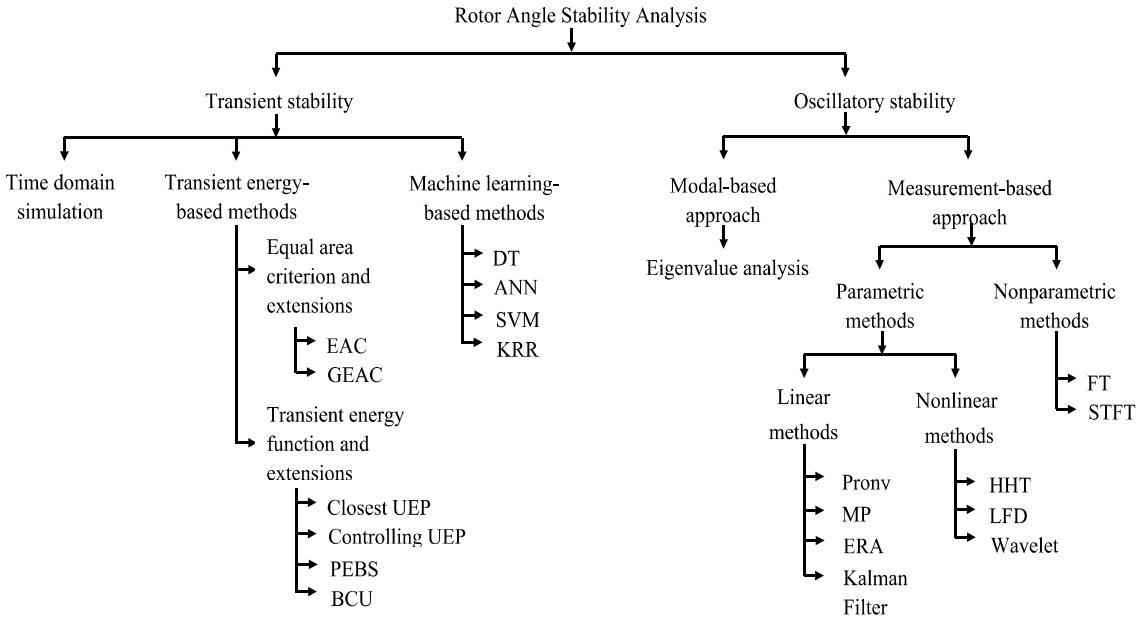

Figure 2.3: Classification of rotor angle stability assessment methods

2.5 Transient stability assessment

The transient stability assessment methods shown in left-hand side of the tree in Fig. 2.3 are briefly reviewed in this section.

2.5.1 Time domain simulation

The stability of the equilibrium point of the post-fault system can be studied by solving the DAEs associated with a given fault scenario. The traditional way of assessing this stability is to perform the time domain simulation (TDS), that is, solve the DAE starting from an initial condition [14], [16]. The different approaches used on this regard can be classified depending on:

- How to interface between differential equations (Eq. 2.10) and algebraic equations (Eq. 2.11).
- The integration method used.
- The method used to solve the algebraic equations.

In a partitioned solution approach, the algebraic equations are solved first to determine **V**, **I** and other nonstate variables, which are then used to update the state variables at the current time step. In contrast, in a simultaneous solution approach, the differential equations are first made algebraic, which are then lumped with Eq. (2.11). The set of larger algebraic equations are solved to update all the variables.

The integration methods used to perform TDS are explicit and implicit integration methods [16]. Euler, predictor corrector and Runge-Kutta are examples of explicit integration methods. These methods update the values of the dependent variables using their values in the previous time steps. In an implicit integration method such as in the trapezoidal method, the value of a variable at the current time step depends on its values at the current and previous time steps. Thus, the approach is complex compared to an explicit integration method. The numerical stability of the integration method is a key factor, which further related with the stiffness of the dynamic system. The stiffness of the power system dynamic model increases with the

increase in modeling complexity. Hence, the time step should be selected depending on the smallest time constant of the system to be simulated. In power system analysis, a small time step of half a cycle of the fundamental frequency (i.e. 1/120 s for a 60 Hz system) is used to perform the TDS.

The TDS approach provides plenty of information about the evolution of the power system variables (generator rotor angles, speeds, real and reactive powers, bus voltages, etc) with the time provided that the power system has been accurately and satisfactorily modelled for the intended study. Thus, the method serves as the reference for the transient stability assessment studies. The stability conclusion in the TDS is derived by using a security measure. For example, the post-fault power system can be concluded as rotor angle stable ($\eta > 0$) or unstable ($\eta \leq 0$) using the criterion $\eta = \frac{(360-\delta_{max})}{(360+\delta_{max})}$, where δ_{max} is the maximum rotor angle separation between the generators in the post-fault system [17].

2.5.2 Transient energy based methods

In Section 2.3.2 of this chapter it was highlighted that if the power system is stable subsequent to a contingency, the state trajectories converge to the stable equilibrium point of the post-fault power system. Hence this stable equlibrium point is asymptotically stable according to Lyapunov stability theory summarized in Section 2.2. In general, a continuous, differentiable and a positive definite[2] candidate Lyapunov function V is constructed to assess the stability of an equilibrium point at the origin of a dynamic system using the Lyapunov stability theory. It is concluded that the equilibrium point is stable if $\dot{V}$ is negative semi-definite and asymptotically stable if

[2]a function $V(x)$ is positive definite if $V(0) = 0$ and $V(x) > 0$ for $x \neq 0$. $V(x)$ is positive semi-definite if $V(0) = 0$ and $V(x) \geq 0$ for $x \neq 0$. $V(x)$ is negative definite if $-V(x)$ is positive definite. $V(x)$ is negative semi-definite if $-V(x)$ is positive semi-definite

$\dot{V}$ is negative definite [5], [12].

The synchronous generators in a power system gain/lose energy during the faulted period due to acceleration/deceleration of their rotors. After the fault clears, the stability depends on the energy absorbing capability of the post-fault system. Let the total energy of the synchronous generators at the time of clearing the fault is $V(t_c)$ and the maximum energy that the post-fault system can absorb is V_{cr}. It is clear that if $V(t_c) < V_{cr}$, the post-fault system is stable and unstable otherwise. Thus, the scalar function V representing the total energy of the system is a Lyapunov function and the surface $V(t_c) = V_{cr}$ is a Lyapunov surface [5]. The stability of the post-fault system can be studied using this approach.

This section summarizes the transient stability assessment techniques based on the aforementioned concept. The equal area criterion (EAC) method and the transient energy function method are two such techniques.

Equal area criterion method and its extensions

The EAC method is widely used to illustrate the fundamentals of the transient stability problem in power systems. Thus, the concept is explained in detail in books describing the transient stability of power systems [13], [14], [18]. This method combines the rotor angle dynamics of a synchronous generator given by the swing equation shown in Eq. (2.22) with the power angle relationship shown in Eq. (2.23). The synchronous generators and the loads are modeled using the classical generator model and the constant admittance load model respectively as explained in Section 2.3.1 for the analysis. Fig. 2.4 illustrates the rationale behind this criterion using a single generator connected to an infinite bus[3].

[3]an infinite bus represents a constant voltage source at constant frequency

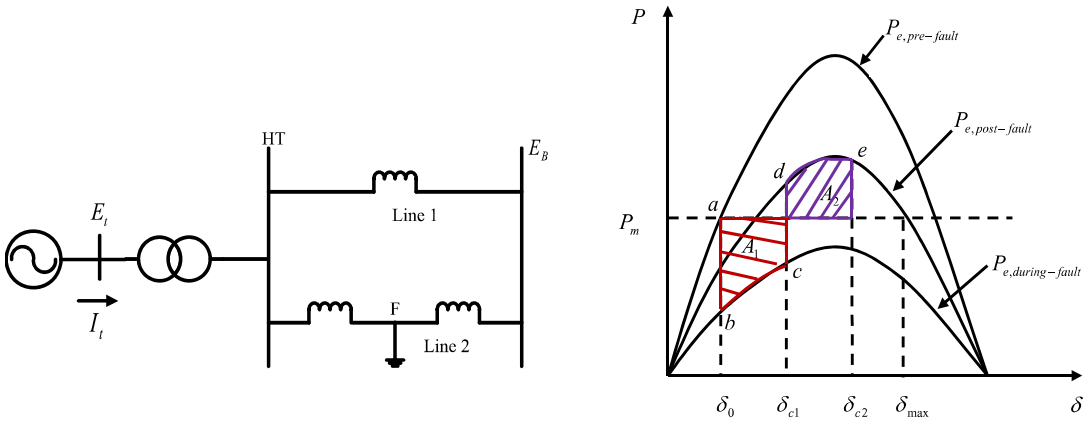

Figure 2.4: Illustration of the concept of equal area criterion

$$\frac{2H}{\omega_0}\frac{d^2\delta}{dt^2} = P_m - P_e - \frac{K_D}{\omega_0}\frac{d\delta}{dt} \tag{2.22}$$

$$P_e = \frac{EE_B}{X}\sin\delta \tag{2.23}$$

where, H is the inertia constant of the generator, ω_0 is the synchronous speed, E is the generator internal voltage, E_B is the voltage at the infinite bus, X is the equivalent reactance between the generator and the infinite bus, δ is the angle between E and E_B, P_m is the input mechanical power in per unit, P_e is the electrical power injected by the generator to the infinite bus in per unit, and K_D is the mechanical damping of the generator.

The system is at steady state initially and $P_m = P_{e,prefault}$. The real power injected by the generator to the network changes during the fault and after clearing the fault as shown by $P_{e,duringfault}$ and $P_{e,postfault}$ respectively in Fig. 2.4. Let the fault occurs at the point denoted by letter a and clears at the point denoted by the letter c in the figure. Assuming that the mechanical power input to the generator, P_m remains

constant, the total energy gained by the generator during the fault on period is given by area A_1 and the total energy transferred to the post-fault system is given by area A_2. The post-fault system is stable since $A_1 = A_2$. The maximum energy that the post-fault system can absorb is given by the integral $\int_{\delta_{c1}}^{\delta_{max}} (P_{e,postfault} - P_m) d\delta$, where δ_{c1} is the rotor angle at this fault clearing time. If $A_1 > A_2$ at a given fault clearing time, then the post-fault system becomes unstable.

The EAC and its theoretical derivations based on an one machine infinite bus (OMIB) system are important to understand the factors influencing the transient stability of the power system. Thus, attemps have been made in the power system literature to extend the approach into transient stability analysis of multi-machine power systems. These attempts have been summarized in [13] and are based on the observation that the loss of synchronism in a multi-machine power system originates due to irrevocable separation of its machines into two groups, a) critical cluster of machines, and b) noncritical cluster of machines. Each group of machines can then be replaced by an equivalent machine. The resulting two equivalents are replaced by a time-invariant OMIB system given by Eq. (2.24).

$$M\frac{d^2\delta}{dt^2} = P_m - P_{max}\sin(\delta - \nu) \tag{2.24}$$

where, M, P, P_{max} and ν are constant values.

Subsequently, the stability of the system can be analyzed using the EAC as explained above. The extended equal area criterion (EEAC) [19], [20], [21] uses this approach to a multi-machine power system assuming the simplified classical generator model and the static load models.

The EAC and the EEAC are direct applications of Lyapunov's second method of stability analysis into power systems. The use of simplified models in the analy-

sis limits the application of the method in deriving valid conclusions for large scale power systems. Thus, the power system literature presents the genaralized equal area criterion (GEAC) method. In this approach also the power system is reduced to an equivalent form given by Eq. (2.24) such that P, P_{max} and ν are no longer constants. The single machine equivalent (SIME) method [13] is an example for the application of GEAC into transient stability analysis in power systems.

The SIME method accommodates the detailed generator models with their auxiliary controls in the transient stability assessment process and uses the step-by-step TDS in during-fault and pre-fault situations. The generators are distinguished as critical and noncritical machines considering their angle differences at each time step. After identifying the two groups of machines, their equivalent parameters are determined using appropriate equations and the stability is assessed. The method further provides the stability margin of the power system. The SIME method is used in commercially available software for offline analysis of transient security assessment in power systems [17]. Further, this approach can also be used in an online security assessment program. Chapter 5 of this thesis compares the results of the proposed transient security assessment method using the concept of Lyapunov exponents with the SIME method.

The transient energy function method and its extensions

Power system transient stability analysis using the energy function given in Eq. (2.25) has gained attention by the power system researchers. Different methods relying on this energy function are also referred to as *direct methods* of transient stability analysis even though the step-by-step TDS is used in the solution procedure. Theoretical derivations of the energy function and the stability analysis are explained in detail in

books [18], [22], [23].

$$\begin{aligned} V = & \frac{1}{2}\sum_{i=1}^{n} J_i\omega_i^2 - \sum_{i=1}^{n} P_{mi}^{/}(\theta_i - \theta_i^s) \\ & - \sum_{i=1}^{n-1}\sum_{j=i+1}^{n} [C_{ij}(\cos\theta_{ij} - \cos\theta_{ij}^s) - \int_{\theta_i^s+\theta_j^s}^{\theta_i+\theta_j} D_{ij}\cos\theta_{ij} d(\theta_i + \theta_j)] \end{aligned} \tag{2.25}$$

All the variables in Eq. (2.25) have their usual notations. The first term represents the kinetic energy and the subsequent three are the potential energy terms. For the stability analysis, this method first calculates the total energy of the system at the fault clearing time using Eq. (2.25). The computed energy is then compared against the critical energy (V_{cr}) of the system and the stability status is concluded. Different direct methods are available in the literature depending on the method used to determine the critical energy. The potential energy boundary surface (PEBS), the closest unstable equilibrium point (UEP), the controlling UEP and the boundary of stability-region-based controlling UEP (BCU) are examples of such methods. The details of these methods can be found in [18], [22], [23]. These methods can be used to determine the stability of the equilibrium point of the post-fault system and the maximum allowable fault clearing time or the critical clearing time of a contingency. However, the computational burden associated with the direct methods, especially when determining V_{cr} and the difficulty of accommodating complex generator models into Eq. (2.25) are considered as limitations for transient security assessment in power systems.

2.5.3 Machine learning-based methods

A significant attention has been given in recent literature to apply artificial intelligence-based techniques to online transient stability assessment and control in power systems. In this approach, a database is created for a given network by considering possible conditions and a classifier is trained using one of the learning techniques. The input to the classifier may be the pre-fault power system variables such as the bus voltage magnitude and angle, active and reactive power flows, etc or the post-fault system dynamic features such as the generator rotor angle, bus voltage magnitude, etc. The automatic learning may be done using the fuzzy-logic rules [24], neural networks (NN) [25], decision trees (DT) [26], extreme learning machines [27], support vector machines (SVM) [28], etc. Thus, once the classifier is trained, it can be used to assess the transient stability of the power system subsequent to the occurrences of anticipated credible contingencies and hence to initiate the preventive control actions or to predict the transient stability status subsequent to the actual occurrence of a contingency and hence to initiate the emergency control actions. References [29] and [30] propose to train classifiers using two regression analysis techniques, kernal ridge regression (KRR) and Lasso to determine the transient stability boundary. This boundary can be incorporated into a dynamic security constrained optimal power flow program to determine the optimum preventive control actions in power systems.

It is clear that these artificial intelligence-based techniques determine the transient stability within a less computing time once the classifiers have been trained extensively in an offline environment. This feature makes such approaches more suitable for online DSA purposes. However, the effort required to train the network may be significant. The recent publication [31] shows that the size of the training data set can be reduced using the input features as the energy terms of the transient energy function given in

Eq. (2.25).

2.6 Oscillatory stability assessment

This section summarizes the oscillatory stability assessment techniques shown in the right-hand side of the tree in Fig. 2.3.

2.6.1 Eigenvalue analysis

The information on whether the current operating point of the power system has a potential of becoming oscillatory unstable can be checked by looking at the eigenvalues associated with the rotor angle modes. The eigenvalues of the state matirx can be determined using the QR transformation method [32]. The size of the state matrix increases with the number of dynamic devices in a large power system, thus limiting the use of QR transformation to accurately calculate the eigenvalues. Therefore, special techniques have been developed to study the small-signal stability of large power systems. Analysis of essentially spontaneous oscillations in power systems (AESOPS) [33] and modified Arnoldi method (MAM) [34] are two special techniques used to determine a selected set of eigenvalues. The AESOPS algorithm can only determine the rotor angle modes[4] and the MAM can compute the eigenvalues associated with any system mode [14]. The QR transformation is used inside both of the algorithms to compute the eigenvalues of a matrix, which is a subset of the overall state matrix.

This model-based approach has a limitation on the number of states and hence the number of eigenvalues. For example, the number of states in the linearized model cannot exceed 1000 in small-signal analysis tool (SSAT) [35]. Thus, a significant

[4]these are the oscillatory modes associated with the movements of the generator rotors around the synchronous speed

attention has been given in literature to determine the dynamic performance of the system from the outputs of the transient simulation programs or from the measured data under ring-down conditions in the power system. Section 2.6.2 describes these measurement-based approaches.

2.6.2 Measurement-based approaches

The measurement-based approaches in right hand side of the tree in Fig. 2.3 are either parametric methods or nonparametric methods. The parametric methods first select a possible model for the measurements and determine the mode parameters based on this model. In contrast, the nonparamteric methods do not make any assumptions about the measured data. Instead they work on the data to estimate the characteristics of the data itself [36]. The parametric methods can be either linear or nonlinear depending on whether the methods originate from the linearity assumptions or not.

Prony analysis

Prony analysis is a linear parametric technique, which fits an observed signal using a sum of complex sinusoidal oscillations [37]. This analysis first constructs a linear prediction model that best fits the measured signal and the coefficients of the prediction model are determined using a least square approach. The roots of the polynomial equation associated with the linear prediction model determine the modes of the system. The theory, derivations and limitations of Prony analysis are presented in detail in Section 4.2 in Chapter 4.

Matrix pencil method

The matrix pencil (MP) method also approximates an observed signal using a sum of complex sinusoidal oscillations. However, the procedure of deriving the solution of the MP method is different from that of the Prony analysis. The MP method constructs two matrices Y_1 and Y_2 including time-shifted measurements of the measured signal. It is shown that the z-domain roots associated with the complex sinusoidal oscillations can be found as a generalized eigenvalue problem of the matrix pair $\{[Y_2], [Y_1]\}$ [38]. This method has been applied into power systems in [39]. The MP method is more robust to noise than the Prony analysis.

Eigen realization algorithm

Referring to Eq. (2.20), the linearized state space model of the power system with usual notations is given by Eq. (2.26).

$$\begin{cases} \dot{x} = Ax(t) + Bu(t) \\ y(t) = Cx(t) \end{cases} \tag{2.26}$$

Considering the transition matrix $\Phi(t) = e^{At}$, the equivalent discrete system of the continuous system given in Eq. (2.26) for a zero-order hold and a sampling time T can be written as in Eq. (2.27).

$$\begin{cases} x(k+1) = Fx(k) + Gu(k) \\ y(k) = Cx(k) \end{cases} \tag{2.27}$$

where, $F = \Phi(T)$ and $G = [\int_0^T \Phi(\tau)d\tau]B$.

The eigen realization algorithm (ERA) numerically determines the matrices (F, G, C)

and/or (A, B, C) assuming an impulse type input in the system. The ERA proposed in [40] applies the singular value decomposition (SVD) to a Hankel block-matrix[5] to determine (F, G, C) such that a minimal realization of the original system is preserved. The discrete system is then converted back to the continuous domain and (A, B, C) are determined. Reference [40] shows that the eigenvalues of matrix A are the minimum number of eigenvalues required to represent the original system. In [41], the minimal realization approach has been improved by constructing a matrix, which is the product of the Hankel matrix and its transpose.

Kalman filter

Kalman filter uses an auto-regressive (AR) model to approximate the observed data. The coefficients of the AR model are determined such that the error between the actual value and the predicted value by the model is minimized. This is achieved using a recursive algorithm. Once the coefficients are found, the roots of the characteristic equation give the eigenvalues of the system. Thus, the Kalman filter algorithm can be used to determine the modal content in the output signals of transient simulation programs. A detailed comparison between the Kalman filters and the Prony analysis can be found in [42].

The recursive Kalman filter algorithm has been used in [43] to track the dominant oscillatory mode in the online environment. In [44], the algorithm has been improved to track multiple oscillatory modes.

[5] a Hankel matrix has the property of $a_{i,j} = a_{i-1,j+1}$ for $i \neq 1$, where $a_{i,j}$ is the $(i, j)^{th}$ element

Fourier transform

Reference [45] presents an algorithm using the Fourier transform (FT) to determine the frequencies and damping ratios of the dominant modes present in the outputs of transient simulations. First, the frequency content of a ring-down oscillation is obtained via the frequency spectrum. Based on the dominant frequency, the length of a data window and the gap between the adjacent data windows are determined. FT is applied on these multiple data windows and the real part of the eigenvalue associated with the oscillation mode is determined by taking the ratio of the FTs at the selected oscillation frequency.

The damping ratio estimations of this approach are sensitive to the length and the seperation between the data windows. Furthermore, the presence of multiple modes in the ring-down oscillation interferes on the calculated values. Therefore, it is recommended to eliminate the neighbouring model interactions before the analysis. An improved algorithm using the FT applied on multiple measurements in power systems is proposed in [46] to monitor the power system oscillations in an online environment. It is shown in [46] that the damping ratio of an oscillatory mode can be determined as the rate of decay of its energy.

Short time Fourier transform

The discrete short time Fourier transform (STFT) is essentially a discrete FT of a sampled signal over a short time data window. Thus, at each time instant, the STFT is related with the FT of the signal in the vicinity of that time instant, which makes it an appropriate tool to determine the time-dependent variation of a spectral content of a signal. The usage of STFT to determine the time-frequency distribution of energy of electromechanical oscillations is given in [47]. The frequencies of the dominant

modes are identified by the peaks of the energy spectrum. A scenario of oscillatory instability is represented by an unbounded increase in the kinetic energy determined at the dominant frequency. This method is more suitable to observe the patterns of system dynamic behavoir. Nevertheless, it lacks of providing an accurate damping estimation.

Wavelet transform

The continuous Wavelet transform (CWT) of a time domain signal $y(t)$ is given by Eq. (2.28).

$$CWT(b,a) = \frac{1}{\sqrt{a}} \int_{-\infty}^{\infty} y(t)\phi(\frac{(t-b)}{a})dt \tag{2.28}$$

where, a is a scalar parameter, b is a time parameter and ϕ is a wavelet function. In literature [48], it has been demonstrated that the Morlet wavelet has the property of preserving damping information of a signal. Reference [48] shows that the CWT can be used for online monitoring the oscillatory stability in power systems. First the measured responses are processed by the CWT. Then Eq. (2.29) can be used with the Wavelet spectral analysis to determine the time distribution of the damping of the oscillatory modes.

$$\sigma = \frac{1}{(b_2 - b_1)} \ln \frac{|CWT(b_1,a)|}{|CWT(b_2,a)|} \tag{2.29}$$

where, b_1 and b_2 are two time instants.

Hilbert-Huang Transform

The Hilbert-Huang transform (HHT) is a two step procedure [49]. First, the input signal is processed by a process known as empirical mode decomposition (EMP), which generates a number of intrinsic mode functions (IMFs). Each IMF represents an oscillation mode imbedded in the input data. The Hilbert transform as defined in Eq. (2.30) is used in order to construct an analytical siganl given in Eq. (2.31) corresponding to each IMF. Using the analytical signal, the instantaneous amplitude, instantaneous phase angle and the instantaneous frequency of the dominant IMFs can be calculated as shown in Eq. (2.32), Eq. (2.33) and Eq. (2.34) respectively.

$$c(t) = \frac{1}{\pi} p.v. \int_{-\infty}^{\infty} \frac{IMF(\tau)}{t-\tau} d\tau \tag{2.30}$$

$$z(t) = c(t) + jc\bar{(t)} = a(t)e^{j\psi(t)} \tag{2.31}$$

$$a(t) = \sqrt{c(t)^2 + c\bar{(t)}^2} \tag{2.32}$$

$$\psi(t) = \tan^{-1} \frac{c(t)}{c\bar{(t)}} \tag{2.33}$$

$$\omega(t) = \frac{d}{dt}\psi(t) \tag{2.34}$$

This method has been applied to determine the instantaneous frequencies and the dampings of modes in power system response signals in [50]. However, the HHT method has the drawback of generating fictitious IMFs, which do not reflect the true dynamic performance of the powe system. A robust algorithm has been proposed in [51], which first process the input signals using a linear filter bank and the dominant signals are identified using a Teager-Kaiser energy operator. The dominant signals are then analyzed using eigen realization algorithm to determine the damping of the modes.

The Wavelet transform, HHT and the Teager-Kaiser energy operator based approach have been applied in online monitoring of power system oscillations [48], [50], [51] . However, still these methods can also be used to process the outputs of the transient simulation programs to determine the frequencies and the damping ratios of the dominant oscillatory modes.

2.7 Chapter summary

This chapter systematically derived a scenario of rotor angle stability analysis in power systems starting from the stability theory of a nonlinear dynamic system. The rotor angle stability analysis is a subset of the tasks in DSA in power systems. This chapter reviewed the literature on rotor angle stability assessment under the two main categories of transient stability and oscillatory stability. Pros and cons of each method were highlighted and their applicability into online DSA and online oscillation monitoring were discussed.

This thesis presents two algorithms for rotor angle stability assessment in power systems. These are; a) transient stability assessment technique based on the concept of Lyapunov exponents (LEs), and b) oscillatory stability assessment using an improved Prony algorithm. The LEs is a theoretically sound approach to study the stability of nonlinear dynamic systems. A comprehensive stability analysis by applying this concept into power systems was not available in literature before this work. Further, the Prony algorithm has been treated as the reference for comparing the results of different oscillation monitoring algorithms presented in Section 2.6. This thesis presents a simple approach to improve the Prony algorithm to extract only the dominant oscillatory modes present in ring-down oscillations. These new approaches are discussed in Chapter 3 and Chapter 4 respectively.

Chapter 3

Transient Stability Assessment using the Concept of Lyapunov Exponents

3.1 Introduction

The conclusion on whether the generators can remain in synchronism subsequent to large-magnitude disturbances in a power system or the transient stability of a power system is in general ranked as a first requirement in a dynamic security sssessment (DSA) program. Such conclusions are to be taken as early as possible allowing the operator to initiate necessary actions to continue the secure operation. This chapter presents a theoretically sound nonlinear analysis technique based on the concept of Lyapunov exponents (LEs) to derive the said stability conclusion in a DSA program.

The objectives of this chapter are: 1) describe the concept of LEs and the procedure of calculating a spectrum of LEs from the dynamic model, 2) investigate the applicability of LEs for transient stability assessment in power systems, and 3) de-

velop a modified algorithm for accurate and early predicting the transient stability in the power system.

3.2 The concept of LEs

The concept of LEs is based on the fundamental assumption that the nearby trajectories in the state space are evolving exponentially [52],[53]. Thus, the LEs measure the exponential rates of divergence or convergence of nearby trajectories in the state space. Reference [52] defines a spectrum of LEs of an $n-$dimensional system based on the long term growth rate of an infinitesimal $n-$dimensional hypersphere of initial conditions around an initial operating point in the state space. The $n-$dimensional hypersphere would become an $n-$dimensional ellipsoid during the evolution. The i^{th} LE (Λ_i) is then defined in terms of the length of the ellipsoidal principal axes as in Eq. (3.1).

$$\Lambda_i = \lim_{t\to\infty} \frac{1}{t} \ln \frac{\|\Delta x_i(t)\|}{\|\Delta x_i(t_0)\|}, \qquad i = 1, 2, \cdots, n \tag{3.1}$$

where, $\|\Delta x_i(t)\|$ and $\|\Delta x_i(t_0)\|$ represent the lengths of the i^{th} principal axes of the ellipsoid at the current time and the initial time respectively. The existence of the above limit is known by Oseledec multiplicative ergodic theorem [54]. However, in practical calculations, the finite-time LEs are defined by Eq. (3.2).

$$\Lambda_i = \frac{1}{t} \ln \frac{\|\Delta x_i(t)\|}{\|\Delta x_i(t_0)\|}, \qquad i = 1, 2, \cdots, n \tag{3.2}$$

In the limit as $t \to \infty$, the finite-time LEs converge to the true LEs of the system. The key properties of the LEs are as follows:

- The LEs are related to the contraction and expansion of different directions in

the state space. A negative exponent reflects an axis which is contracting on average.

- The sum of n LEs represents the average contraction/expansion rate of an $n-$volume element in the state space.
- The signs of the LEs indicate the asymptotic performance of a dynamic system. If all the exponents are negative, the trajectories from all the directions in the state space converge to an exponentially stable equilibrium point. If at least one of the exponents is positive, the trajectories diverge along one direction and the system is said to has a chaotic or strange attractor.
- The LEs do not depend on the initial conditions, that is, all the LEs starting from different initial conditions converge to the same value as long as these initial conditions lie within the same stability region of the equilibrium point.
- The concept of LEs is related with the exponential stability of a dynamic system. If a system is exponentially stable, it is also asymptotically stable [5].

3.3 Estimation of LEs from a mathematical model

Estimation of LEs from a mathematical model has been well established. Wolf et al. [52] pioneered the work and developed the standard algorithm for LE estimation from mathematical models. During the calculation procedure, the reference trajectory of an $n-$dimensional continuous time system given by $\dot{\mathbf{x}} = \mathbf{f}(\mathbf{x})$ is determined by the action of the nonlinear equations of motion on an initial condition. The nearby trajectories are defined by the evolution of the principal axes of $n-$hypersphere via the linearized equations of motion. This gives rise to the simultaneous solution of the set of equations shown in Eq. (3.3):

$$\begin{Bmatrix} \dot{x} \\ \dot{\varphi}_t \end{Bmatrix} = \begin{Bmatrix} f(x) \\ J\varphi_t \end{Bmatrix} \tag{3.3}$$

where, $x(t) = [x_1(t), x_2(t), \cdots, x_n(t)]$ is a vector of state variables, φ_t is the state transition matrix of the linearized system; $\Delta x(t) = \varphi_t \Delta x(0)$ and J is the $n \times n$ Jacobian matrix defined as in Eq. (3.4);

$$J_{ij} = \frac{\partial f_i}{\partial x_j}\Big|_{x=x(t)} \tag{3.4}$$

The initial conditions of the above integration are $x(t_0) = x_0$ and $\varphi(t_0) = I$, where I represents the identity matrix.

The principal axes of the initial $n-$hypersphere would tend to fall along the direction of the most rapid growth during the above integration. In order to avoid this misalignment of vectors, the resulting vectors by solving the linearized equations of motion, $\Delta x_1, \Delta x_2, \cdots, \Delta x_n$ are processed using Gram-Schmidt reorthonormalization (GSR) at each integration time step. The GSR first results in a set of orthogonalized vectors, $\Delta u_1, \Delta u_2, \cdots, \Delta u_n$ and then a set of orthonormalized vectors, $\Delta v_1, \Delta v_2, \cdots, \Delta v_n$ determined by Eq. (3.5), where $<>$ represents the inner product of vectors.

$$
\begin{aligned}
&\Delta u_1 = \Delta x_1, && \Delta v_1 = \frac{\Delta u_1}{\|\Delta u_1\|} \\
&\Delta u_2 = \Delta x_2 - < \Delta x_2, \Delta v_1 > \Delta v_1, && \Delta v_2 = \frac{\Delta u_2}{\|\Delta u_2\|} \\
&&& \vdots \\
&\Delta u_n = \Delta x_n - < \Delta x_n, \Delta v_{n-1} > \Delta v_{n-1} - \cdots - < \Delta x_n, \Delta v_1 > \Delta v_1, && \Delta v_n = \frac{\Delta u_n}{\|\Delta u_n\|}
\end{aligned}
\tag{3.5}
$$

Fig. 3.1 shows the geometrical interpretation of the orthonormalization of two principal axes at the j^{th} time step.

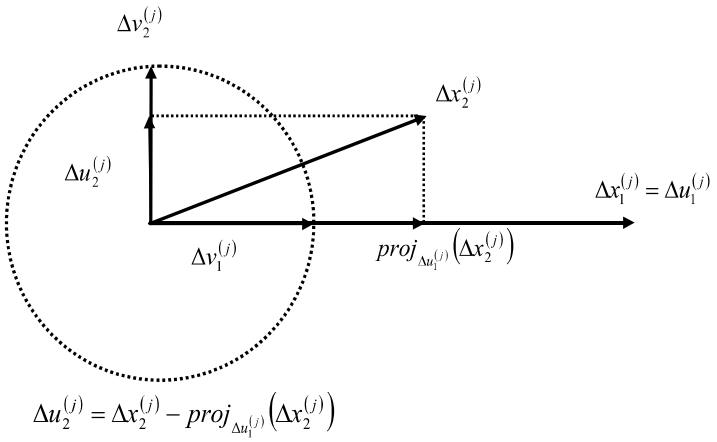

Figure 3.1: Geometrical interpretation of GSR of two principal axes: $\Delta x_1^j \& \Delta x_2^j$ (j represents the number of integration step). $\Delta x_1^j \& \Delta x_2^j$ are first orthogonalized into $\Delta u_1^j \& \Delta u_2^j$ and orthonormalized into $\Delta v_1^j \& \Delta v_2^j$

Once the orthogonal vector frame is available by GSR, for a sufficiently large integer k, the i^{th} LE can be estimated using Eq. (3.6).

$$\Lambda_i \approx \frac{1}{n\Delta t}\sum_{j=1}^{n} \ln \|\Delta u_i^{(j)}\|, \qquad i = 1, 2, \cdots, n \tag{3.6}$$

where, Δt is the integration time step.

According to the above procedure, it is observed that this computation involves simultaneous solution of $n(n+1)$ number of equations, n equations for the reference trajectory and n copies of tangent map equations.

3.3.1 Spectrum of LEs of a two-dimensional system

Consider the two-dimensional system[1] given in Eq. (3.7) and Eq. (3.8) to illustrate the calculation procedure of the spectrum of LEs as explained in Section 3.3.

$$\frac{d}{dt}x_1 = 0.13 - 0.16\sin(x_2) - 1.43x_1 \tag{3.7}$$

$$\frac{d}{dt}x_2 = 377x_1 \tag{3.8}$$

The time varying Jacobean matrix of the linearized system is:

$$J_{x(t)} = \begin{bmatrix} -1.43 & -0.16\cos(x_2) \\ 377 & 0 \end{bmatrix}.$$

The spectrum of LEs of this system can be determined using the following steps:

1. Numerically integrate the dynamic equations given in Eq. (3.7) and Eq. (3.8) starting from an initial condition.

   In this study, 4^{th} order Runge-Kutta method was used selecting the initial

[1] this represents the post-fault system dynamic behavior of the single machine infinity bus system given in [14]

conditions as $(x_{10}, x_{20}) = (0.0102, 0.8926)$. This gave the reference trajectory shown in purple line in Fig. 3.2

2. Numerically solve the equation $\dot{M} = J_{t=t_0} M$ to evolve the nearby trajectories.

   At $t = t_0$, a set of nearby trajectories are formed by selecting their initial conditions inside a circle of unit radius. As shown in Fig. 3.2, $\vec{X_{11}} = 1 + j0$ and $\vec{X_{21}} = 0 + j1$ were used as the initial conditions of the above integration. The two vectors, $\vec{X_{12}}$ and $\vec{X_{22}}$ at time, $t = t_0 + \Delta t$ were the results of this integration.

3. Orthonormalize the vectors.

   $\vec{X_{22}}$ was first orthogonalized with respect to $\vec{X_{12}}$ to form the vector $\vec{U_{22}}$ and then normalized to obtain the vector $\vec{V_{22}}$. $\vec{V_{12}}$ is the unit magnitude vector corresponding to $\vec{X_{12}}$.

4. Calculate the first approximation of the spectrum of LEs.

   The two LEs were calculated as $\frac{1}{\Delta t} \ln |U_{12}|$ and $\frac{1}{\Delta t} \ln |U_{22}|$ respectively.

5. Evolve the nearby trajectories over the next time step selecting the orthonormalized vectors as the initial conditions of $\dot{M} = J_{t=t_0+\Delta t} M$.

6. Continue this process for sufficiently long time and average the individual LEs to obtain the spectrum of LEs of the dynamic system.

Fig. 3.2 shows the evolution of the reference trajectory and the principal axes during the calculation.

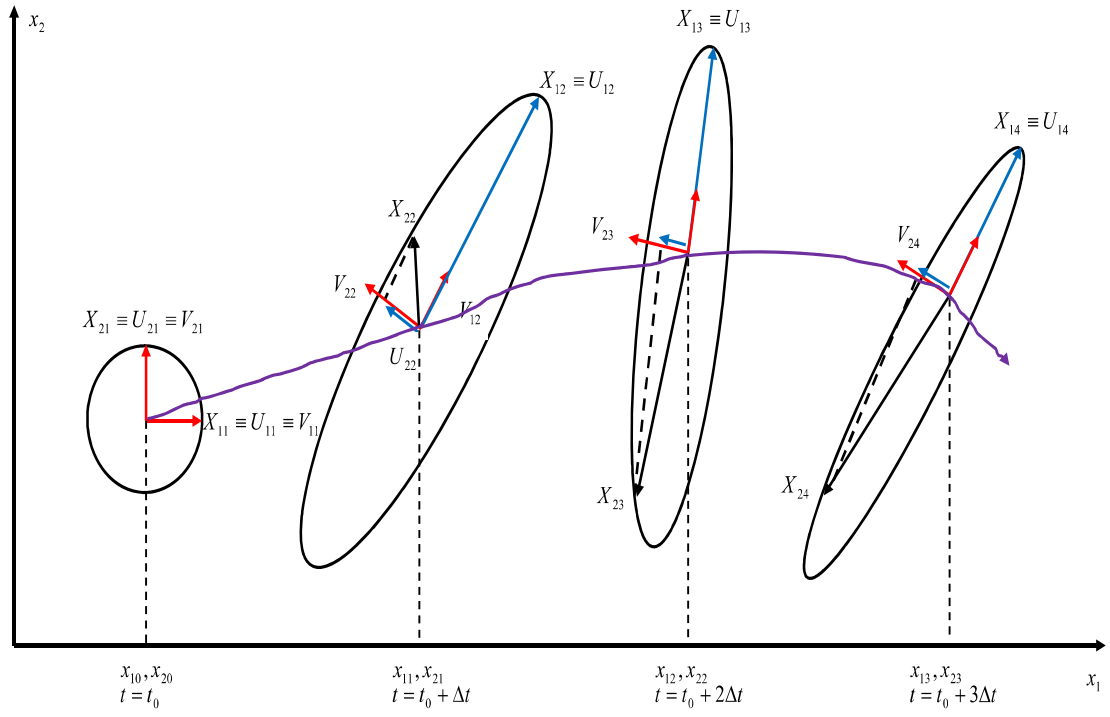

Figure 3.2: Evolution of the reference trajectory and nearby trajectories of a two-dimensional system : purple line - reference trajectory, blue lines - orthogonalized vectors, red lines - orthonormalized vectors, $\vec{X_{11}} = 1 + j0, X_{21} = \vec{0} + j1, \vec{X_{12}} = 0.9869 + j3.1217, X_{22} = -0.00\vec{08} + j0.9987, \vec{V_{12}} = 0.3014 + j0.9535, V_{22} = 0.95\vec{35} + j0.3014$

3.4 Investigation of the applicability of LEs for large-disturbance rotor angle stability assessment in power systems

This section presents a comprehensive stability analysis using the concept of LEs for transient stability assessment in power systems using a test power system. The purpose behind this analysis is to investigate the applicability of the LEs to study the said stability in power systems.

3.4.1 Test power system

The test system [18] shown in Fig. 3.3 has 3 generators and 9 buses and the geneara-tors are connected at the buses 1, 2 and 3. The steady state operating parameters and the dynamic data of the test system are given in Section B.1 in Appendix B.

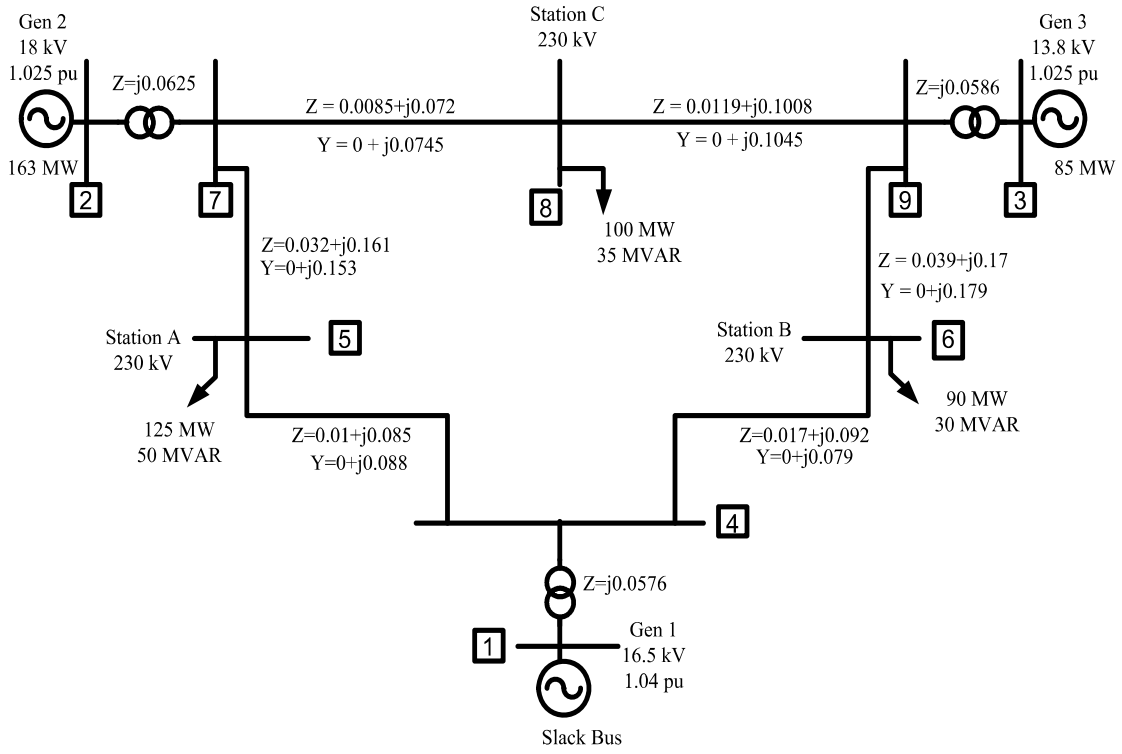

Figure 3.3: 3-generator 9-bus test system [18]

In order to study the transient stability of the system, the dynamic model of the test system was derived using the following assumptions.

- Generators were modeled using the classical generator model with a voltage source of constant magnitude behind its transient reactance as shown in Fig. 3.4.

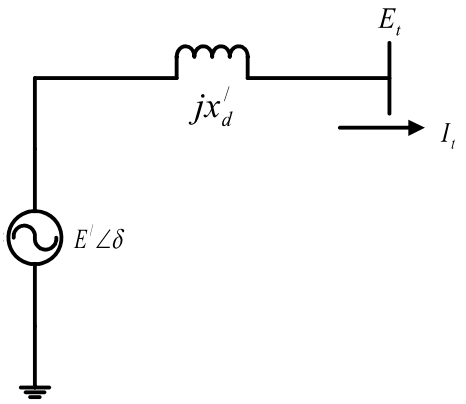

Figure 3.4: Classical generator model:$x_d^{'}$ is the generator transient reactance, $E^{'}\angle\delta$ is the generator internal voltage

- Loads were modeled as constant admittances connected in shunt at the respective bus bars.
- Bus 1 was considered as an infinite bus, that is, the dynamics of the generator connected to bus 1 was not modelled, instead it was treated as a constant voltage source.

The dynamic behaviour of a generator is given by Eq. (3.9).

$$\frac{2H}{\omega_0}\frac{d^2\delta}{dt^2} = \bar{T_m} - \bar{T_e} - \frac{K_D}{\omega_0}\frac{d\delta}{dt} \tag{3.9}$$

where, ω_0 is the synchronous speed, $\bar{T_m}$ is the input mechanical torque of the generator in pu, and $\bar{T_e}$ is the generator air gap torque output in pu. Eq. (3.9) can be expressed using two first order differential equations as given in Eq. (3.10) and Eq. (3.11).

$$\frac{1}{\omega_0}\frac{d}{dt}\delta = \Delta\omega \tag{3.10}$$

$$\frac{d}{dt}\Delta\omega = \frac{1}{2H}(\bar{T_m} - \bar{T_e} - K_D\Delta\omega) \tag{3.11}$$

where, δ and $\Delta\omega$ represent the angle of the generator internal voltage in radians and the pu generator speed deviation from the synchronous speed respectively.

When the generator is operating around the pre-fault equilibrium point, the mechanical torque input $\bar{T_m}$ of the generator equals the generator air gap torque $\bar{T_e}$. These $\bar{T_m}$ values were kept constant throughout the simulation and $\bar{T_e}$ was determined using Eq. (3.12) approximating the rotor speed to be 1.0 pu.

$$T_{ei} \approx |E_i|^2 G_{ii} + |E_i^{/}| \sum_{j=1, j\neq i}^{3} |E_j^{/}||Y_{ij}| \cos(\delta_{ij} - \theta_{ij}) \tag{3.12}$$

where, $E_i^{'} = |E_i|\angle\delta_i$ is the generator internal voltage, $Y_{ij} = G_{ij} + jB_{ij}$ is the equivalent admittance between i^{th} and j^{th} generators.

Combining Eq. (3.10), Eq. (3.11) and Eq. (3.12), the state space model of the test system was formulated as given in Eq. (3.13).

$$\begin{cases} \frac{d}{dt}\delta_i = \omega_0\Delta\omega_i \\ \frac{d}{dt}\Delta\omega_i = \frac{T_{m_i}}{2H_i} - \frac{|E_i^{/}|^2 G_{ii}}{2H_i} - \frac{|E_i^{/}|}{2H_i}\sum_{j=1, j\neq i}^{3} |E_j^{/}||Y_{ij}| \cos(\delta_{ij} - \theta_{ij}) - \frac{K_{D_i}}{2H_i}\Delta\omega_i \end{cases} \tag{3.13}$$

Eq. (3.13) is in the form of $\dot{X} = f(X)$, where $X = [\delta_2, \Delta\omega_2, \delta_3, \Delta\omega_3]$.

$|Y_{ij}|\angle\theta$ values in Eq. (3.13) change depending on the pre-fault, during-fault and post-fault network configuration. The equilibrium point of the pre-fault system

($\delta_{2,pre}, \Delta\omega_{2,pre}, \delta_{3,pre}, \Delta\omega_{3,pre}$) was obtained by equating Eq. (3.13) to zero. Assuming that the system operating at steady state subjects to a specified fault scenario, the resulting dynamic equations during the faulted period were integrated and the values of the state variables ($\delta_{2d}, \Delta\omega_{2d}, \delta_{3d}, \Delta\omega_{3d}$) at the fault clearing time were determined. These were then used to solve the post-fault system dynamic equations and to determine the LEs associated with the equilibrium point of the post-fault system.

Conceptually, convergence of the LEs is an important criterion to derive the stability conclusions. The convergence criterion was accommodated as a constraint as given in Eq. (3.14).

$$|LLE_{t=T} - LLE_{t=(T-100)}| \leq 0.001 \tag{3.14}$$

where, LLE is the largest Lyapunov exponent and T is the current time window.

3.4.2 Stability analysis

As explained in Section 2.3 in Chapter 2, an event-type disturbance is characterized by a specific fault scenario with a known fault clearing time. Such a scenario is known as a contingency. The interest is on the stability of the equilibrium point of the post-fault system subsequent to the contingency. This section presents the results of the rotor angle stability analysis performed on the 3-generator 9 bus test system shown in Fig. 3.3 under different contingencies. The analysis was done in MATLAB using the 4^{th} order Runga-Kutte method at 1/120 s time step as the numerical integration method. This time step is a standard time step used in power system time domain simulations.

System stability subsequent to an event-type disturbance

Consider the stability of the test system subsequent to a three phase solid fault in the line 9-8, very close to the bus bar 9 and was cleared after 100 ms by disconnecting the faulted line from the network. Table 3.1 shows the estimated LEs up to the 4^{th} decimal place at different time intervals.

Table 3.1: LEs of 3-generator 9 bus system

Time (s)	1^{st}LE	2^{nd}LE	3^{rd}LE	4^{th}LE
10	-0.1231	-0.2311	-0.0721	-0.0730
100	-0.1159	-0.1495	-0.0869	-0.1470
800	-0.1019	-0.1103	-0.1399	-0.1471
900	-0.1012	-0.1100	-0.1409	-0.1472
1000	-0.1013	-0.1086	-0.1407	-0.1481

Accordingly, all the four LEs have converged to negative values. This ensures that the trajectories have converged to an exponentially stable equilibrium point. Fig. 3.5 shows the time domain trajectories of the four state variables $(\delta_2, \delta_3, \Delta\omega_2, \Delta\omega_3)$. It can be seen that these trajectories reach the equilibrium point showing exponentially decaying oscillations. The long computation time for the convergence is due to the oscillatory nature of the state trajectories. Furthermore, the concept of LEs is related with the exponential stability of a dynamic system. The exponentially decaying nature of the power system oscillations subsequent to a stable contingency highlights that the LEs is a theoritically sound approach to study the transient stability problem in power system.

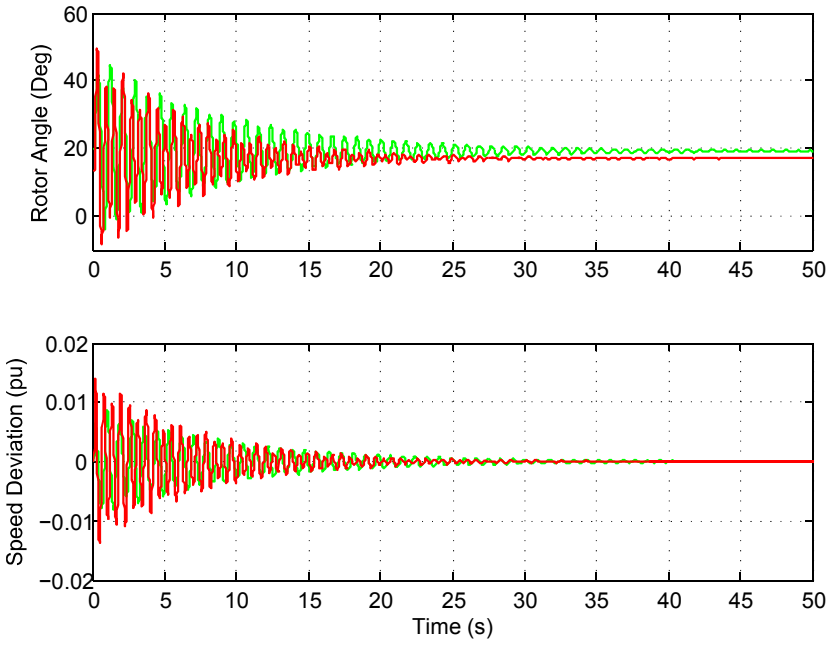

Figure 3.5: Evolution of state trajectories; red - generator 2 and green - generator 3

System stability region and the critical clearing time

The maximum allowable fault clearing time of a contingency so that the post-fault system remains stable is known as the *critical clearing time (CCT)*. In order to determine the CCT of the given contingency, the fault clearing time was changed in steps of the time step used to peform the numerical integration, that is, 1/120 s in this case. The LEs of the post-fault equilibrium point were calculated starting from the state values at the fault clearing time. Hence, the change in the fault clearing time disturbs the initial conditions of the LE estimation. Fig. 3.6 shows the variation of the LLE with the fault clearing time.

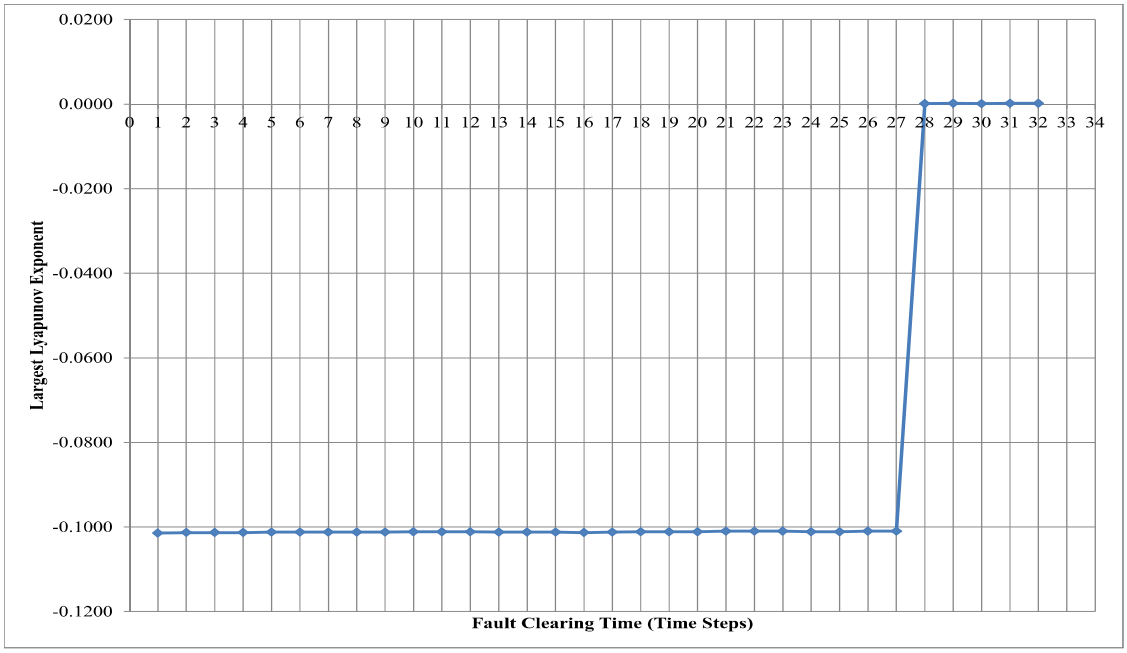

Figure 3.6: Change in LLE with fault clearing time

The LLEs starting from state values corresponding to different fault clearing times have converged to the same negative value irrespective of the fault clearing time up to a critical value ($27\Delta t, \Delta t = 1/120s$). The LLE is a small positive number (0.001 in this case) for fault clearing times beyond this critical value. Visual inspection of the time domain trajectories corresponding to fault clearing times beyond the critical value shows diverging trajectories. Therefore, this critical time is the maximum possible fault clearing time or the CCT of the contingency.

The change in fault clearing time does not change the equilibrium point of the post-fault system. Therefore, the CCT is the boundary of the stability region of the equilibrium point. The importance of this analysis is that as long as the fault clearing time is less than the CCT, the LLEs converge to the same negative value. Therefore, the magnitude of the LLE cannot be used as a stability index to determine

the closeness of the current operating point to instability.

Effect of the post-fault system topology on LEs

A power system can subject to different faults anywhere in the system. Even the same fault can occur at different locations leading to outages of different elements from the network. Hence, the post-fault network topology may change subsequent to different fault scenarios. In order to investigate the change in the LEs with the post-fault system topology, first, a series of solid three phase bus faults were applied at different bus bars of the test system and cleared after 100 ms without disconnecting any lines from the network. Since the network topology doesn't change during these cases, the steady state stable attractors of the post-fault systems remain the same. However, depending on the location of the bus fault, the system dynamic equations during the fault situation change which in turn give different initial conditions for the post-fault system dynamic equations even for the same fault clearing time. The calculated LLE values for this situation are given in Table 3.2.

The estimated LLE values are all negative and identical up to the 5^{th} decimal place irrespective of the fault location. The negative LLE indicates the stability of the post-fault systems equilibrium point. The occurrence of the equal LLE values under all these cases is to be expected since the post-fault system equilibrium point remains unchaged due to no topological changes in the system.

Table 3.2: Variation of LLE with faults at different locations without system topological changes

Scenario No	Faulted Bus	LLE
1	4	−0.108456
2	5	−0.108456
3	6	−0.108455
4	7	−0.108457
5	8	−0.108456
6	9	−0.108456

Next, a series of fault scenarios were considered by applying three-phase solid faults in transmission lines near the bus bars (e.g., bus bar 4, 7, 9) in Fig. 3.3 followed by disconnecting the respective transmission lines (e.g., line 4-5, line 4-6, line 7-5, etc) from the network after 100 ms. The estimated LLE values during these scenarios are shown in Table 3.3.

Table 3.3: Variation of LLE with system topology

Scenario No	Faulted Bus	Line Disconnected	LLE
1	4	Line 4–5	−0.10736
2	4	Line 4–6	−0.11610
3	7	Line 7–5	−0.10800
4	7	Line 7–8	−0.10094
5	9	Line 9–6	−0.10000
6	9	Line 9–8	−0.10138

For the considered clearing time, all the LLE values shown in Table 3.3 are negative confirming that the trajectories have converged to the exponentially stable equilibrium

point. Depending on the disconnecting line, the network power flow changes which in turn results in different stable attractors for the post-fault system trajectories. Each different, negative LLE value uniquely identifies these different stable attractors of different post-fault system topologies.

3.5 Faster identification of transient stability using the concept of LEs

A systematic stability analysis using the concept of LEs for large-disturbance rotor angle stability assessment was discussed in detail in Section 3.4.2. It was highlighted that the LEs need long computation time for the convergence mainly due to the presence of exponentially damped sinusoidal oscillations in a stable post-fault power system. For example, the LEs were calculated over a data window in length longer than 1000 s to make sure the convergence upto the 3^{rd} decmal place in all above scenarios. Calculation of the LEs over a long time window for rotor angle stability assessment is not recommended due to following reasons:

1. A proposed application of this thesis is the rotor angle security assessment in an online DSA program. Fast assessment of the stability of the current operating point for multiple contingencies is critical since the operating conditions keep on changing.

2. The unstable generators are tripped by the power system protection during the actual operation. Hence, realistically, the trajectories from unstable generators won't be there for a long time period.

Therefore, this thesis proposes a modified algorithm as shown in Fig. 3.7 to derive the stability conclusion of the post-fault power system. This modified algorithm

calculates the finite-time LEs.

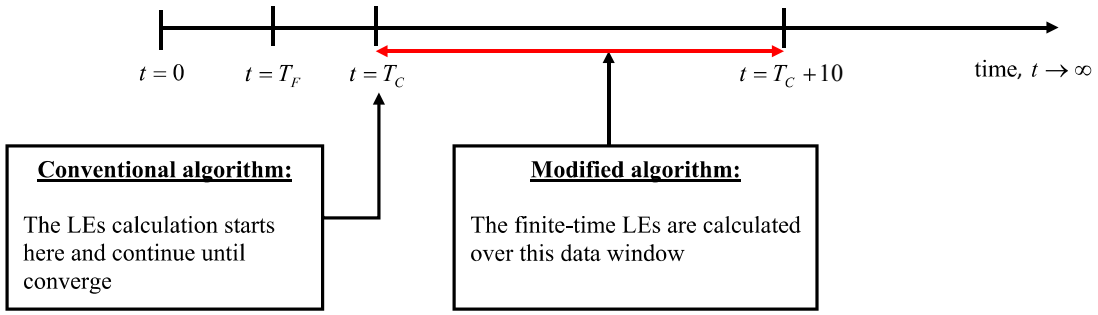

Figure 3.7: Proposed transient stability prediction algorithm using finite-time LEs: T_F-time at which the fault occurs, T_C-time at which the fault clears

The finite-time LEs have been discussed in literature for stability assessment of nonlinear dynamic systems [55], [56] and they are related with the time-average local divergence rate. Thus, mathematically, the modified algorithm shown in Fig. 3.7 derives the stability conclusion by calculating a function, $D(x,T), T = k\delta T$ given in Eq. (3.15).

$$\Lambda_{FT} = \frac{1}{k\Delta T}\sum_{j=1}^{k} \ln \|\Delta u^{(j)}\| \tag{3.15}$$

where, ΔT s the integration time step and Δu is the orthogonalized vector.

For, $k = 1$, $D(x, \Delta T)$ is the local divergence rate over the first time step and for $k \to \infty, D(x, \infty)$ is the true LE. Thus, calculating $D(x,T)$ for $1 \leq k < \infty$ provides the information on the local predictability of the finite-time LEs.

In order to check the local predictability of the transient stability of the power system by the finite-time LEs, consider the contingency of clearing a solid three-phase bus fault applied in the transmission line 4-5 very close to the bus bar 4 after a known time period of the 3-generator 9 bus system shown in Fig. 3.3. In this case, two fault

clearing times, 100 ms and 250 ms, were considered. The post-fault power system was stable at 100 ms clearing time and was unstable at 250 ms clearing time according to the time domain simulated trajectories. Fig. 3.8 and Fig. 3.9 show the time domain simulated trajectories and the time variation of the local divergence rate of the LLE under the two scenarios. In this thesis, the finite-time LE associated with the LLE is referred to as the *largest average exponential rate*.

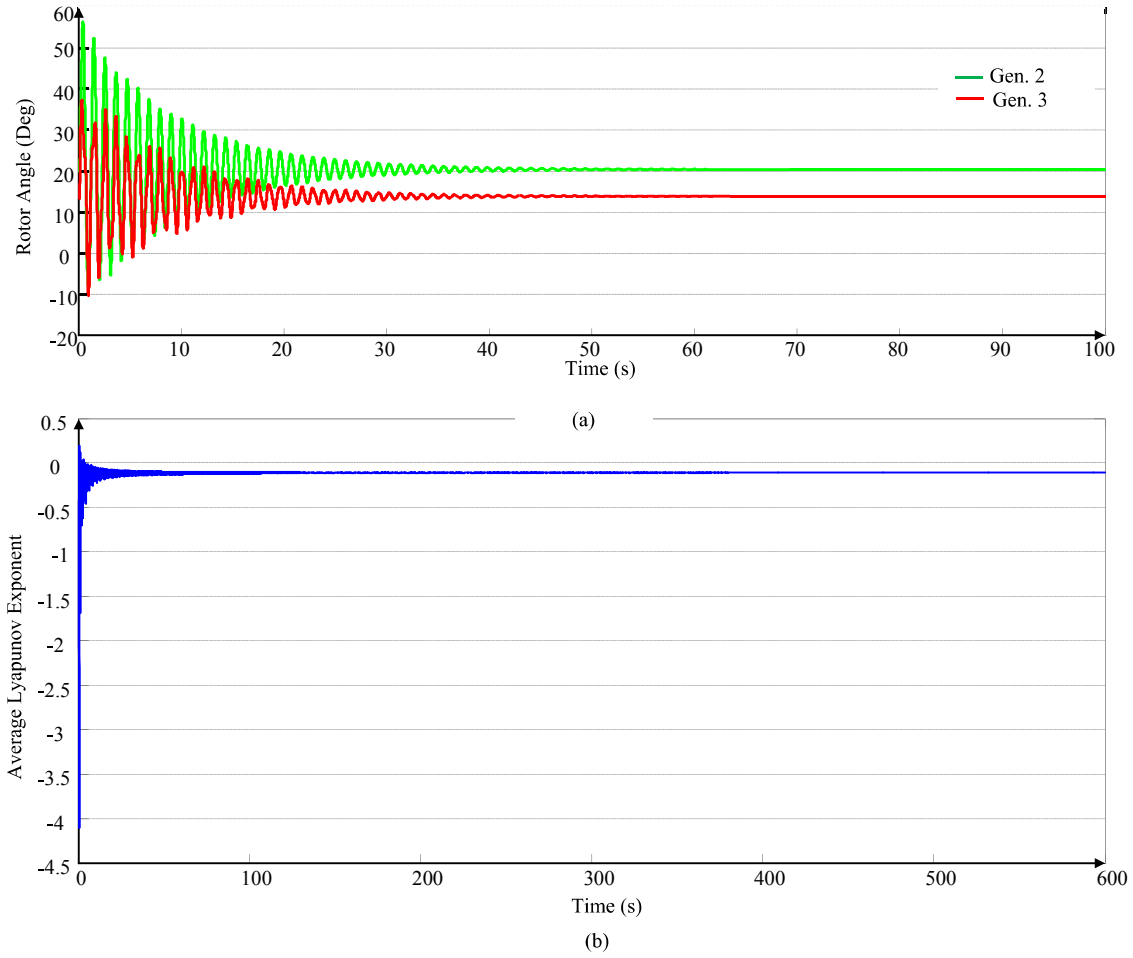

Figure 3.8: Finite-time LEs:stable scenario, (a) time domain trajectories of the rotor angle, (b) evolution of the largest average exponential rate

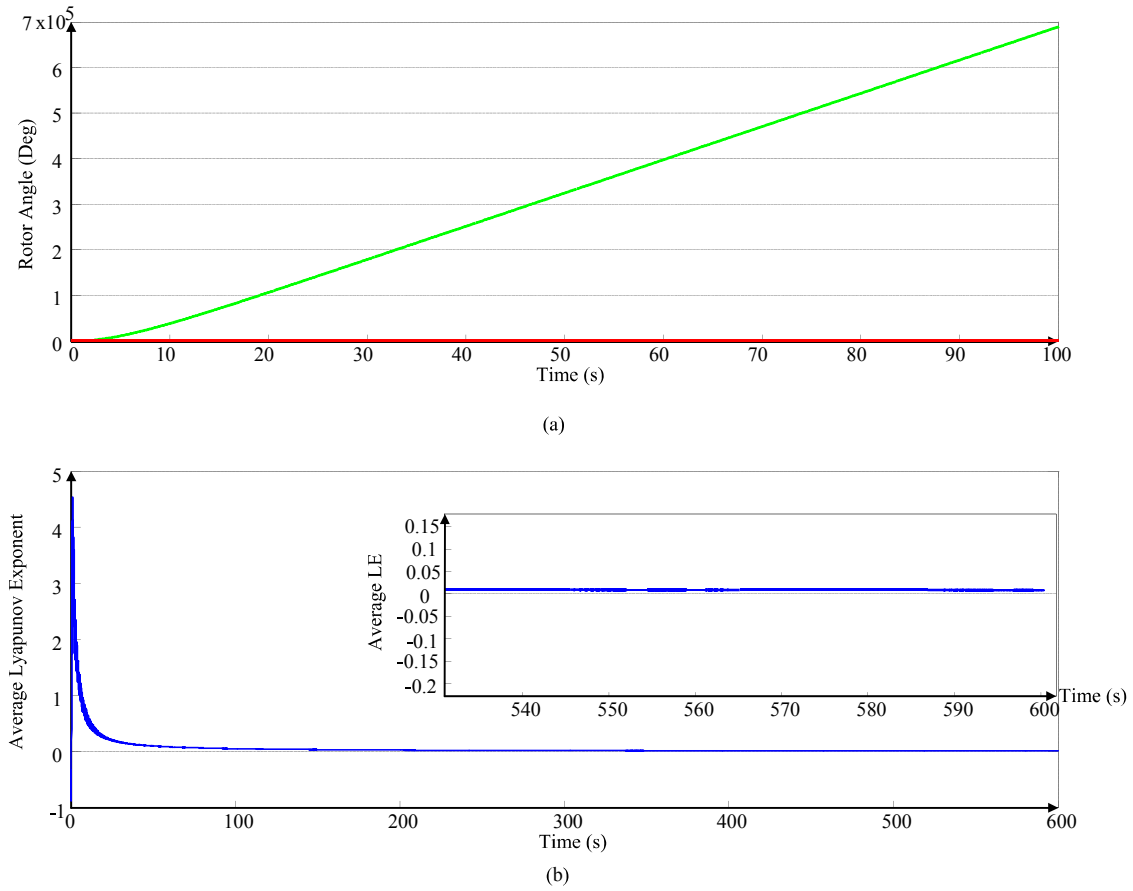

Figure 3.9: Finite-time LEs:unstable scenario, (a) time domain trajectories of the rotor angle, (b) evolution of the largest average exponential rate

It is seen from Fig. 3.8 and Fig. 3.9 that the largest average exponential rate remains negative after some time when the post-fault power system is rotor angle stable and is positive when the post-fault power system is rotor angle unstable. Thus, the same stability conclusion derived by the true LEs can be accurately derived by the finite-time LEs calculated over a shorter data window. The reason for this local predictability by the finite-time LEs is that the time domain simulated trajectories of the state variables exponentially decay under stable scenarios and drastically increase under first-swing unstable scenarios. Further, the LEs are associated with the expo-

nential decaying rates of the trajectoris. Therefore, the final sign of the true LEs can be accurately predicted by the finite-time LEs while reducing the computational burden.

The performance of the proposed algorithm was tested with the 3-generator 9 bus system under three fault scenarios with two fault clearing times, 100 ms and 250 ms respectively. The three fault scenarios were: 1) fault on the line 4-5 closer to the bus 4 cleared by isolating the line 4-5, 2) fault on the line 7-5 closer to the bus 7 cleared by isolating the line 7-5, and 3) fault on the line 9-8 closer to the bus 9 cleared by isolating the line 9-8. Visual inspection of the time domain trajectories showed converging trajectories at 100 ms and diverging trajectories at 250 ms fault clearing times for the three scenarios. Accordingly, the expected sign of the largest average exponential rates is negative for the first three cases and positive for the latter three cases. The stability analysis results of these six contingencies using the modified algorithm is presented in Table 3.4.

Table 3.4: Largest average exponential rates of 3-generator 9 bus system

Case No	Fault Duration (ms)	Largest average exponential rates				
		T_C - $(T_C + 5.0)s$	T_C- $(T_C + 10)s$	T_C- $(T_C + 20)s$	T_C- $(T_C + 30)s$	T_C - $(T_C + 40)s$
1	100	-0.0253	-0.1452	-0.0806	-0.0876	-0.0963
2	100	-0.0858	-0.0578	-0.0384	-0.0499	-0.0603
3	100	-0.1155	-0.2447	-0.1166	-0.1776	-0.1094
4	250	1.3049	0.6227	0.243	0.1632	0.1188
5	250	0.9335	0.4754	0.2588	0.1717	0.129
6	250	0.2277	0.1396	0.0794	0.0523	0.0343

Table 3.4 shows that the stability of the equilibrium points has been correctly determined by the sign of the largest average exponential rate calculated over a short time window. Based on the observations, a 5 s long data window starting from the initial conditions at the time of clearing the fault was sufficient to derive the stability conclusion of the power system. The benefits of the proposed algorithm for accurately predicting the transient stability is further demonstrated with large power systems in Chapter 5.

The applications of the finite-time LEs into power systems stability analysis have been reported in recent literature [57], [58], [59]. The work presented in this thesis is different from the work presented in these references in the following aspects.

- This thesis uses the mathematical model of the post-fault power system to calculate the finite-time LEs. In [57],[59], and [60], the finite-time LEs have been estimated using time series data.

- Chapter 5 of the thesis shows that the largest average exponential rate determined using the post-fault system trajectories can be used as a security measure to conclude the transient rotor angle stability. Thus, the finite-time LEs are used in an online dynamic security assessment algorithm. However, the references [57],[59], and [60] show that the finite-time LEs can be used in real-time stability monitoring applications using the synchronized data available from phasor measurement units.

3.6 Chapter summary

The main contribution of this chapter is that it has presented a novel algorithm based on the concept of LEs to accurately predict the transient stability status of a

power system subsequent to a contingency. These contributions were published in References [61] and [62] during this PhD study.

- At the beginning, the concept of LEs and the procedure for determining a spectrum of LEs from a mathematical model were presented. Subsequently, a detailed stability analysis was presented using a test power system model. The major findings of this analysis were:
  - The post-fault system equilibrium point can be completely characterized by a spectrum of all negative LEs if the power system is stable subsequent to the contingency. Otherwise, the LLE becomes a small positive number.
  - The LLE converges to the same negative value, if the fault clearing time is less than the CCT, beyond which the system becomes unstable. Thus, the power system stability regions can be determined using this invariance property of LEs from the initial conditions within the same stability region.
  - The computational burden of the exponents for convergence is significant.
- The above observations were the impetus behind the modified algorithm developed in this chapter. The modified algorithm accurately derived the stability conclusion starting from the state values at the fault clearing time and limiting the computation for a short time interval.

Being a nonlinear stability analysis technique, the concept of LEs become an ideal technique to study the transient stability of the power system since the nonlinear behavior needs to be treated for such an analysis. The developed algorithm in Section 3.5 will be used in Chapter 5 to classify the stable and unstable contingencies as the first process in the proposed rotor angle security assessment tool.

Chapter 4

Extracting Dominant Oscillatory Modes from Transient Stable Power Swings using an Improved Prony Algorithm

4.1 Introduction

If the post-fault power system is stable subsequent to a contingency as discussed in Chapter 3, the time responses of the states and other measured power system variables show exponentially damped oscillations. This situation is referred to as a ring-down condition in the power system. The Lyapunov exponents measure the average decaying rate of the trajectories in the state space. However, they do not provide the damping ratios of the dominant oscillations present in the ring-down oscillations. The damping ratio of an electromechanical oscillation as defined in Eq. (2.21) in Chapter 2 is a measure of the degree of small-signal rotor angle stability of

the equilibrium point of the post-fault power system. The main goal of this chapter is to extract the dominant oscillatory modes present in the ring-down oscillations and to determine their frequencies and damping ratios using an improved Prony algorithm.

The Prony algorithm is a linear parametric technique which can directly estimate the frequency, damping, strength and phase angle of modes present in an input signal. Theory of the Prony algorithm and its applications into power systems are well documented in the literature. A few examples of its applications are; 1) analyzing responses of noise-free linear time invariant systems [37], 2) studying outputs of transient stability programs [37], 3) constructing the standard form impulse response models to be used in extended analysis and in control system design [63] , and 4) offline analyzing of field measured data [64].

The proposed rotor angle security assessment tool in this thesis first uses the algorithm developed in Chapter 3 to determine the transient stability of the power system. Such stable cases are then processed using an improved Prony algorithm as explained in this chapter. The purpose is to extract the dominant oscillatory modes present in the ring-down oscillations and to determine their damping. Hence, the small-signal rotor angle stability around the equilibrium point of the post-fault power system can be determined without calculating the eigenvalues. The dominant modes may cause severe threats to system security due to poorer damping.

The objectives of this chapter are; i) present the theory of the Prony algorithm and the solution procedure, ii) highlight the limitations of the conventional algorithm and the proposed techniques in literature to overcome such problems, iii) develop an improved Prony algorithm to be used in the proposed rotor angle security assessment tool, and iv) present the performance of the proposed algorithm using a small test power system.

4.2 Theory of Prony Algorithm

Consider a linear, time invariant dynamic system given by $\dot{\mathbf{x}}_{p\times 1} = A_{p\times p}\mathbf{x}_{p\times 1} + B_{p\times p}\mathbf{u}_{p\times 1}$, where, $\mathbf{x}$ is the state vector, $\mathbf{u}$ is the input vector and p is the order of the linearized system. The system is initially operating at a state x_0 at time, $t = t_0$. If the input to the system is removed and if there are no further inputs, the system responds according to a set of differential equations given by $\dot{\mathbf{x}}_{p\times 1} = A_{p\times p}\mathbf{x}_{p\times 1}$. Let, $\mathbf{x} = \Phi\mathbf{Z}$, where $\mathbf{Z}$ is a new state vector and the columns of Φ are the right eigenvectors of A. Then, the following mathematical manipulations derive the solutions of the original set of differential equations.

$$\Phi\dot{\mathbf{Z}} = A\Phi\mathbf{Z} \tag{4.1}$$

$$\dot{\mathbf{Z}} = \Lambda\mathbf{Z} \tag{4.2}$$

where, $\Lambda = \Phi^{-1}A\Phi$ is a diagonal matrix containing all the eigenvalues of A. Thus, each element in the new state vector $\mathbf{Z}$ are now decoupled from the rest of the elements.

$$\dot{Z}_i(t) = \lambda_i Z_i(t), \quad i = 1, 2, \cdots, p \tag{4.3}$$

$$Z_i(t) = Z_i(0)e^{\lambda_i t} \tag{4.4}$$

$$x(t) = [\phi_1 \quad \phi_2 \quad \cdots \quad \phi_p] \begin{bmatrix} Z_1(t) \\ Z_2(t) \\ \vdots \\ Z_p(t) \end{bmatrix} \tag{4.5}$$

$$x(t) = \sum_{i=1}^{p} \phi_i Z_i(0) e^{\lambda_i t} \tag{4.6}$$

$$x(t) = \sum_{i=1}^{p} \phi_i (\psi_i x_0) e^{\lambda_i t} \tag{4.7}$$

$$= \sum_{i=1}^{p} R_i x_0 e^{\lambda_i t} \tag{4.8}$$

where, ϕ_i and ψ_i are the right eigenvector and the left eigenvector of the i^{th} eigenvalue respectively. x_0 is the initial state vector.

Assuming a single output of this dynamic system, mathematically, it can be expressed as a linear combination of the p eigenvalues as given in Eq. (4.9).

$$Y(t) = Cx(t) \tag{4.9}$$

$$= \sum_{i=1}^{p} B_i e^{\lambda_i t} \tag{4.10}$$

$$= \sum_{i=1}^{p} A_i e^{\sigma_i t} \cos(2\pi f_i t + \alpha_i) \tag{4.11}$$

where, B_i are referred to as signal residues, $\lambda_i = -\sigma_i \pm j2\pi f_i$, A_i and α_i are the amplitude and the phase angle of the i^{th} mode respectively.

Prony analysis fits a measured time domain signal using a sum of sinusoidals as given in Eq. (4.11) and estimates the parameters $\sigma, f, A, \& \ \alpha$. Consider N samples

of the measured signal shown in Fig. 4.1, where Y_k is the value of the signal at k^{th} sampling time, $t_k = k\Delta t$, Δt is the sampling interval and $k = 0, 1, \cdots, N-1$. Thus, Eq. (4.10) can be written to estimate Y_k as given in Eq. (4.12) and Eq. (4.13).

$$Y(t_k) = \sum_{i=1}^{p} B_i e^{\lambda_i t_k} = \sum_{i=1}^{p} B_i e^{\lambda_i k\Delta t} = \sum_{i=1}^{p} B_i z_i^k \tag{4.12}$$

$$z_i = e^{\lambda_i \Delta t} \tag{4.13}$$

z_i in Eq. (4.13) are the discrete domain eigenvalues corresponding to λ_i. Thus, z_i are the roots of an p^{th} order polynomial as given in Eq. (4.14).

$$z^p - a_1 z^{p-1} - a_2 z^{p-2} - \cdots - a_p = 0 \tag{4.14}$$

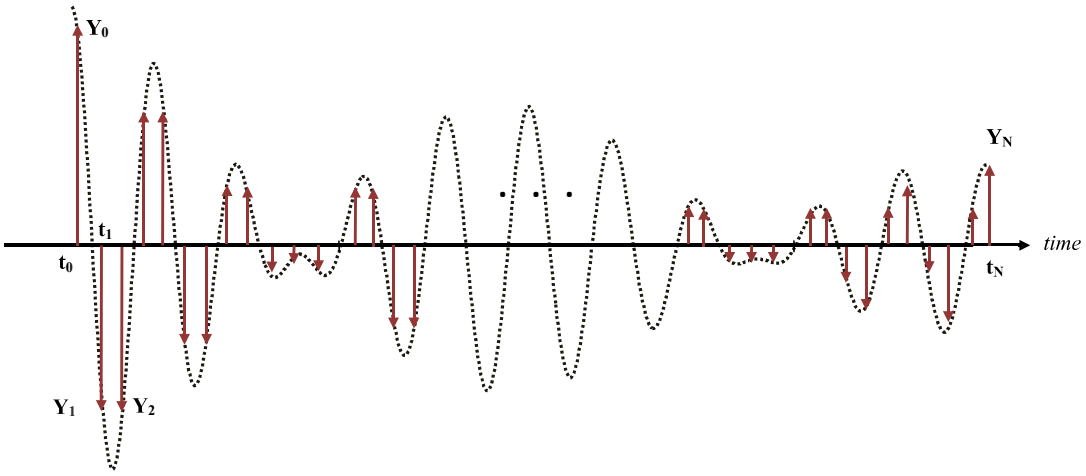

Figure 4.1: Discrete time domain measured output signal

The mathematical manipulations mentioned hereafter establishes the solution procedure of the Prony algorithm to determine the mode parameters.

- Estimate Y_k at each sampling instant. This will produce an overdetermined set

of equations given in Eq. (4.15).

$$\begin{bmatrix} Y(0) \\ Y(1) \\ \vdots \\ Y(N-1) \end{bmatrix} = \begin{bmatrix} z_1^0 & z_2^0 & \cdots & z_p^0 \\ z_1^1 & z_2^1 & \cdots & z_p^1 \\ \vdots & \vdots & \ddots & \vdots \\ z_1^{N-1} & z_2^{N-1} & \cdots & z_p^{N-1} \end{bmatrix} \begin{bmatrix} B_1 \\ B_2 \\ \vdots \\ B_p \end{bmatrix} \tag{4.15}$$

$$Y = ZB \tag{4.16}$$

- Construct the vector $\bar{A}_{1\times N} = [-a_p - a_{p-1} \cdots - a_1 \quad 1 \quad 0 \quad 0 \quad \cdots \quad 0]$.

$$\bar{A}Y = \bar{A}ZB \tag{4.17}$$

$$\bar{A}Y = [-a_p \cdots - a_1 \quad 1 \quad \cdots \quad 0][Y(0) \quad Y(1) \cdots \quad Y(N-1)]^T \tag{4.18}$$

$$= Y(p) - a_pY(0) - a_{p-1}Y(1) - \cdots - a_1Y(p-1) \tag{4.19}$$

$$\bar{A}ZB = \begin{bmatrix} z_1^p - a_1z_1^{p-1} - a_2z_1^{p-2} - \cdots - a_p \\ z_2^p - a_1z_2^{p-1} - a_2z_2^{p-2} - \cdots - a_p \\ \vdots \\ z_p^p - a_1z_p^{p-1} - a_2z_p^{p-2} - \cdots - a_p \end{bmatrix}^T \begin{bmatrix} B_1 \\ B_2 \\ \vdots \\ B_p \end{bmatrix} \tag{4.20}$$

$$\bar{A}ZB = 0, \quad \textit{based on Eq. (4.14)} \tag{4.21}$$

- Using Eq. (4.17), Eq. (4.19) and Eq. (4.21), $\bar{A}Y = \bar{A}ZB = 0$

$$Y(p) = a_1Y(p-1) + a_2Y(p-2) + \cdots + a_pY(0) \tag{4.22}$$

The linear prediction model given in Eq. (4.22), which is the core of the Prony algorithm states that the value of the measured signal at the $(p+1)^{th}$ sample can be written as a linear combination of the prevoius p samples. The above re-

lationship can be used to derive an overdetermined set of equations to determine the unknown coefficients of the linear prediction model.

$$\begin{bmatrix} Y(p) \\ Y(p+1) \\ \vdots \\ Y(N-2) \\ Y(N-1) \end{bmatrix} = \begin{bmatrix} Y(p-1) & Y(p-2) & \cdots & Y(0) \\ Y(p) & Y(p-1) & \cdots & Y(1) \\ \vdots & \vdots & \ddots & \vdots \\ Y(N-3) & Y(N-4) & \cdots & Y(N-p-2) \\ Y(N-2) & Y(N-3) & \cdots & Y(N-p-1) \end{bmatrix} \begin{bmatrix} a_1 \\ a_2 \\ \vdots \\ a_{p-1} \\ a_p \end{bmatrix} \tag{4.23}$$

The procedure of determining the mode parameters using the Prony algorithm can be summarized as follows:

1. Construct a discrete linear prediction model that best fits the recorded signal as given in Eq. (4.22).

2. Construct Eq. (4.23) and determine the least square solution for the coefficients of the linear prediction model.

3. Determine the roots of the characteristic equation given in Eq. (4.14). Then, find the corresponding eigenvalues using Eq. (4.13).

4. Solve Eq. (4.15) using the discrete domain roots of the characteristic polynomial to determine the amplitude and the phase angle of each mode.

4.3 Improved Prony algorithm for extracting dominant oscillatory modes

This section presents an improved Prony algorithm which overcomes the limitations of the conventional Prony algorithm.

4.3.1 Limitations of the Prony algorithm

Even though the Prony algorithm can determine the frequency, damping, strength and the phase angle of modes present in the ring-down oscillations, its performance depends on the data window length, the sampling time used and the order of the Prony model. Reference [65] theoretically proves that both small and large sampling steps lead to errors in damping estimations, thereby, proposing an adaptive sampling scheme. It is recommended in [66], to capture at least four cycles of the smallest frequency waveform as the data window length. In the proposed rotor angle security assessment tool, more cycles are available at a sampling rate of $\frac{1}{\Delta T}\ samples/s$, where ΔT is the time step used in the time domain simulation. Further, more cycles provide a clearer picture of the system dynamics. Thus, the user can specify the data window length and the sampling time. The recommended settings in this thesis are given in Section 4.3.5.

Let the data window length and the sampling rate have been selected in the Prony algorithm. The issue then is to set the order of the Prony model since the roots of the linear prediction model are associated with the system dynamics. In order to suppress the effect of noise and the signal offset, it is the usual practice to over-fit the input signal. For example, the order of the Prony model p is selected as $p \leq \frac{N}{3}$, where N is the total number of samples in the data window [67]. Therefore, fictitious modes are

artificially introduced to the calculation in addition to the true modes present in the input signal. These fictitious modes do not reflect the system dynamics and some of them may have poorer damping than the true modes of the system. Therefore, it is important to extract the true modes from the fictitious modes. Different approaches have been proposed in the literature to address the said issue in the Prony analysis.

The energy of an oscillatory mode (E_i) can be calculated as $E_i = \sum_{k=0}^{N-1} |x_i(k)|^2$ over a data window having N samples. It can be assumed that the modes carrying significant amount of energies are the dominant modes of the input signal [67]. Therefore, the dominant modes can be extracted if the energy of the mode is above a threshold value. This threshold setting is difficult since 1) the total energy of the input signal does not equal the sum of the energies of the individual modes [67], and 2) when the input signal has a dc component, it subsequently carries a significant amount of energy. Another effort on this regard is to process multiple inputs simultaneously as proposed in [68] and [69]. This method is based on the assumption that an oscillatory mode can appear in different power system variables once the power system is disturbed, hence the purpose is to determine a one set of mode estimates from multiple inputs. This method produces a large set of overdetermined equations in Eq. (4.23) to determine the mode parameters, which can still produce fictitious modes. The model reduction algorithm based on Akaike Information Criterion [70] and the minimal realization method based on the singular value decomposition algorithm [71] try to find the reduced order model for the Prony input signal. Eventually, performance of each method is based on the closeness of the fitting of the reduced order model to the actual input to the algorithm. The recent publication [67] proposes applying a stepwise regression method to sort the dominant modes. The stepwise regression is an iterative procedure that adds and removes terms from the linear model

based on their statistical significance in a regression. The authors claim that this method works well under low signal-to-noise ratio conditions as well. However, the damping ratio estimations of the Prony algorithm are sensitive to the presence of noise in the input signal. Further, the inputs to the Prony algorithm in the proposed rotor angle security assessment tool are noise free signals.

This chapter presents a simple technique to modify the Prony algorithm to extract the dominant modes in the ringdown oscillations. The novelty of the proposed algorithm is based on the observation that the dominant modes, which are characteristics of the power system, consistently appear in a measured response irrespective of the order of the Prony model. Such modes can then be extracted using a sorting method. Thus, the proposed algorithm is well suited to conclude the small-signal rotor angle stability in the rotor angle security assessment tool proposed in this thesis.

4.3.2 Rationale behind the proposed algorithm

The waveform shown in Fig. 4.1 is a synthetically generated signal at a known sampling rate. This signal consists of two oscillatory modes at 0.5 Hz and 0.6 Hz frequencies and 1.5% and 1.6% damping ratios respectively. Consider two data sets of the waveform; $\mathbf{Y}_1 = [Y_0, Y_1, Y_2, \cdots, Y_N]_{1\times N}$ and $\mathbf{Y}_2 = [Y_0, Y_2, Y_4, \cdots, Y_N]_{1\times(1+\frac{N}{2})}$, where Y_k is the value at the k^{th} sampling time. Note that the lengths of the two data sets are different. Such different length data sets of the same waveform can be selected using two approaches, 1) change the length of the data window keeping the sampling time fixed, and 2) down-sample the data keeping the data window length fixed. Coefficients of the two LP models given in Eq. (4.24) and Eq. (4.25) can be determined using the Prony analysis as explianed in Section 4.2 on these two data sets. Note that the orders of the two LP models p_1 and p_2 are different since the sizes

of the two data sets are different.

$$\mathbf{Y}_1 \rightarrow Y_1(k) = a_1 Y_1(k-1) + \cdots + a_{p_1} Y_1(k-p_1) \tag{4.24}$$

$$\mathbf{Y}_2 \rightarrow Y_2(k) = b_1 Y_2(k-1) + \cdots + b_{p_2} Y_2(k-p_2) \tag{4.25}$$

These two LP models have the characteristic equations given in Eq. (4.26) and Eq. (4.28), where the roots of the characteristic equations are the discrete domain poles of the associated linear system.

$$(1) \rightarrow z^{p_1} - a_1 z^{p_1-1} - \cdots - a_{p_1-1} z - a_{p_1} \tag{4.26}$$

$$= (z - z_{11})(z - z_{12}) \cdots (z - z_{1p_1}) \tag{4.27}$$

$$(2) \rightarrow z^{p_2} - b_1 z^{p_2-1} - \cdots - b_{p_2-1} z - b_{p_2} \tag{4.28}$$

$$= (z - z_{21})(z - z_{22}) \cdots (z - z_{2p_2}) \tag{4.29}$$

The number of roots in Eq. (4.27) and Eq. (4.29) are p_1 and p_2 respectively, where $p_1 \neq p_2$. However, the two characteristic equations Eq. (4.26) and Eq. (4.28) describe an identical linear system. Therefore, theoretically there should be common roots (4 in this case) among p_1 and p_2 number of roots. These roots describe the true dynamic behavior of the linear system and the remaining roots ($(p_1 - 4)$ in Eq. (4.27) and $(p_2 - 4)$ in Eq. (4.29)) are the fictitious roots produced by the linear fitting.

In order to illustrate the said theoretical explaination, consider the linear system shown in Fig. 4.2, which consists of three oscillatory modes with the parameters as mentioned in Table 4.1. This system was simulated in MATLAB/SIMULINK using 60 samples/s sampling rate, which adheres with the IEEE standard for synchrophasor

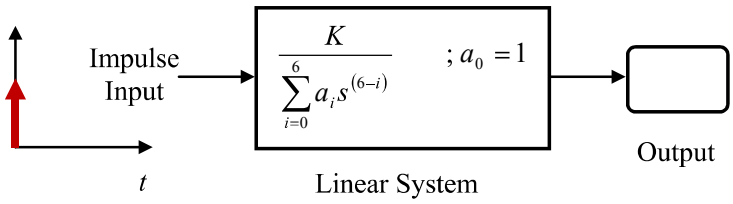

Figure 4.2: Test Linear System

Table 4.1: Test signal I parameters

Mode No	Frequency (Hz)	Real Part of Eigenvalue	Damping Ratio (%)
1	0.5	-0.0471	1.5
2	0.6	-0.0603	1.6
3	0.7	-0.5541	12.5

measurements in power systems [7]. Prony analysis was done on the output of this system using two data windows of different lengths, as shown in Fig. 4.3. The lengths of the two data windows were 7 s and 8 s respectively. Table 4.2 shows the frequencies and the real parts of the eigenvalues determined in these two cases. Only the modes with frequencies less than 5 Hz are shown.

It is observed from Table 4.2 that consistently appearing modes in the two windows are the true modes of the input signal. By selecting data windows of different lengths, the order of the linear prediction model used in the Prony analysis is changed. Table 4.2, shows that a change in the order of the polynomial eventually impacts on the fictitious modes but not on the true modes of the input signal.

The order of the linear fitting in the Prony analysis can also be changed by changing the sampling time while keeping the data window length fixed. This approach is applicable when the data are availabe at a higher sampling rate. An 8 s long data window of the above signal was analyzed using 10, 15 and 30 samples/s sampling

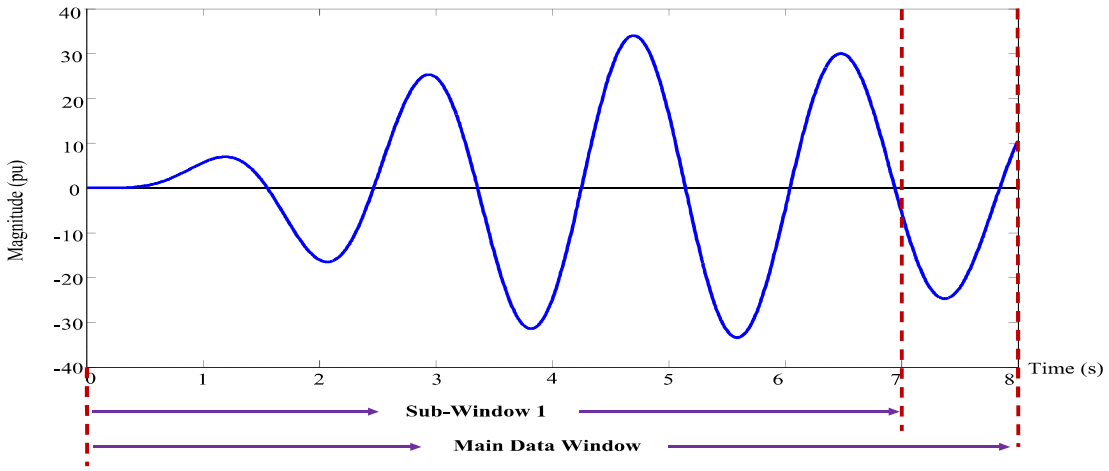

Figure 4.3: Illustration of the rationale behind the proposed algorithm

Table 4.2: Modes Appearing in Different Length Data Windows

Window 1 (0 - 7 s)		Window 2 (0 - 8 s)	
Fre. (Hz)	Real Part of EV	Fre. (Hz)	Real Part of EV
0.5	**-0.0471**	**0.5**	**-0.0471**
0.6	**-0.0603**	**0.6**	**-0.0603**
0.7	**-0.5541**	**0.7**	**-0.5541**
1.4777	-0.5420	1.3763	-0.7802
1.9417	-0.6705	1.7855	-0.9865
2.3874	-0.7636	2.1781	-1.1396
2.8260	-0.8378	2.5643	-1.2634
3.2612	-0.8999	2.9471	-1.3681
3.6942	-0.9534	3.3280	-1.4589
4.1259	-1.0004	4.8421	-1.7365
4.5567	-1.0424	3.7077	-1.5393
4.9868	-1.0804	4.0864	-1.6114
		4.4645	-1.6767

rates. This analysis showed that the true modes appear consistently. Therefore, the true modes of the input signal can be extracted using a sorting method.

4.3.3 Extracting true modes of the input signal

This study uses the comparison of the Euclidean distances in the complex plane between individual modes as the technique to extract the consistently appearing modes. Assume that p_1 and p_2 are the number of modes identified by the Prony analysis using two data windows or sampling steps as explained in Section 4.3.2. Thus, the true modes can be extracted using the following logic.

$$\begin{aligned} if, \quad \sqrt{(f_i - f_j)^2 + (\sigma_i - \sigma_j)^2} \leq \tau \quad & i = \ 1, 2, \cdots, p_1 \\ & j = \ 1, 2, \cdots, p_2 \end{aligned}$$

$$\begin{aligned} f &= \frac{f_i + f_j}{2} \\ \sigma &= \frac{\sigma_i + \sigma_j}{2} \end{aligned} \tag{4.30}$$

where, τ is the threshold assigned for the Euclidean distance in order to identify the close modes, and f & σ refer to the frequency and the real part of the eigenvalue respectively.

The threshold value to extract the true modes was determined based on number of simulations using different test systems. These are discussed in Chapter 5 and Chapter 6.

4.3.4 Improved Prony algorithm

The procedure of the improved Prony algorithm is summarized below:

1. Specify the main data window length and the sampling time step.

2. Change the order of the linear prediction model used in the Prony analysis. Two possible options for changing the order are as follows:

- Reduce the length of the data window in intervals of 1 s while keeping the specified sampling time fixed. Multiple sub-windows can be generated inside the main data window via this approach. Let us refer to this as **Shrinking Window Improved Prony algorithm**.
- Change the sampling time while keeping the data window length fixed. Let us refer to this as **Multiple Sampling Time Improved Prony algorithm**.

3. Perform the Prony analysis individually under each case. Extract only the eigenvalues with positive frequencies less than 5 Hz.
4. Extract the true modes as explained in Section 4.3.3.
5. Average the frequency and the real part of the eigenvalue of each mode calculated in different data windows or different sampling steps to get the parameters of the modes.

The complex eigenvalues always occur in conjugate pairs, where each pair corresponds to a single oscillatory mode. Further, the interest is on the low-frequency oscillatory modes. Hence, the number of combinations to be checked to extract the true modes can be greatly reduced by selecting only the positive-frequency eigenvalues with frequency less than 5 Hz.

This thesis uses the improved Prony algorithm for two applications in power systems, 1) dynamic security assessment studies, and 2) online monitoring of power system oscillations. The results presented in this thesis are based on the Shrinking Window Improved Prony algorithm.

4.3.5 Implementation

For the dynamic security assessment studies, it is recommended to set the length of the data window to be 10 - 20 s. This is acceptable since the electromechanical oscillations are typically in the range of 0.1 - 2 Hz [15], thus the 10 s long data window covers atleast one cycle of a 0.1 Hz mode. The sampling rates can be selected as 10, 12, 15, 20, 30, and 60 samples/s. These sampling rates satisfy the Nyquist criterion[1] for the intended application and are the recommended PMU reporting rates for a 60 Hz system[2] [7].

The flow chart of the Shrinking Window Improved Prony algorithm with two sub-windows inside the main data window is shown in Fig. 4.4. The order p of the Prony model is selected as $\frac{N}{3}$, where N is the total number of samples in the data window. The least-squares solution for the coefficients of the linear prediction model is determined using truncated singular value decomposition [71]. The energy ratio (ER) as defined in Eq. (4.31) is used to identify the truncation parameter. The dominant singular values can be selected when the ER value is sufficiently close to unity.

$$ER(q) = \frac{\sum_{i=1}^{q} \sigma_i^2}{\sum_{i=1}^{p} \sigma_i^2} \tag{4.31}$$

where σ_i is the i^{th} singular value of the data matrix.

In this study, the rotor angle security assessment is done using the Shrinking Window Improved Prony algorithm. Chapter 6 of this thesis investigates the applicability of the proposed improved Prony algorithm for online oscillation monitoring in power

[1]Nyquist criterion states that the sampling frequency must be greater or equal to twice the cut-off frequency in order to avoid aliasing errors

[2]the sampling rates were selected based on the IEEE standard for synchrophasor measurements in power systems since the same algorithm is used in Chapter 6 for online oscillation monitoring in power systems.

systems. The sensitivities of the algorithm for the data window length, sampling time, number of sub-windows inside the main data window of the Shrinking Wndow algorithm are presented in Chapter 6.

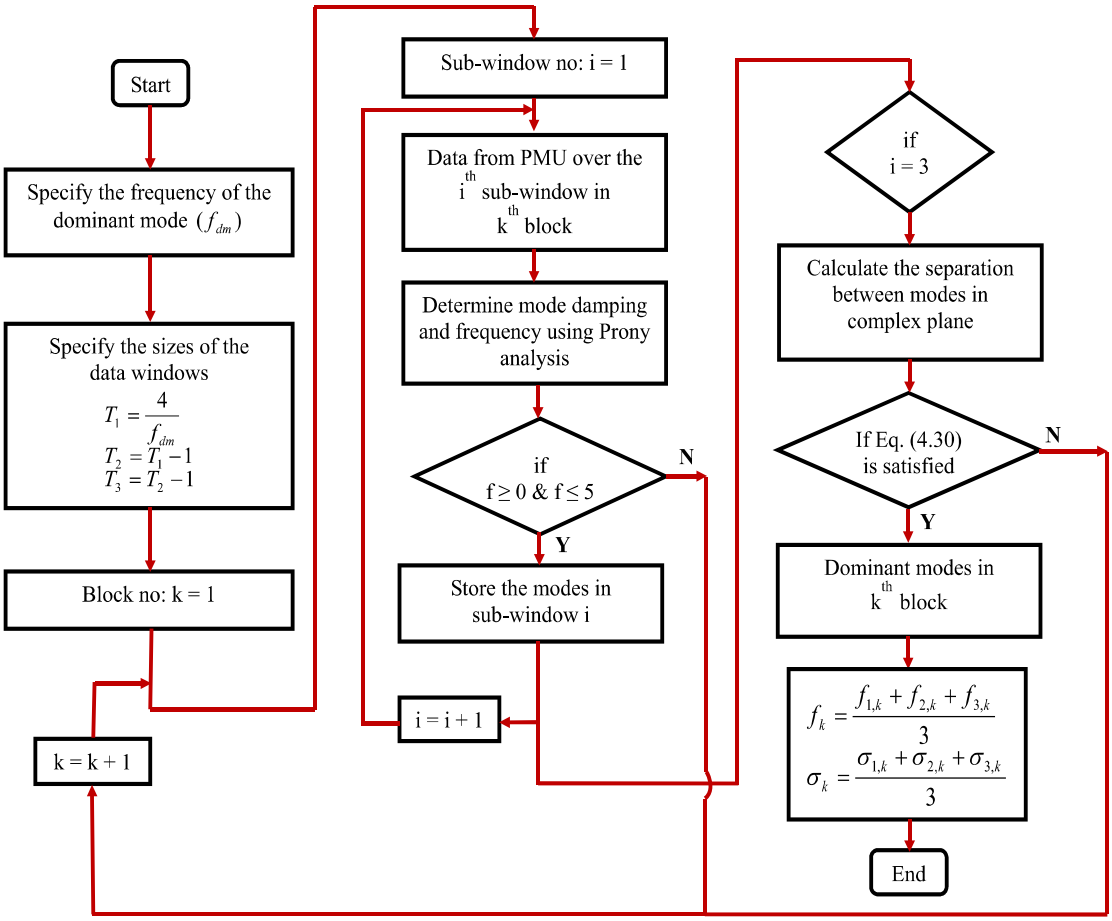

Figure 4.4: Flow chart of the Shrinking Window Improved Prony algorithm

4.4 Performance evaluation of the improved Prony algorithm

This section presents the true mode extraction capability of the Shrinking Window Improved Prony algorithm using the 3 generator 9 bus test system shown in Fig. 3.3 in Chapter 3. The modeling assumptions used were same as explianed in Section 3.4.1

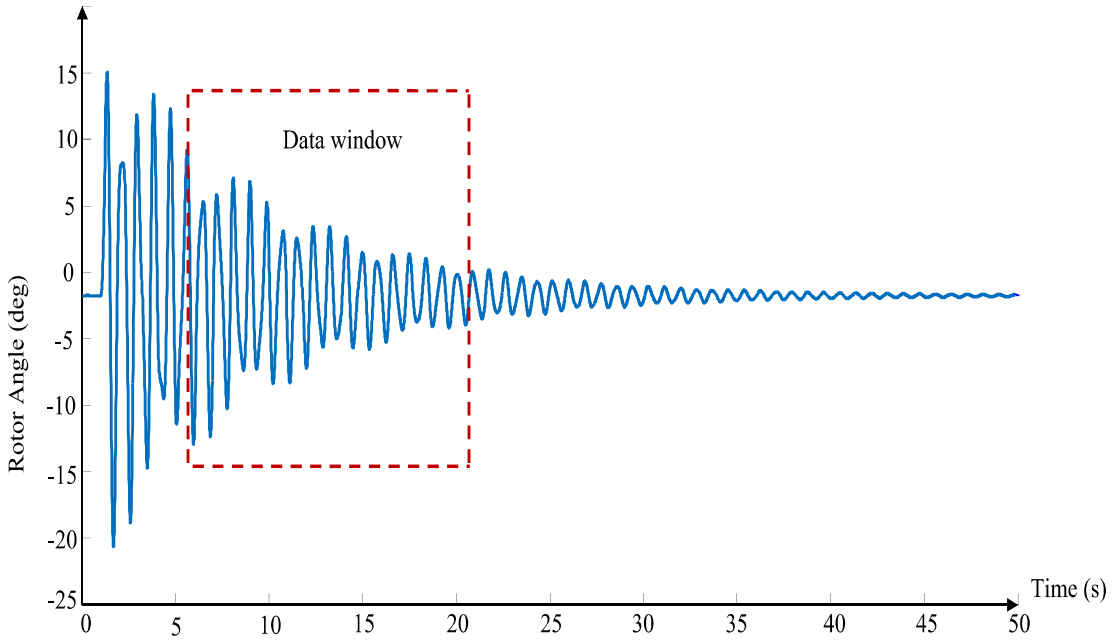

Figure 4.5: Generator 2 rotor angle subsequent to a three-phase solid fault at bus 4

in Chapter 3. The contingency considered was a solid three-phase fault very close to the bus bar 4 cleared after 100 ms without any topology change in the network. Fig. 4.5 shows the time variation of the generator 2 rotor angle subsequent to the fault scenario.

This signal was processed using the Shrinking Window Improved Prony algorithm with two sub-windows inside the main data window as explained in Section 4.3.4 to extract the dominant oscillatory modes present in the signal. The data window was selected after 5 s of clearing the fault as shown in Fig. 4.5. The power system response just after the disturbance is nonlinear, hence processing such data using the Prony algorithm gives wrong damping estimations since the Prony algorithm is a linear analysis method. This is further explained in Chapter 6. The length of the data window was set to be 15 s as explained in Section 4.3.5 and the sampling rate used was 10 samples/s. The threshold was set as 0.01 to extract the consistently

appearing modes.

The improved algorithm first applies the Prony algorithm individually on each window inside the main data window. The total number of modes identified by the Prony algorithm on sub-window 1, sub-window 2 and the main data window were 23, 26 and 26 respectively. However, the proposed algorithm extracted the modes shown in Table 4.3 as the true modes of the input signal.

Table 4.3: True modes of 3 generator 9 bus test system

Mode No	Frequency (Hz)	Damping Ratio (%)
1	0	100
2	1.1737	1.4616
3	2.1206	1.0604

Validation of the results of the improved algorithm

After identifying the true modes of the input signal as shown in Table 4.3, the next step is to confirm that the extracted modes are actually the true modes. This can be done by using an eigenvalue analysis. The state matrix of the system was determined by linearizing Eq. (3.13) given in Section 3.4.1 in Chapter 3 around the equilibrium point of the post-fault system. This state matrix has the oscillatory modes given in Table 4.4.

Table 4.4: Oscillatory modes of 3 generator 9 bus test system

Mode No	Frequency (Hz)	Damping Ratio (%)
1*	1.1736	1.47
2*	2.1223	1.06

The eigenvalue analysis at an operating point determines the oscillatory modes of the power system. The parameters of the modes in Table 4.4 are almost same as

those given in Table 4.3 except the mode 1. The mode 1 in Table 4.3 corresponds to the dc offset of the input signal to the algorithm. Therefore, the true modes extracted by the improved algorithm are the actual modes representing the dynamic behavior of the test power system. Based on this observation, it is recommended to remove the dc component before applying the improved Prony algorithm on the waveform.

4.5 Chapter summary

The main contribution of this chapter is that it has presented an improved Prony algorithm, which can extract the true dominant oscillatory modes present in the ring-down oscillations in power systems.

The damping ratios of the dominant oscillatory modes indicate the degree of small-signal rotor angle stability of the power system. The Prony algorithm can determine the frequencies and the damping ratios of the oscillatory modes. However, generation of the fictitious modes by the Prony algorithm in addition to the true modes is a major limitation of the algorithm. Therefore, the true mode extraction capability of the algorithm is important to derive valid conclusions.

The performance of the improved algorithm was tested using the 3 generator 9 bus test system. The extracted true modes by the algorithm was validated against the oscillatory modes identified using the eigenvalue analysis.

If the power system is transient stable subsequent to the contingency, the ring-down oscillations present in the system are then analyzed using the improved Prony algorithm in the proposed rotor angle security assessment tool in this thesis. Chapter 5 presents the results of the improved Prony algorithm for rotor angle security assessment in larger test power systems and Chpater 6 uses the algorithm to develop an online oscillations monitoring algorithm.

Chapter 5

A Hybrid Algorithm for Rotor Angle Security Assessment in Power Systems

5.1 Introduction

Transient rotor angle stability assessment and oscillatory rotor angle stability assessment subsequent to a contingency are integral components of dynamic security assessment (DSA) in power systems. This chapter proposes a hybrid algorithm to determine whether the post-fault power system is secure due to both transient and oscillatory rotor angle stability subsequent to a set of known contingencies. The hybrid algorithm first uses the new security measure developed based on the concept of Lyapunov exponents (LEs) presented in Chapter 3 to determine the transient stability of the post-fault power system. Next, the transient stable power swing curves are analysed using the improved Prony algorithm presented in Chapter 4 determine the oscillatory stability. The objectives of this chapter are; i) present the proposed

algorithm for rotor angle security assessment in power systems, and ii) evaluate the performance of the proposed algorithm using a 16-generator 68-bus test system and a 50-generator 470-bus test system.

5.2 Proposed algorithm for rotor angle security assessment in power systems

The hybrid algorithm proposed in this thesis to determine the security of the power system with respect to rotor angle stability is shown in Fig. 5.1. The algorithm starts using the data of the current operating point and concludes the security of the operating point after processing all the steps as shown in the figure. Then, the algorithm is reset and waits until the data of the next operating point are received. Thus, the algorithm shown in Fig. 5.1 assesses the security of the power system with respect to the rotor angle stability in finite time intervals, which is the usual practice of power utilities.

The steps of the algorithm are described below:

Current snapshot

Power system is monitored in real-time to obtain the current operating point. As explained in Chapter 1, this can be done via SCADA systems or WAMS. The real-time measurements of power systems include i) analog measurements such as bus voltage magnitudes and angles, active and reactive power flows through transmission lines and active and reactive power injections (i.e. generation or demand at buses), and ii) logic measurements such as status of switches, transformer tap positions and status of circuit breakers.

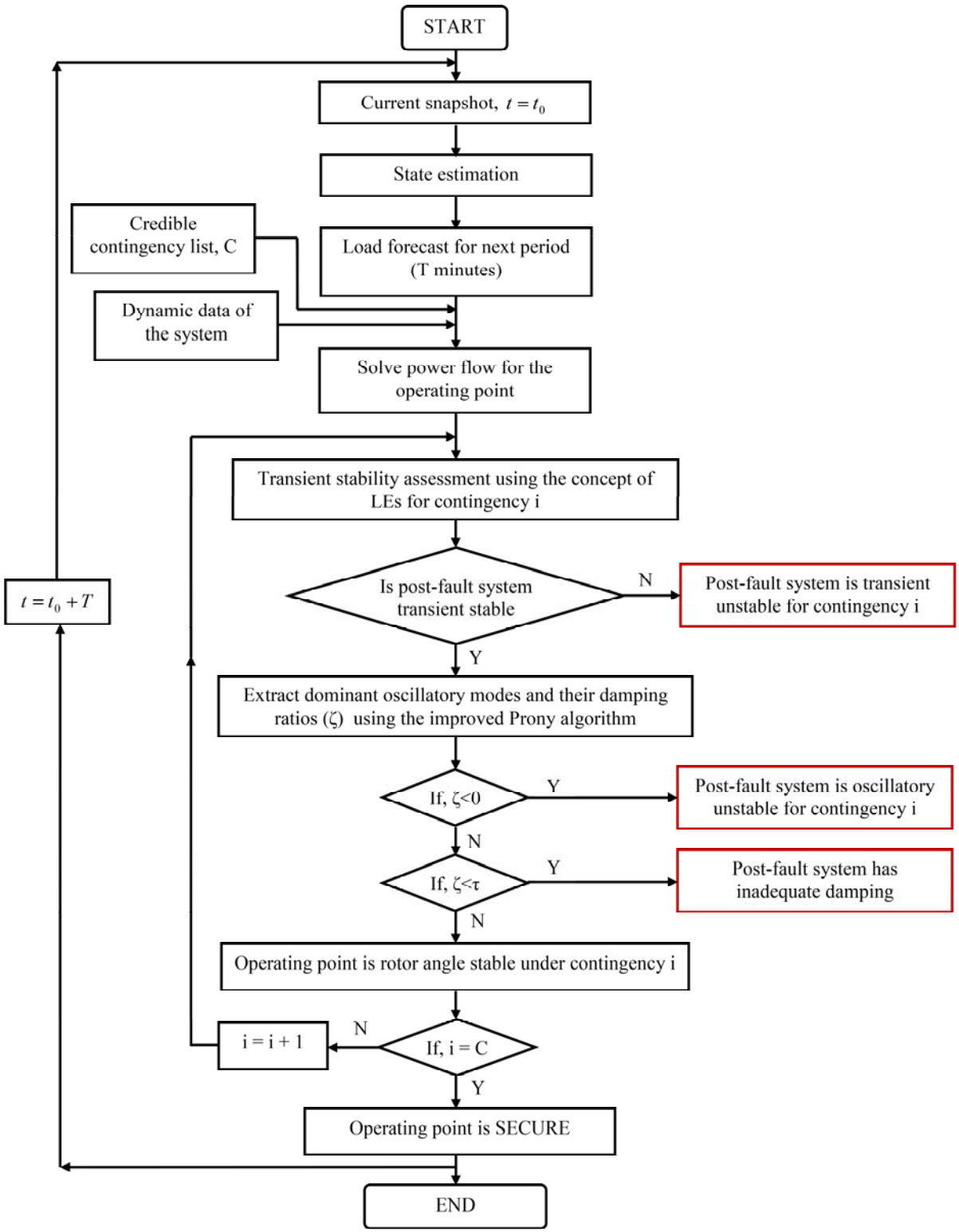

Figure 5.1: Proposed rotor angle security assessment tool: t_0 - initial time, T - computation cycle, C - no. of contingencies, ζ - percentage damping ratio, τ - threshold of damping

State estimation

These measured data are in general corrupted with errors and may contain bad data as well. Therefore, a state estimation algorithm is used to determine the best estimate of the state variables of the power system based on the measured data [10].

Load forecast

Short term load forecast in 15 minutes intervals is carried out at the control center using the current snapshot [6]. Then, the power generation and the load demand is balanced using automatic generation control (AGC). Subsequently, the security of the operating point of the power system to an anticipated list of credible contingencies where the system can experience can be investigated. The hybrid algorithm shown in Fig. 5.1 is used for this purpose.

Power flow solution

The power flow solution is the starting point of any dynamic simulation in a power system [14]. A power flow program determines the bus voltage magnitudes and angles, active and reactive power outputs of the generators, the line current flows, etc so as to satisfy the condition that the total power generation equals the system load and the losses. The operating point considered is an acceptable operating point if the power flow solution converges without violating the operational constraints (static security assessment). However, for the operating point to be secure, it must be able to survive from a list of credible contingencies (dynamic security assessment).

Transient security assessment

The proposed hybrid algorithm first uses the modified algorithm based on the concept of Lyapunov exponents (LEs) developed in Chapter 3 to assess the transient security of the power system. In this study, the time-varying Jacobean matrix required in the LEs calculation process was derived using the simplified classical generator model. Furthermore, the $N-1$ criterion, which is the general industry practice was used [4] to assess the transient security. This criterion assesses the security of a power system having N number of components subsequent to a loss of a single unit, that is, a loss of a transmission line, a generating unit, a large load, etc subsequent to a fault in the system.

Oscillatory security assessment

If it is determined that the post-fault power system is secure subsequent to a fault scenario by the LEs-based algorithm, a selected set of rotor angle trajectories are then analyzed by the improved Prony algorithm developed in Chapter 4 in order to extract the dominant oscillatory modes and to determine their frequencies and damping ratios. The damping ratio is a security measure about the oscillatory stability of the post-fault power system subsequent to the contingency.

In order to select a set of rotor angle waveforms to be processed by the improved Prony algorithm and hence to automate the security assessment process, the rotor angle trajectories were ranked using the following approach:

Fig. 5.2 shows the rotor angle separation subsequent to a contingency in a power system. Consider a T s long data window starting from the first peak of the waveform as shown in the figure. Let, δ_{t_0} and δ_{nt} are the magnitudes of the angle at the first peak and at time $t = T_1 + T$ respectively. Since the rotor angle separation is exponentially

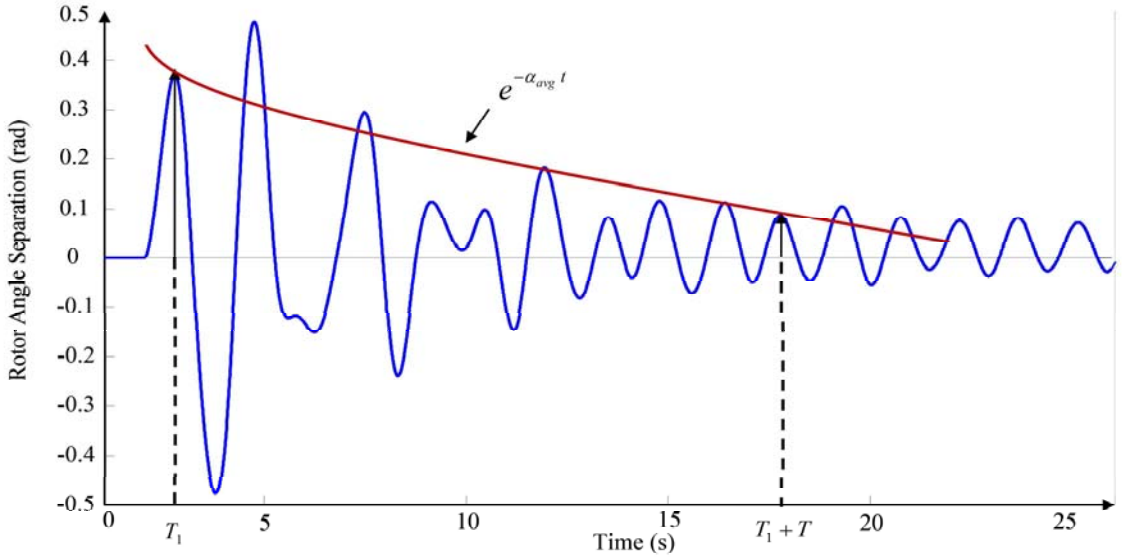

Figure 5.2: Selection of rotor angle trajectories

converging when the post-fault system is stable subsequent to a fault scenario, δ_{t_0} and δ_{nt} can be related as; $\delta_{nt} = e^{\alpha_{avg} t}\delta_{t_0}$, where, α_{avg} is the average decaying rate over the data window. α_{avg} can be calculated as shown in Eq. (5.3).

$$\alpha_{avg} = \frac{1}{t}\ln\frac{\delta_{nt}}{\delta_{t_0}} \tag{5.1}$$

$$= \frac{1}{t}\ln\frac{\delta_{t_1}}{\delta_{t_0}}\frac{\delta_{t_2}}{\delta_{t_1}}\cdots\frac{\delta_{nt}}{\delta_{(n-1)t}} \tag{5.2}$$

$$= \frac{1}{n\Delta t}\sum_{i=1}^{n}\ln\frac{\delta_{it}}{\delta_{(i-1)t}} \tag{5.3}$$

α_{avg} calculated in this way can be ranked from least negative to the most negative and the rotor angle trajectories selected via this approach were used to extract the dominant modes and to determine their parameters in the hybrid algorithm proposed in this thesis. Following specifications were used in the Shrinking Window Improved Prony algorithm.

- Sampling rate as 10 samples per second.

  The time domain simulations were done using a time step of $\frac{1}{120}$ s. Thus, the waveforms were downsampled to get a 10 samples per second sampling rate. This sampling rate is adequate to observe the electromechanical oscillations.

- 20 s long data window, where the data window was selected after a 5 s delay of clearing the fault.

  The power system response soon after the disturbance is nonlinear and the Prony algorithm is a linear parametric approach. Hence, damping estimations by the Prony algorithm deviate from those obtained using the eigenvalue analysis if a data window soon after the disturbance is used.

- Two sub-windows inside the data window generated by reducing the window lengths in steps of 1 s.

- 0.01 threshold to extract the true modes

5.3 Performance evaluation of the proposed hybrid algorithm

This section presents the results of the rotor angle security assessment using a 16-generator 68-bus tets system [72] and a 50-generator 470-bus test system [73].

5.3.1 16-generator 68-bus test system

The 16-generator 68-bus test system shown in Fig. 5.3 is a reduced order equivalent of the interconnected New England Test System (NETS) and the New York Power System (NYPS). The test system was modeled in detail as given in Appendix A for the stability analysis. The dynamic simulation was done using PSS/E software.

The time domain simulation trajectories were then read to the rotor angle security assessment tool developed in MATLAB in the PC environment for the analysis.

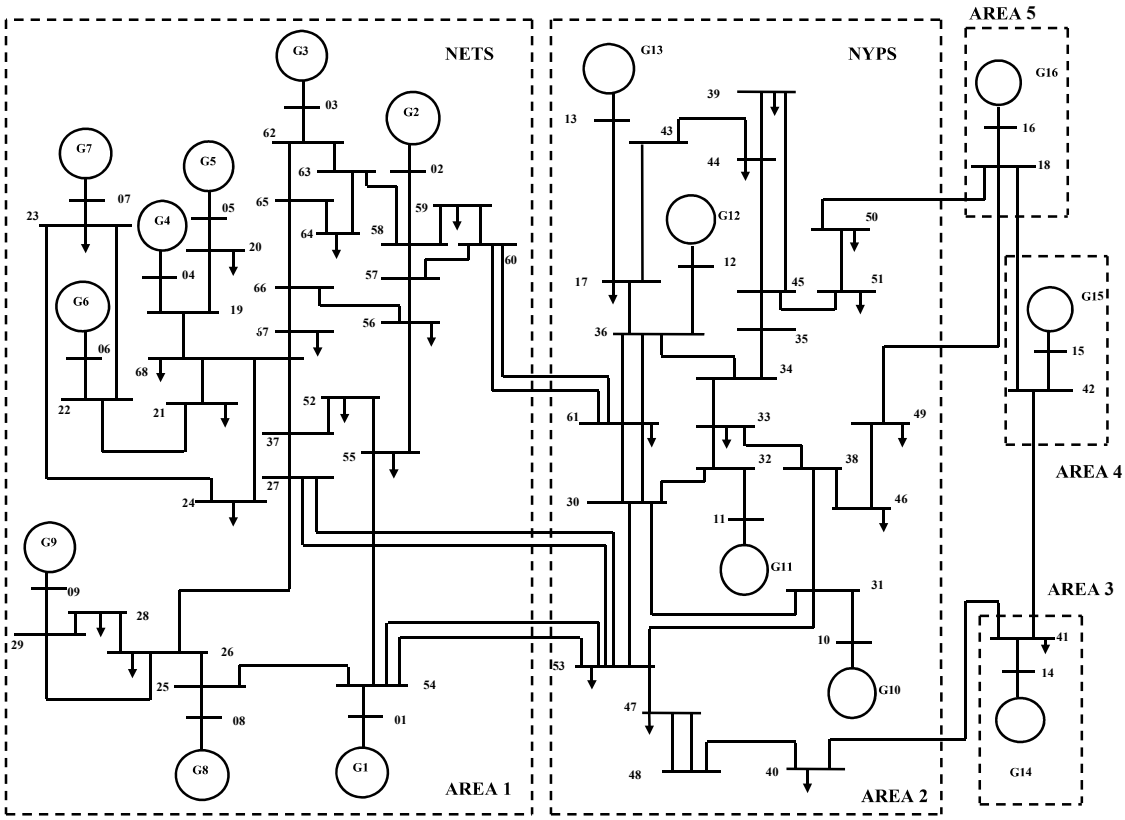

Figure 5.3: 16 generator 68 bus test system [72]

Transient rotor angle security assessment of the test system

Table 5.1 shows the transient rotor angle security assessment results of the 16-generator 68-bus test system. The fault scenarios considered were the occurrences of faults very close to the bus bars shown in the first column cleared after 100 ms by disconnecting the transmission lines connecting the buses shown in column 2 of the table. The transient security assessment results derived using the finite time LEs (i.e. LAERs) were compared with the standard time domain simulation (TDS) and

the generalized equal area criterion (GEAC) described in Section 2.1. The decision of stability using TDS was made by visual inspection of the rotor angle trajectories. The GEAC based assessment was done using the power swing-based stability index (PSSI) in TSAT software.

Table 5.1: Transient security assessment results under different contingencies of the 16-generator 68-bus test system

Faulted bus	Tripping line	Largest average exponential rate				Swing stability index	Time domain simulation
		T_C*$-T_C+5$	T_C-T_C+10	T_C-T_C+15	T_C-T_C+20		
18	–	-0.0903	-0.0467	-0.0521	-0.0428	61.53	Stable
17	17-43	-0.0810	-0.0310	-0.0247	-0.0197	58.81	Stable
22	22-23	-0.0807	-0.0339	-0.0240	-0.0245	54.72	Stable
38	38-46	-0.0758	-0.0320	-0.0247	-0.0240	63.69	Stable
43	43-44	-0.1005	-0.0445	-0.0348	-0.0282	64.27	Stable
55	55-56	-0.0765	-0.0319	-0.0285	-0.0165	57.36	Stable
60	60-61	-0.1962	-0.0360	-0.0743	-0.0343	58.25	Stable
17	17-36	0.7107	0.7021	0.5593	0.5728	-99.33	Unstable
19	19-68	0.2338	0.3403	0.4386	0.5398	-71.77	Unstable
36	36-17	0.8903	1.0136	0.8150	0.6549	-99.39	Unstable
42	42-41	0.4774	0.4044	0.4013	0.3363	-99.53	Unstable
50	50-51	0.6297	0.9713	1.1080	1.0948	-98.8	Unstable
50	50-69	0.7247	0.9367	1.2387	1.4934	-98.58	Unstable
23	23-24	-0.0654	-0.0566	-0.0135	-0.0154	39.84	Unstable
27	27-37	-0.0440	-0.0442	-0.0380	-0.0273	28.5	Unstable

*Fault clearing time

Following conclusions can be made based on these results.

- With reference to the time domain simulation result, it is seen from Table 5.1 that all the stable and unstable scenarios have been classified correctly by the proposed stability identification algorithm except the last two cases.

- The largest average exponential rates calculated over a short time window after

clearing the fault are indicators of the large-disturbance rotor angle stability of the post-fault power system. If the largest average exponential rate is negative, the post-fault power system is stable, and unstable, if it is positive.

- The power swing-based stability index gives a positive number if the post-fault power system is stable and a negative number, otherwise.

The last two scenarios are two special cases. The largest average exponential rates are negative and the power swing-based stability indices are positive indicating that the post-fault power systems are stable subsequent to the considered fault scenarios. However, visual inspection of the time domain trajectories showed oscillations with slowly increasing amplitudes. Thus, these two scenarios are two oscillatory instability scenarios. The largest average exponential rates calculated over the data window $(T_C - T_C + 50)$ gave positive values in these two cases. Fig. 5.4 shows the rotor angle trajectories of two selected generators under first-swing stable, first-swing unstable and oscillatory unstable scenarios.

Oscillatory security assessment

The transient secure scenarios were then analyzed using the improved Prony algorithm to extract the dominant oscillatory modes and to determine their parameters. Table 5.2 shows the results of a few selected scenarios.

In order to validate the oscillatory security assessment results of the improved Prony algorithm, the parameters of the critical oscillatory modes[1] determined by the eigenvalue analysis of the test system was used. The eigenvalue analysis performed around the equilibrium point of the pre-fault system using SSAT software [35] identified three critical modes with frequencies 0.5568 Hz, 0.6915 Hz, 1.0149 Hz

[1]oscillatory modes with damping ratio $\leq 3\%$ were treated as the critical modes

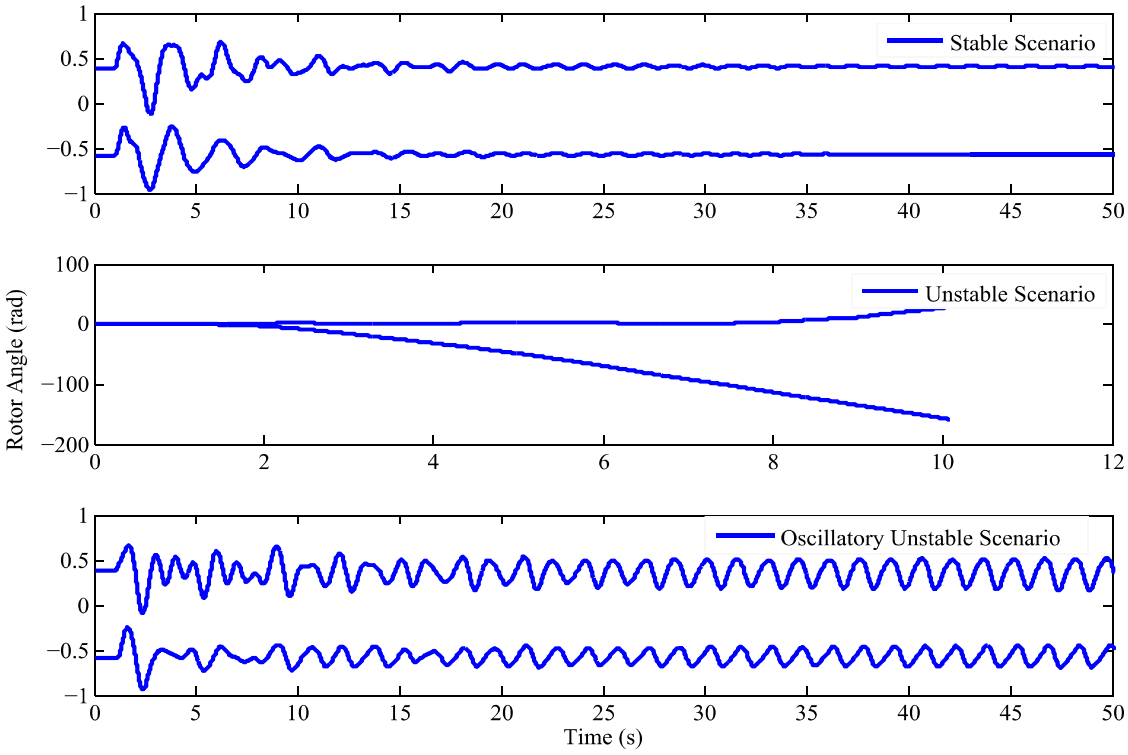

Figure 5.4: Rotor angle trajectories of 16 generator 68 bus test system under different scenarios

and damping ratios 2.41%, 1.40%, 2.26% respectively. The poorly-damped 0.6915 Hz mode is an inter-area mode between NETS and NYPS with the highest participation from the speed of the generator 5.

The first scenario shown in Table 5.2 is a bus fault scenario, where a bus fault applied at bus 18 was cleared after 100 ms without any topology change in the network. It is seen from Table 5.2 that the improved Prony algorithm has extracted two modes in this case and their parameters are close (error < 0.01) to those determined by the eigenvalue analysis. An eigenvalue analysis gives oscillatory modes at the equilibrium point. However, only a few modes are excited by a given fault scenario. Furthermore, the ranking logic explained in Section 5.2 has identified the generator 5 rotor angle as the input signal to the improved Prony algorithm.

Table 5.2: Oscillatory security assessment under different contingencies of the 16-generator 68-bus test system

Faulted Bus	Tripped line	Input signal	Dominant modes		Conclusion
			Fre. (Hz)	Dam. ratio (%)	
18	-	Gen. 5 relative angle	0.6911 0.5562	1.37 2.37	Post-fault system has inadequate damping
17	17-43	Gen. 2 relative angle	0.6824 1.0125 0.4220	1.20 2.22 8.78	Post-fault system has inadequate damping
22	22-23	Gen. 13 relative angle	0.6904 0.5565 0.4307	1.37 2.38 8.03	Post-fault system has inadequate damping
43	43-44	Gen. 12 relative angle	0.6825 0.5546 1.1153 0.4228	1.14 2.52 4.34 8.50	Post-fault system has inadequate damping
55	55-56	Gen. 12 relative angle	0.6908 0.5570 1.1239 0.4306	1.36 2.54 3.02 7.80	Post-fault system has inadequate damping
60	60-61	Gen. 15 relative angle	0.6666 0.5548 0.4274	1.34 2.47 6.86	Post-fault system has inadequate damping
23	23-24	Gen. 10 relative angle	0.6650 0.5592 0.4109	-0.19 2.64 6.07	Post-fault system is oscillatory unstable
27	27-37	Gen. 12 relative angle	0.6719 0.5591 0.4149	-0.32 2.73 6.63	Post-fault system is oscillatory unstable

Referring to the last two rows in Table 5.2, it is seen that the oscillatory instability of the post-fault power system subsequent to the two fault scenarios has been correctly identified by the improved Prony algorithm. A negatively damped low-frequency mode has been excited under the two scenarios. The amplitude of this mode slowly grew with time eventually leading to a collapse in the power system. Furthermore, it can be seen from Table 5.2 that the damping ratios of the critical modes have changed subsequent to different fault scenarios. This emphasises the importance of having the

improved prony algorithm in the proposed hybrid algorithm.

5.3.2 50-generator 470-bus test system

The 50-generator 470-bus test system used for the security assessment studies in this thesis is same as given in [73]. The test power system has 2 areas with 14 thermal generators in the area 1 and 23 thermal generators and 13 hydro generators in the area 2. This system was simulated in TSAT software [17] using the modelling details given in Section B.4 in Appendix B.

Transient rotor angle security assessment of the test system

Table 5.3 shows the security assessment results of the test system subsequent to different fault scenarios. In power systems operation, faults are cleared by the primary protection systems. If in case the primary protection fails, the fault clearing is done by the backup protection system. Thus, in this case, two fault clearing times were considered for each scenario. The largest average exponential rates were calculated considering 5 s long data windows after clearing the fault, that is, the data window was; $T_C - T_C + 5$.

Table 5.3 also shows that the stable and unstable cases have been accurately identified by the negative and positive largest average exponential rates respectively. The same observation was done in the analysis of the 16-generator test system.

Oscillatory security assessment of the test system

The oscillatory rotor angle security of the post-fault power system subsequent to different fault scenarios was determined using the improved Prony algorithm. The eigenvalue analysis performed using SSAT identified a poorly-damped low-frequency

Table 5.3: Transient security assessment results under different contingencies of the 50-generator 470-bus test system

Faulted	Tripped	Clearing time = 100 ms			Clearing time = 300 ms		
bus	element	LAER*	PSSI**	TDS***	LAER	PSSI	TDS
5	-	-0.1025	51.94	Stable	0.3458	-98.20	Unstable
10	-	-0.0785	53.17	Stable	-0.0762	27.56	Stable
15	-	-0.2152	56.60	Stable	0.2712	-98.71	Unstable
16	-	-0.2707	55.01	Stable	0.2694	-98.76	Unstable
20	-	-0.1603	57.29	Stable	0.2040	-99.29	Unstable
56	line 56-92	-0.1624	57.20	Stable	-0.1587	55.47	Stable
81	line 81-82	-0.1841	55.00	Stable	0.1588	-98.52	Unstable
85	line 85-88	-0.2127	54.41	Stable	2.0359	-98.45	Unstable
130	line 130-166	-0.0714	56.11	Stable	-0.0429	49.58	Stable
171	line 171-173	-0.0948	57.08	Stable	-0.0783	38.63	Stable
197	line 197-271	-0.1705	56.64	Stable	-0.1787	47.75	Stable
210	line 210-307	-0.1963	56.58	Stable	-0.2200	47.26	Stable
250	line 250-321	-0.1222	57.22	Stable	-0.1408	56.67	Stable
276	line 276-308	-0.1788	56.77	Stable	-0.1916	46.07	Stable
329	line 329-330	-0.0644	51.84	Stable	0.0348	-98.73	Unstable
5	generator 5	-0.0895	56.09	Stable	-0.1269	44.90	Stable
30	generator 30	-0.1239	57.67	Stable	-0.1350	57.39	Stable

*Largest Average Exponential Rate

**Power Swing-based Stability Index

*** Time Domain Simulation

mode at 0.8228 Hz frequency, and 2.55% damping ratio. The speed of the generator 16 highly participated in this mode.

Consider the fault scenario of a clearing of a solid three-phase bus fault applied at bus 16 after 100 ms without any topology change in the network. The post-fault power system is transient rotor angle stable in this case as shown in 4^{th} raw of Table 5.3. The rotor angle of the generator 16 was identified as the input to the improved Prony algorithm and two modes were extracted. The frequencies and the damping ratios of the two modes were 0.8225 Hz, 1.1413 Hz and 2.84%, 5%

respectively. According to the eigenvalue analysis, the system has a mode at 1.1417 Hz frequency and 5.32% damping ratio. Note that in this case, the 20 s long data window for the improved Prony algorithm was selected as $t = (5 - 25)$ s as mentioned in Section 5.2. However, when the data window was selected as $t = (20 - 40)$ s, the improved Prony algorithm extracted only the dominant mode with frequency 0.8223 Hz and damping ratio 2.60%.

Similarly, the proposed hybrid algorithm identified the oscillatory stability status of the post-fault power system subsequent to the different fault scenarios analyzed.

5.4 Discussion

In this study, the power systems were modeled in detail using the auxiliary controls of the generators in order to assess the transient rotor angle security. The time domain simulated trajectories were then analyzed using the LEs-based algorithm and the power swing-based stability index to derive the stability conclusions. A comparison between the two methods is given below.

- Both methods employ a criterion based on the simplified generator models in predicting the stability even though the power system is modeled in detail in the time domain simulation. In the power swing-based stability index method, the rotor angle separations between all the generators are compared at each time step to group them into the critical cluster and the noncritical cluster of generators. The two groups are further simplified into their equivalent single generator models to use the EAC and hence to derive the stability conclusion. The LEs-based algorithm is less complex compared to this approach. The LEs determine whether the rotor angles converge or not to the equilibrium points by using a time-varying Jacobean matrix to evolve the nearby trajectories in

the state-space.

- Unlike the power swing-based stability index, the major limitation of the LEs-based approach is that the magnitude of the largest average exponential rate does not provide the indication on how close is the post-fault power system to instability. However, it was shown in Section 3.4.2 in Chapter 3 that subsequent to a fault scenario, the LEs converge to the same negative value irrespective of the fault clearing time upto the critical clearing time, beyond which the system becomes unstable. Thus, the only way to evaluate the closeness to the instability by the LEs-based algorithm is to determine the critical clearing time associated with a given fault scenario.

Computational complexity of the hybrid algorithm

The proposed rotor angle security assessment tool uses the LEs-based algorithm and the improved Prony algorithm to derive the stability conclusions using the time domain simulated trajectories. The average computational burden of these two algorithms to process one fault scenario was around 0.0576 s in the case of 16-generator 68-bus test system and 0.0644 s in the case of 50-generator 470-bus test system. These computations were done on a PC having Intel Core i7 (3.40 GHz) processor with 8 GB RAM.

The 5 s long data window used to calculate the largest average exponential rates derived the stability conclusions accurately in the test power systems used in this study. A longer data window can be used on this regard if the additional computational burden is acceptable. Further, assuming that there is no prior knowledge about the frequencies of the dominant modes, a 20 s long data window was used for the improved Prony algorithm. The data window length can be set based on the frequency

of the dominant mode, for example, four cycles of the dominant mode, if the operator has an idea about the dominant mode of the system. Thus, it is recommended to perform an offline analysis first in order to set the data window lengths before using the proposed algorithms in the actual power system operation.

5.5 Chapter summary

The contribution of this chapter is that it has presented a hybrid algorithm to perform the dynamic security assessment with respect to both transient and oscillatory rotor angle stability under multiple contingencies of the power system. The proposed hybrid algorithm first used the LEs-based algorithm developed in Chapter 3 to determine the large-disturbance rotor angle stability. Such stable cases were further processed using the Shrinking Window Improved Prony algorithm developed in Chapter 4 in order to determine the oscillatory stability of the post-fault power system. Further, the input signal to the improved Prony algorithm was selected using a ranking logic.

In this chapter, the rotor angle security assessment results obtained using the LEs-based algorithm were compared with the generalized equal area criterion. It was shown that both methods derived the stability conclusions accurately. Furthermore, the results of the improved Prony algorithm were also compared with the eigenvalue analysis. It was shown that the proposed hybrid algorithm determines the transient rotor angle security and the oscillatory rotor angle security of the post-fault power system with a computation time which is acceptable for online applications. The above contributions were published in Reference [74] during this PhD study.

Chapter 6

Online Monitoring of Power System Oscillations using an Improved Prony Algorithm

6.1 Introduction

Presence of oscillations is an inherent property of an interconnected electrical power system. These oscillations do not cause a threat to the security of the power system as long as they are sufficiently damped. However, a poorly-damped oscillation brings the power system into an alert state where a preventive action needs to be taken. The presence of an unstable oscillation can lead even to a blackout if no corrective actions are timely taken. Therefore, it is important to continuously monitor these oscillations and alert the system operator if they are not acceptable. The availability of synchrophasor data from phasor measurement units (PMUs) in todays power systems enables the monitoring of such oscillations. The main goal of this chapter is to show that the improved Prony algorithm presented in Chapter 4 can also be used to

monitor power system oscillations in an online environment.

Among different types of power system oscillations, inter-area oscillations have gained the attention of power system engineers since a stable inter-area mode can become a poorly-damped or negatively-damped mode due to changes in the network structure, load characteristics, system operating conditions, etc [75]. These low-frequency oscillations with frequencies 0.1 - 0.8 Hz correspond to oscillations between generators in different areas. The blackout in the Western Interconnection in 1996 [76] renewed the interest in monitoring inter-area oscillations. Several algorithms have been proposed in literature to monitor inter-area oscillations [44], [50], [51], [67], [77] and some have been implemented.

Sub-synchronous oscillations on the other hand are the oscillations with frequencies less than the fundamental frequency. These oscillations are generated when a circuit involving a resistor, inductor, capacitor (RLC circuit) is connected in series with the network. For example, a scenario of sub-synchronous resonance can arise when a transmission line is series compensated, which can lead to turbine-generator shaft failure and electrical instability at frequencies less than the nominal system frequency [78]. The 1971 incident at the Mohave generating station [79] emphasised the importance of studying sub-synchronous interactions in power systems. However, the monitoring of sub-synchronous oscillations using PMU data has not been widely discussed in the literature.

This chapter shows that the improved Prony algorithm presented in Chapter 4 can also be used to monitor power system oscillations including inter-area and sub-synchronous modes in the online environment using synchronized phasor measurements. The objectives of this chapter are; i) develop the online oscillation monitoring algorithm, ii) show the performance of the algorithm for extracting low-frequency

modes, and iii) show the performance of the algorithm for extracting sub-synchronous modes.

6.2 Online monitoring of power system oscillations

In order to illustrate how the improved Prony algorithm presented in Section 4.3 in Chapter 4 can be used to power system's oscillation monitoring, consider a scenario where both low-frequency inter-area modes and sub-synchronous modes are excited in a measured signal as given in Eq. (6.1) with mode parameters as given in Table 6.1.

$$x(t) = c + \sum_{i=1}^{3} a_i e^{-\sigma_i t} \cos(2\pi f_i t) + \omega(n) \tag{6.1}$$

where, $c = 1$ was used in this study and a_i, σ_i, f_i are mode strength, real part of the eigenvalue and frequency of the i^{th} mode respectively. $\omega(n)$ represents a zero-mean Gaussian white noise. The sampling rate used was $\frac{1}{120}$ s, which is equivalent to 120 fps[1] reporting rate of a PMU [7]. This sampling rate was used in this study, thus a maximum of 60 Hz signal can be monitored according to the Nyquist criterion.

Table 6.1: Parameters of the oscillatory modes

Mode No	Frequency (Hz)	Real Part of Eigenvalue	Damping Ratio (%)	Mode Strength (pu)
1	0.5	-0.0471	1.5	2.5
2	0.6	-0.1131	3.0	2.5
3	25	-0.7854	0.5	2.5

Fig. 6.1 shows the noise added input signal. Here the noise has been added such that the signal-to-noise ratio (SNR) is 30 dB. The first 5 s long data window is zoomed

[1]fps means frames per second

in top right hand side of the figure.

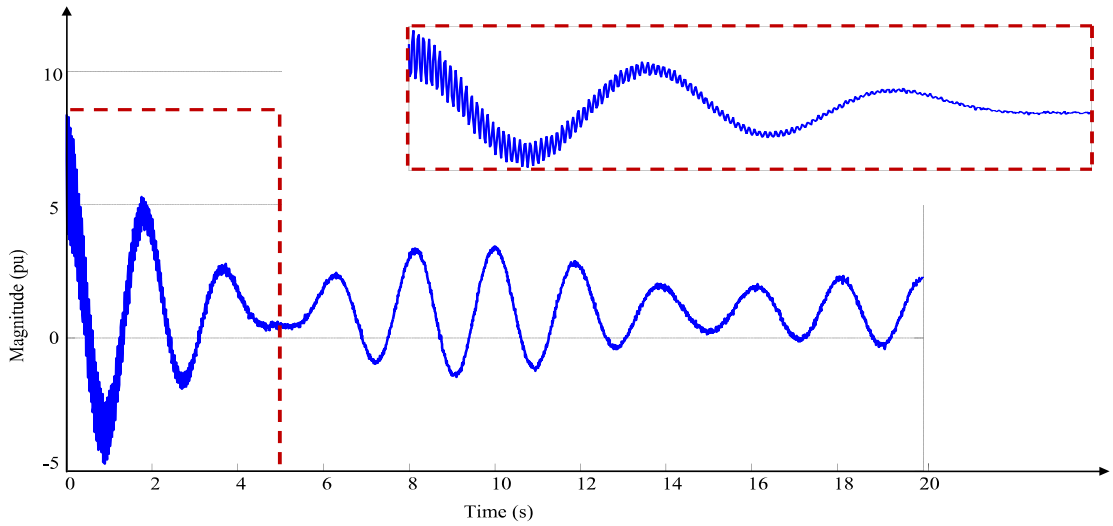

Figure 6.1: Synthetic signal with inter-area and sub-synchronous modes

In order to determine the parameters of the modes present in the input signal $x(t)$, it is not advisable to directly feed this signal into the improved Prony algorithm due to following reasons:

- In order to monitor the low-frequency modes, Section 6.3 of this Chapter recommends to set the length of the Prony window as four cycles of the dominant low-frequency mode if the frequency of the dominant mode is known, that is 8 s in this case. There are 200 ($= 8 \times 25$) cycles of the sub-synchronous mode over this data window. Thus, if the sub-synchronous mode is very poorly-damped, the oscillations might grow leading to a system collapse before we identify a poorly-damped sub-synchronous mode is present in the system.

- When the improved Prony algorithm is applied to an input signal like $x(t)$, it determines the frequencies over a wide range such as 0.1 - 40 Hz. Thus, the

improved Prony algorithm can still generate fictitious modes specially when the measurement noise is present in the signal.

Therefore, it is recommended to preprocess the output signal from the PMU before feeding it to the improved Prony algorithm. The proposed oscillation monitoring algorithm is shown in Fig. 6.2. This oscillation monitoring algorithm was implemented using MATLAB in the PC environment. The purposes of different preprocessing steps are explained below:

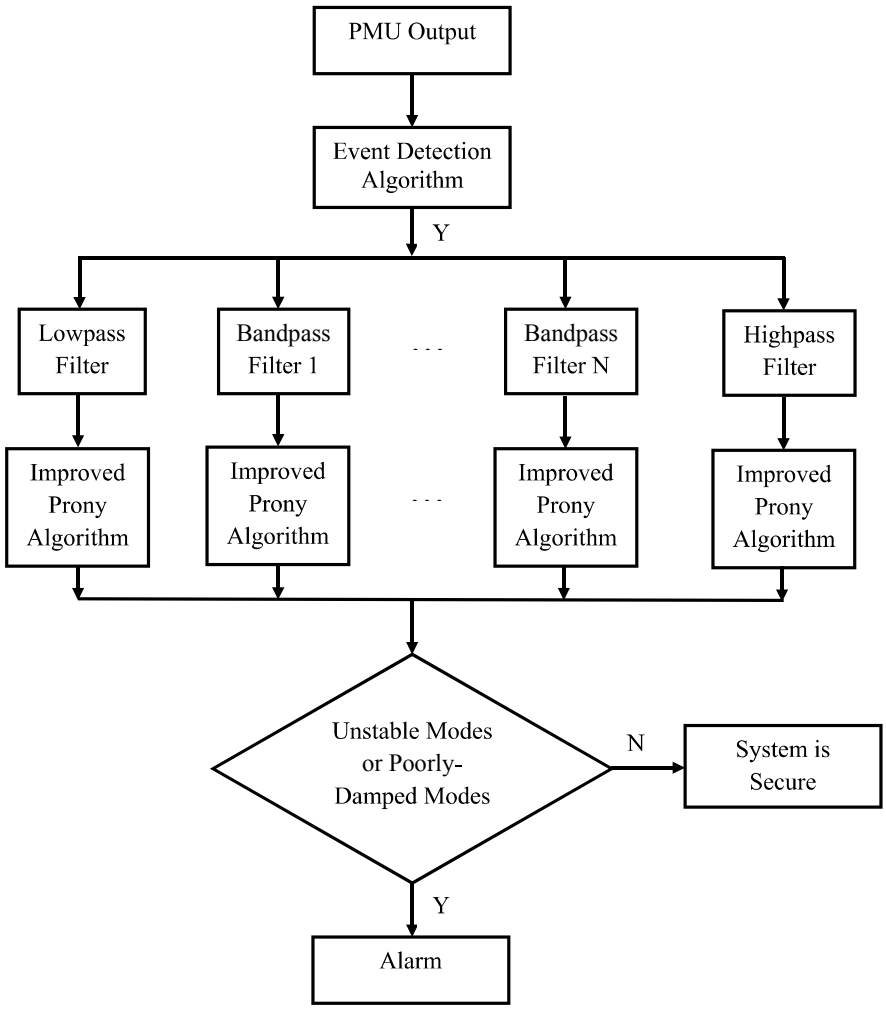

Figure 6.2: Proposed oscillation monitoring algorithm

6.2.1 Event detection algorithm

Throughout the discussions in Chapter 4, 5 and 6 so far, it was pointed out that the Prony algorithm works when there is a noticeable oscillation in the data window or in general under ring-down conditions in the power system. Such a scenario occurs subsequent to a large magnitude disturbance in the power system. In contrast, under normal operating conditions in the power system, the major force behind the mode excitation is the randomly changing load in the system, which can be referred to as ambient noise from signal processing point of view [37]. The power system is operating in a quasi-steady-state without no significant disturbances under ambient conditions [80]. Thus, it is important to trigger the Prony algorithm subsequent to an onset of a ring-down oscillation in the power system. In order to distinguish between the ambient operation and the onset of a ring-down oscillation, the measurement energy, E_k defined by Eq. (6.2) was used in this study.

$$E_k = \sum_{i=k}^{i=k+N-1} |x(i)|^2 \tag{6.2}$$

where N is the total number of samples inside the k^{th} data window.

The energy over a data window of the measured signal is continuously determined using Eq. (6.2). Subsequent to an onset of a ring-down oscillation in the power system, the calculated energy dramatically changes compared to the mean energy in the ambient operation [81]. This feature can be used to detect the onset of a ring-down oscillation and hence to initiate the improved Prony algorithm. In this study, if E_k is continuously changing and if $E_k \geq 1.05 \times mean(E_1 : E_{k-1})$ or $E_k \leq 0.95 \times mean(E_1 : E_{k-1})$, the improved Prony algorithm was initiated.

After initiating the algorithm, it determines whether the system is secure or not. If it is insecure, the execution of the algorithm can be stopped and the operator is

alerted. If the system is found to be secure, that means all the oscillatory modes have adequate damping, and the execution of the algorithm can be stopped.

6.2.2 Signal preprocessing through a filter bank

The purpose of the filter bank is to separate the various frequency components present in the input signal. The input signal is sent through a parallel filter bank as shown in Fig. 6.2 and each output is analyzed by the improved Prony algorithm to extract the dominant modes. The passband frequencies of the filters are adjusted as follows.

- Lowpass filter

  The purpose of the lowpass filter is to separate the low-frequency oscillatory modes. In this study, the pass-band and the stop-band corner frequencies of the lowpass filter were set as 2 Hz and 5 Hz respectively. Further, the lowpass filter reduces the influence of the measurement noise on the parameter estimation of the low-frequency modes by the algorithm.

- Bandpass filters and highpass filter

  The purposes of these filters are to separate oscillations present in other frequency bands. Accordingly, the pass-band corner frequencies of the filters can be set.

  This chapter shows that the improved Prony algorithm can be used to monitor the sub-synchronous oscillatory modes. Power system literature suggests different approaches to study the impact of such modes on the power system. For example, references [82] and [83] present methodologies to study sub-synchronous oscillations in an HVDC-integrated power system and a wind-integrated power system, hence the operator can have a prior knowledge about the frequencies

of such modes. This information can be used to set the pass-band and the stop-band corner frequencies of the bandpass filters.

The pass-band ripple and the stop-band attenuation were considered as 0.2 dB and 20 dB respectively in this study. These two specifications were made based on IEEE standard for synchrophasor measurements in power systems [7]. These filter specifications are same as those given in [7] to improve the dynamic performance of the PMU. These apecifications are shown in Fig. 6.3.

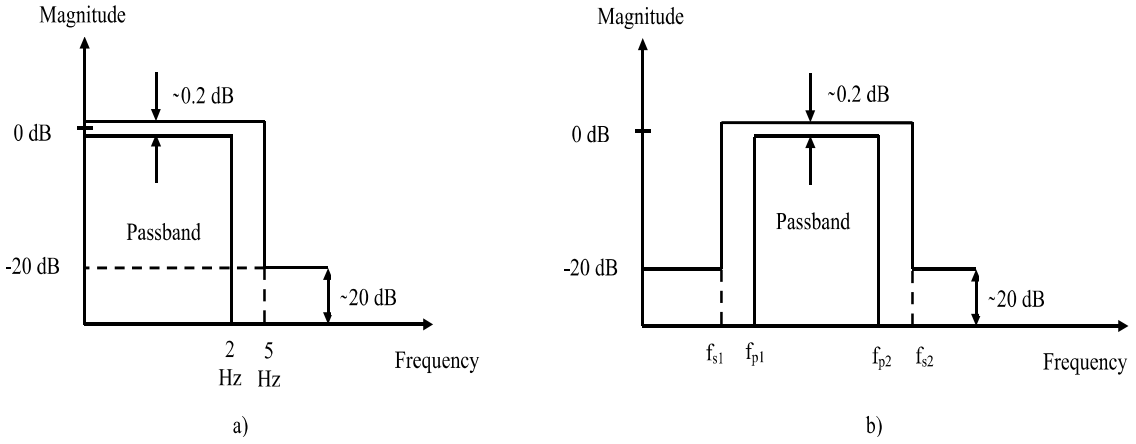

Figure 6.3: Illustration of filter specifications: a) Lowpass filter b) Bandpass filter

Design of filters to meet the design specifications

This section describes the design of a lowpass filter, bandpass filter and a highpass filter to process the input signal given in Eq. (6.1). The pass-band and the stop-band edge frequencies were selected as given in Table 6.2, where Fs refers to the sampling rate. The pass-band ripple and the stop-band attenuation were considered as 0.2 dB and 20 dB respectively.

Finite impulse response (FIR) filters are considered to be efficient filters due to their linear phase characteristics and are always stable [84]. Let $x(n)$ and $y(n)$ are

Table 6.2: Filter specifications for the synthetic input signal

Frequency range	Lowpass filter	Bandpass filter	Highpass filter
Passband (f_{p1}, f_{p2})	(0 , 2)	(15 , 35)	(40 , $\frac{Fs}{2}$)
Stopband (f_{s1}, f_{s2})	(5 , $\frac{Fs}{2}$)	(0 , 10) & (40 , $\frac{Fs}{2}$)	(0 , 35)

the input and the output of an M length FIR filter at discrete time n. Eq. (6.3) shows the relationship between $x(n), y(n)$ and the filter coefficients $\{b_k\}$.

$$y(n) = b_0x(n) + b_1x(n-1) + \cdot + b_{M-1}x(n-M+1) \quad (6.3)$$

$$= \sum_{k=0}^{M-1} b_kx(n-k) \quad (6.4)$$

The system function of the FIR filter is given by $H(z) = \sum_{k=0}^{M-1} b_kz^{-k}$, thus the roots of this polynomial give the zeros of the filter. FIR filters are in general designed based on the well known "brick-wall" concept multiplied by a window function [84]. In this study the *Hamming window*[2] was used and the designs were done using built-in functions available in MATLAB signal processing toolbox.

The orders of the lowpass filter, bandpass filter and the highpass filter were determined as 70, 56 and 46 respectively using a trail-and-error approach to meet the design specifications. Fig. 6.4 shows the input signal and the output signals of the three filters.

[2]M length Hamming window is described by a time-doamin sequence, $h(n) = 0.54 - 0.46\cos\frac{2\pi n}{M-1}$ [84]

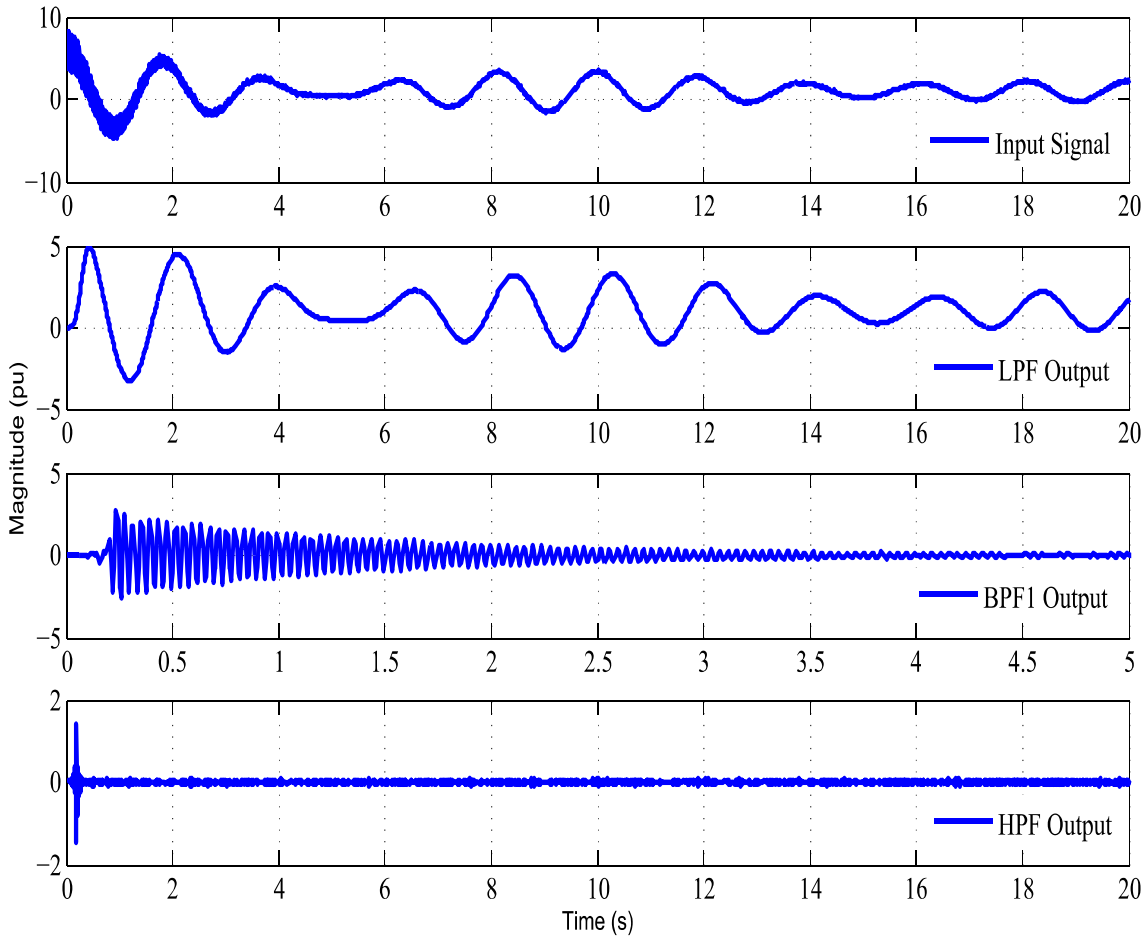

Figure 6.4: Input signal and the output signals of the filters: Test case 1 - the synthetic signal

6.2.3 Improved Prony algorithm

Outputs of each filter are processed individually by the improved Prony algorithm as shown in Fig. 6.2. For the completeness, the Shrinking Window improved Prony algorithm shown in Fig. 4.4 in Chapter 4 is repeated in Fig. 6.5.

The following specifications are recommended for the shrinking window improved Prony algorithm.

- Use a higher sampling rate such as 120 samples per second in order to monitor

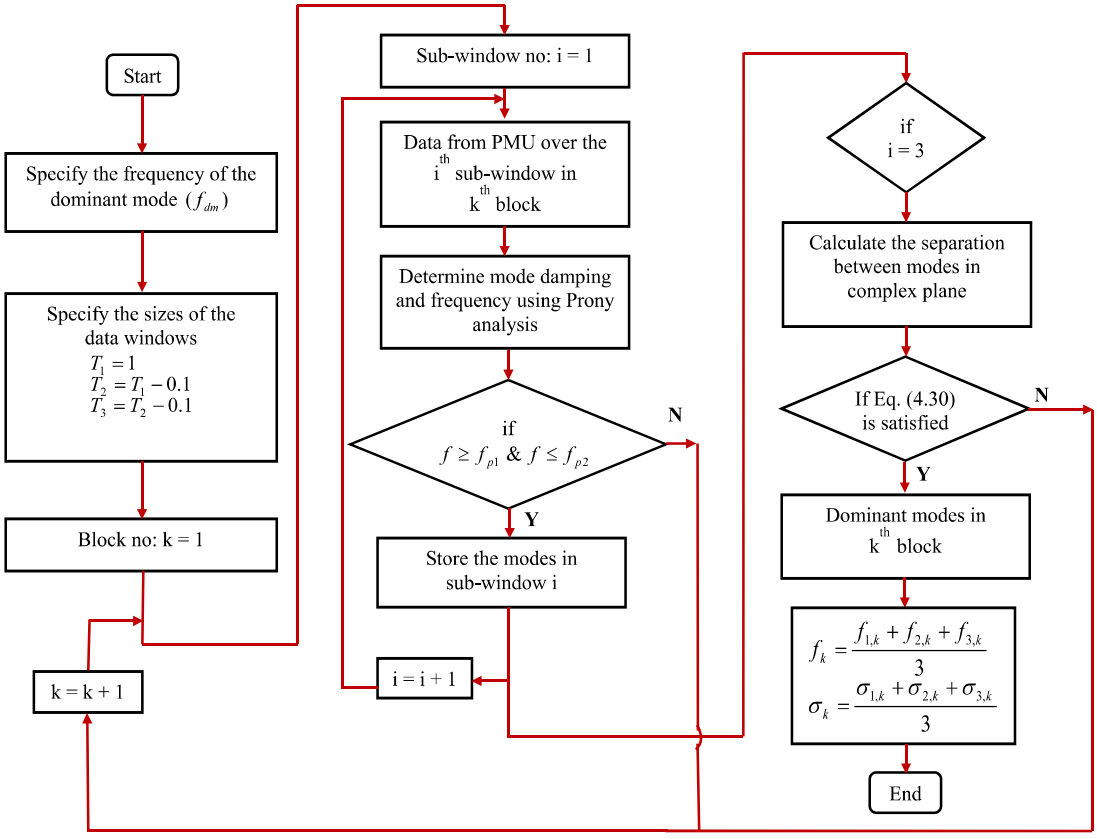

Figure 6.5: Flow chart of the shrinking window improved Prony algorithm for band-pass filter output

sub-synchronous modes. However, if the interest is only on monitoring the inter-area modes, a lower sampling rate such as 10 samples per second can be used. A sensitivity analysis using different sampling rates corresponding to different PMU reporting rates is given in Section 6.3.

- For the lowpass filter output signal, set the data window length as four cycles of the dominant oscillatory mode if there is a prior knowledge about the frequency of that mode. Otherwise, set it between 10 - 20 s, thus there is atleast one cycle of 0.1 Hz low-frequency mode inside the 10 s long data window. Generate multiple sub-windows inside the main data window by reducing the length in

steps of 1 s.

- For the bandpass filter and the highpass filter output, set the data window length as 0.5 s and generate multiple sub-windows by reducing the length in steps of 0.01 s.

- Set the threshold values between 0.01 - 0.03 for the lowpass filter output signal and between 0.2 - 0.3 for the bandpass filter and the highpass filter output signals in order to extract the true modes.

Sensitivity analysis on aforementioned different settings is given in Section 6.3.

Note that, when processing the filter output signals by the improved Prony algorithm, it is recommended to store the modes such that their frequencies lie within the pass-band frequency range of the corresponding filter before checking the consistently appearing modes. This would improve the computational efficiency of the algorithm by limiting the number of combinations to be compared to extract the consistently appearing modes in the input signal to the algorithm.

Extracting true modes of the synthetic signal using the oscillation monitoring algorithm

The three output signals of the lowpass, bandpass and highpass filters shown in Fig. 6.4 were analyzed using the Shrinking Window Improved Prony algorithm using the specifications given in Section 6.2.3. The data windows were selected after some time in order to accommodate the delays of the filters. Table 6.3 shows the extracted modes and their parameters determined by the algorithm.

It is seen that the improved Prony algorithm has performed well with the signal preprocessing using a filter bank. Note that the small deviations of the mode param-

Table 6.3: Parameters of the extracted modes - synthetic input

Filter output	No. of true modes	Frequency (Hz)	Dam. ratio (%)
Lowpass filter	3	0	100
		0.4994	1.4798
		0.6003	3.0874
Bandpass filter	1	25.0150	0.4835
Highpass filter	0	-	-

eters compared to the true parameters given in Table 6.1 are acceptable in this case since 30 dB measurement noise is present in the input signal. Further the output signal of the highpass filter does not carry useful information. This has been reflected since none of the modes has been extracted by the improved Prony algorithm on this signal.

6.3 Sensitivity analysis

The true mode extraction capability of the Shrinking Window Improved Prony algorithm depends on the data window length, the number of sub-windows inside a main data window, and the threshold for extracting the true modes. The effects of these were investigated using the synthetic signal given in Eq. (6.5). This signal has two low-frequency modes with frequencies, 0.25 Hz and 0.39 Hz and damping ratios, 7% and 6.5% respectively. This signal has been used in [67] to illustrate the true mode extraction capability of the Prony algorithm under noisy conditions using a stepwise regression analysis method.

$$x(t) = 2e^{-0.1102t}\cos(1.5708t + 1.5\pi) + 2e^{-0.1596t}\cos(2.4504t + 0.5\pi) + \omega(n) \quad (6.5)$$

Let the simulation time step as $\frac{1}{120}$ s and the SNR as 30 dB. The above signal was sent through the lowpass filter designed in Section 6.2.2. It is the usual practice in power system literature to use a Monte Carlo type method to evaluate the performance of the mode identification algorithms [67], [80]. The Monte Carlo type method uses independent trials to generate different instances of the random noise $\omega(n)$. In this study, 100 independent simulations were done on this regard. Three measures were used to analyze the performance of the algorithm. These three measures were: 1) number of trials in which only the true modes were extracted (γ_1), 2) number of trials in which only one of the true modes was extracted (γ_2), and 3) number of trails in which true modes and fictitious modes were extracted (γ_3) . If $\gamma_1 + \gamma_2 + \gamma_3 < 100$, none of the modes were extracted in some trials. Table 6.5 summarizes the results of the sensitivity analysis. Here the data window length is specified as the number of cycles of the dominant low-frequency (0.25 Hz) mode. The following conclusions can be made on the results shown in Table 6.5.

In order to extract the true modes in the Shrinking Window Improved Prony algorithm, many number of sub-windows have to be used inside the data window when the length of the data window increases. For example, the performance of the algorithm is poor when one sub-window is used inside a data window in length 4 or 5 cycles of the dominant oscillatory mode. However, the performance is acceptable when three sub-windows are used when the threshold value lies between 0.01 - 0.03.

Another important factor to be considered is the computational complexity of the method with different adjustable parameters. For a given threshold value, an increase in the number of sub-windows inside a given data window increases the number of combinations to be compared in order to extract the true modes. Therefore, the objective should be to have better accuracy while maintaining the computational

Table 6.4: Sensitivity analysis of the shrinking window algorithm: Part I

Data Window Length (Cycles)	No. of Sub-Windows	Threshold Value	γ_1	γ_2	γ_3
3	1	0.01	96	0	4
		0.02	82	0	18
		0.03	70	0	30
		0.04	56	0	44
		0.05	41	0	59
	2	0.01	100	0	0
		0.02	99	0	1
		0.03	97	0	3
		0.04	94	0	6
		0.05	85	0	15
	3	0.01	100	0	0
		0.02	100	0	0
		0.03	99	0	1
		0.04	95	0	5
		0.05	93	0	7
4	1	0.01	66	0	34
		0.02	28	0	72
		0.03	11	0	89
		0.04	7	0	93
		0.05	4	0	96
	2	0.01	100	0	0
		0.02	99	0	1
		0.03	96	0	4
		0.04	75	0	25
		0.05	62	0	38
	3	0.01	100	0	0
		0.02	95	0	5
		0.03	87	0	13
		0.04	76	0	24
		0.05	70	0	30

complexity at an acceptable level for the online application. Based on the sensitivity analysis, it can be concluded that a data window of 3 or 4 cycles of the dominant low-frequency oscillatory mode with 2 sub-windows provides acceptable mode extraction

Table 6.5: Sensitivity analysis of the shrinking window algorithm: Part II

Data Window Length (Cycles)	No. of Sub-Windows	Threshold Value	γ_1	γ_2	γ_3
5	1	0.01	46	0	54
		0.02	14	0	86
		0.03	5	0	95
		0.04	0	0	100
		0.05	0	0	100
	2	0.01	93	0	7
		0.02	63	0	37
		0.03	34	0	66
		0.04	16	0	84
		0.05	6	0	94
	3	0.01	98	0	2
		0.02	84	0	16
		0.03	58	0	42
		0.04	34	0	66
		0.05	18	0	82

accuracy for the threshold value between 0.01 - 0.03.

Sensitivity analysis with change in measurement noise

Mode parameter estimations by the Prony algorithm are sensitive to the amount of noise level present in the input signal. In order to investigate the impact of measurement noise on the mode parameter estimation, the input signal given in Eq. (6.5) was corrupted by measurement noise such that the SNR was 5 dB, 10 dB, 15 dB and 20 dB respectively. 100 independent simulations were done at each SNR. A 16 ($\frac{4}{0.25}$) s long data window with 2 sub-windows was used to extract the dominant modes. The threshold used to extract the dominant modes was changed in steps of 0.01. Fig. 6.6 shows one instance of the synthetic signal at each SNR and the lowpass filter output.

Table 6.6 shows the true mode extraction capability of the algorithm. Table 6.7

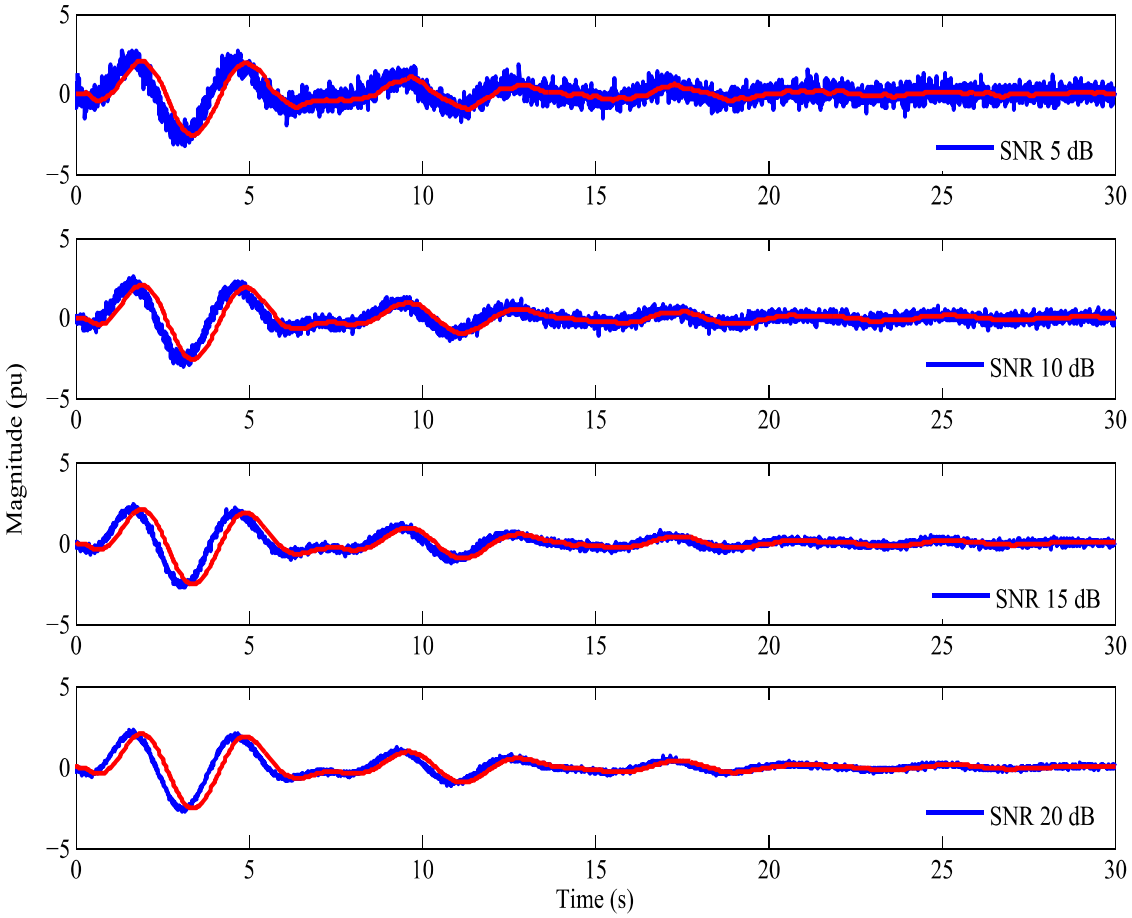

Figure 6.6: Synthetic signal and the lowpass filter output signal at different SNR levels, blue curve - input signal, red curve - lowpass filter output signal

shows the statistical significance of the estimated mode parameters with respect to the true mode parameters of the signal considering the 100 independent simulations. The following conclusions can be made based on the observations from Table 6.6 and Table 6.7.

- The true mode extraction capability of the Shrinking Window Improved Prony algorithm is acceptable for a threshold value of 0.01 - 0.03.
- Presence of measurement noise in the input signal has not degraded the perfor-

Table 6.6: Sensitivity analysis of the Shrinking Window algorithm with measurement noise

Noise Level (dB)	Threshold	γ_1	γ_2	γ_3
5	0.01	89	8	0
	0.02	98	0	2
	0.03	91	0	9
	0.04	82	0	18
	0.05	70	0	30
10	0.01	99	1	0
	0.02	95	0	5
	0.03	90	0	10
	0.04	81	0	19
	0.05	76	0	24
15	0.01	100	0	0
	0.02	97	0	3
	0.03	91	0	9
	0.04	86	0	14
	0.05	79	0	21
20	0.01	100	0	0
	0.02	98	0	2
	0.03	93	0	7
	0.04	89	0	11
	0.05	79	0	21

Table 6.7: Statistical significance of the Shrinking Window algorithm with measurement noise

Noise Level (dB)	Mode No	Fre. (Hz)	std	Real part of EV	std
5	1	0.2475	0.0006	-0.1107	0.0043
	2	0.3861	0.0011	-0.1595	0.0061
10	1	0.2500	0.0005	-0.1100	0.0030
	2	0.3899	0.0009	-0.1597	0.0045
15	1	0.2500	0.0003	-0.1100	0.0015
	2	0.3899	0.0005	-0.1598	0.0024
20	1	0.2500	0.0002	-0.1103	0.0009
	2	0.3900	0.0002	-0.1596	0.0015

mance of the algorithm. The deviations of the frequencies and the dampings of the modes even under noisy conditions are less. This is due to the fact that the input signal is first sent through a lowpass filter. Thus, the filter output signal

is less noise contaminated as observed in Fig. 6.6.

Sensitivity of the improved Prony algorithm with change in sampling rate

IEEE standard for synchrophasor measurements in power systems [7] recommends different PMU reporting rates. These are 10, 12, 15, 20, 30, and 60 fps for a 60 Hz system. Further, high reporting rates such as 100 and 120 fps are also recommended. In this analysis so far a higher reporting rate of 120 fps was considered since the overall goal of the proposed oscillation monitoring algorithm is to monitor both inter-area and sub-synchronous oscillations. However, if the interest is only on monitoring the low-frequency inter-area modes, a lower reporting rate such as 10 fps can be accommodated. This section presents the results of the sensitivity analysis by changing the PMU reporting rate, that is, by changing the sampling rate of the improved Prony algorithm.

Now, the input signal given in Eq. (6.5) was corrupted by measurement noise at 20 dB SNR. A 16 ($\frac{4}{0.25}$) s long data window with 2 sub-windows were used to extract the dominant modes and their parameters. The threshold value used to extract the dominant modes was 0.02. Table 6.8 shows the performance of the algorithm and the statistical significance of the estimated mode parameters using 100 independent simulations. The three performance measures γ_1, γ_2 , and γ_3 are same as explained at the beginning of this section.

Following conclusions can be made based on the results given in Table 6.8.

- The performance of the algorithm for extracting low-frequency modes is acceptable with the different recommended PMU reporting rates by the standard.

Table 6.8: Performance of the shrinking window algorithm with PMU reporting rate

Reporting Rate (fps)	γ_1	γ_2	γ_3	Mode No	Fre. (Hz)	std	Real part of EV	std
10	94	0	6	1	0.2498	0.0007	-0.1107	0.0049
				2	0.3900	0.0011	-0.1611	0.0073
12	92	1	7	1	0.2500	0.0006	-0.1102	0.0039
				2	0.3901	0.0010	-0.1611	0.0065
15	96	0	4	1	0.2500	0.0005	-0.1107	0.0037
				2	0.3901	0.0008	-0.1598	0.0055
20	96	0	4	1	0.2501	0.0004	-0.1106	0.0026
				2	0.3899	0.0007	-0.1591	0.0043
30	92	0	8	1	0.2500	0.0003	-0.1100	0.0022
				2	0.3900	0.0005	-0.1599	0.0036
60	95	0	5	1	0.2500	0.0002	-0.1106	0.0015
				2	0.3900	0.0003	-0.1596	0.0018
100	95	0	5	1	0.2500	0.0002	-0.1102	0.0010
				2	0.3899	0.0003	-0.1594	0.0016

- The standard deviations of the frequencies and the real parts of the eigenvalues determined by the algorithm are very small ($< 10^{-2}$) indicating that the variation of these parameters with the PMU reporting rate is negligible for the purpose of online oscillation monitoring.

6.4 Results

Performance of the Shrinking Window Improved Prony algorithm for monitoring of power system oscillations was tested using different test cases. These test cases were; i) two-area four-generator test system [14], ii) 16-generator 68-bus test system [72], iii) 50-generator 470-bus test system [29], iv) A wind-integrated 12-bus test system [83], and v) an HVDC-integrated test system. The first three test cases show the performance of the algorithm for extracting low-frequency inter-area oscillatory modes and the last two test cases have sub-synchronous oscillatory modes. The input data for

the oscillation monitoring algorithm were generated using simulations of the above test systems in different simulation tools as indicated in Section 6.4.1 and Section 6.4.2.

6.4.1 Monitoring of inter-area oscillatory modes

In this section, the improved Prony algorithm with following specifications was used to monitor the inter-area oscillatory modes: a) sampling rate was $\frac{1}{120}$ s, b) the data window length was set as four cycles of the dominant mode, c) two sub-windows inside the main data window, and d) threshold used to extract consistently appearing modes from the lowpass filter output was 0.03.

Test case 1: Two-area four-generator test system

The two area four generator test system shown in Fig. 6.7 is widely used in power system literature to study the inter-area oscillations [14], [75], [85]. This system was simulated in RSCAD software [86] with following modeling details: all the generators were modeled using the sub-transient equivalent two axis model with one damper winding in the d-axis and two damper windings in the q-axis [14]. Further, the generators were equipped with the exciter, power system stabilizer and the turbine-governor model. The steady state data and the dynamic data of the generators and the associated controls are given in Section B.2 in Appendix B. The small-signal stability analysis of the test system at the given operating point was done using small-signal analysis tool (SSAT) [35]. The frequency and the damping ratio of the inter-area mode were 0.642 Hz and 4.02 % respectively.

The PMU shown in Fig. 6.7 has been fed with the three-phase currents (i_a, i_b, i_c) through the 2^{nd} line connecting the buses 7 and 8 and the three-phase voltages

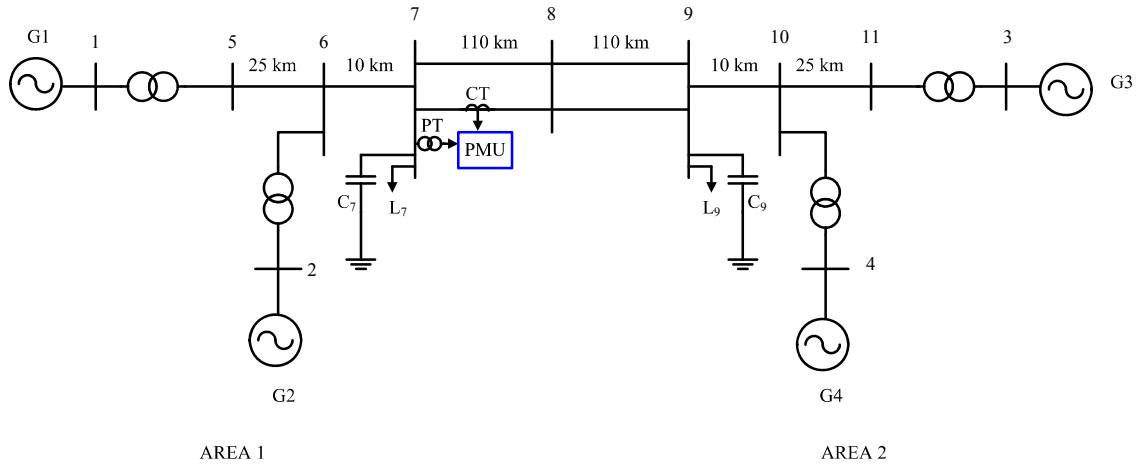

Figure 6.7: Single-line diagram of two-area four-generator test system [14]

(v_a, v_b, v_c) at bus 7. Thus the PMU provides the phasors corresponding to i_a, i_b, i_c, v_a, v_b, &, v_c and the reporting rate used was 120 fps. Note that in this case the PMU model available in RSCAD software was used. The active power flow through the line was determined using the phasors provided by the PMU. Fig. 6.8 shows the active power flow through the line subsequent to a solid three-phase bus fault in bus 7 cleared after 5 cycles of the fundamental frequency (60 Hz) without any topological changes in the system.

30 dB of measurement noise was added to the input signal shown in Fig. 6.8 before analyzing it using the oscillation monitoring algorithm. The event detection logic identified an onset of a ring-down oscillation at time, $t = 6.34$ s and initiated the improved Prony algorithm for extracting the dominant modes. In this case also, 100 independent simulations were done to generate different instances of the random noise.

In order to highlight the statistical significance of the mode parameter estmation, two data windows were selected soon after and few seconds later triggering the improved Prony algorithm. Table 6.9 shows the average values of the mode parame-

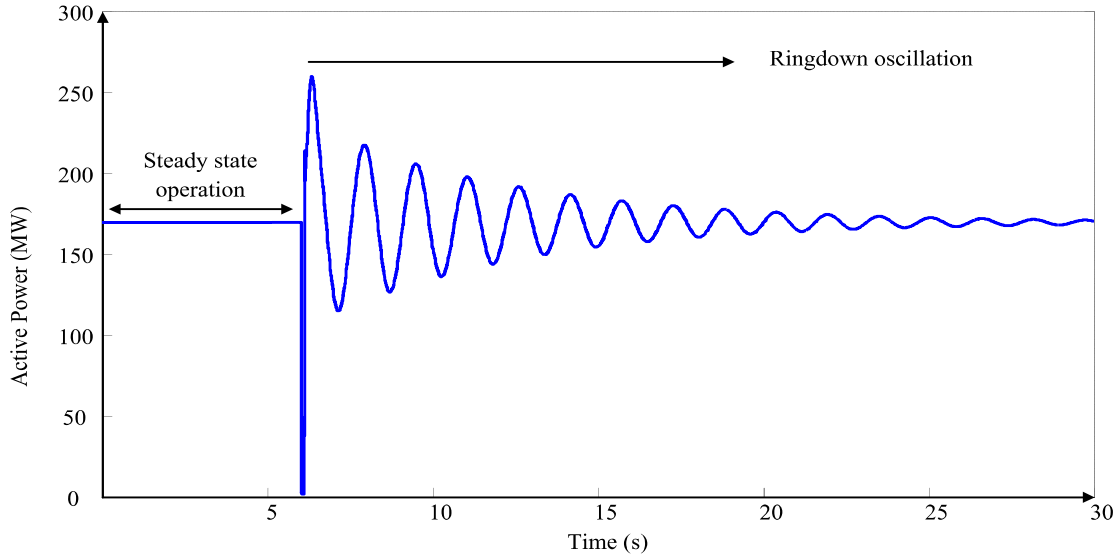

Figure 6.8: Active power flow along the line 7-8 subsequent to a contingency

ters considering the 100 cases and their standard deviations with respect to the true mode parameters obtained via the eigenvalue analysis. Furthermore, among these 100 cases, the improved Prony algorithm extracted only the true mode in 97 cases in the data window 1 and 98 cases in the data window 2. Thus, the true mode extraction capability and the parameters of the true modes given in Table 6.9 show that the proposed oscillation monitoring algorithm can be used in the online environment for inter-area oscillation monitoring in power systems.

Table 6.9: Mode Parameter Estimations: 2-area 4-generator test system

Data Window		(6.93- 14.93) s		(10.0 -18.0)s	
Mode No	Parameter	Mean Value	Std. Deviation	Mean Value	Std. Deviation
1	Fre. (Hz)	0.6415	0.0005	0.6420	0.0001
	Real Part of Eigenvalue	-0.1638	0.0016	-0.1620	0.0007

Test case 2: 16-generator 68-bus test system

The 16-generator 68-bus test system shown in Fig. 5.3 in Section 5.3.1 in Chapter 5 was used to evaluate the performance of the proposed oscillation monitoring algorithm. This is a reduced order equivalent of the interconnected New England Test System (NETS) and the New York Power System (NYPS) [72]. The test system was modeled as given in Appendix A for the stability analysis of the system.

It is the usual practice in power systems oscillation monitoring to receive the data from highly observable locations of the modes. The observability calculation based on the eigenvalue analysis at the given operating point can be used to identify the highly observable locations of the modes. Due to the difficulty in performing the observability calculations using SSAT, an analytical program written in MATLAB for the small-signal stability assessment of the 16-generator 68-bus test system was first validated against SSAT. The four inter-area modes given in Table 6.10 were identified using this small-signal stability assessment program. The inter-area modes with frequencies 0.52 Hz and 0.70 Hz are two poorly-damped modes.

Table 6.10: Inter-area modes of 16 generator 68 bus test system

Fre. (Hz)	Real Part of Eigenvalue	Dam. Ratio (%)	Inter-Area Mode
0.41	-0.3349	12.89	Group of generators in NETS and NYPS against generators in area 4
0.52	-0.0480	1.47	Generator 14 against generator 16
0.70	-0.0673	1.53	Group of generators in NETS against generator 13 in NYPS
0.79	-0.2206	4.44	Generator 15 against generator 14

The analytical program was then used to determine the observability indices of these inter-area modes from different measurable power system variables. Appendix

C shows the steps of deriving the small-signal stability model, the validation of the program, the procedure of doing the observability calculations and the observability indices of the modes. Through this analysis, it was found that both the poorly-damped modes are observable in the active power flows along the tie lines connecting NETS and NYPS. Furthermore, the measuring devices like PMUs are usually installed to measure the power system variables in major tie lines connecting different areas in large interconnected power systems.

Dynamic simulation of the system for a contingency of clearing a solid three-phase bus fault at bus bar 18 after 5 cycles of the fundamental frequency (60 Hz) was done using transient stability analysis tool (TSAT) [17] using a time step of $\frac{1}{120}$ s. Fig. 6.9 shows the active power flow along one of the tie lines connecting the buses 60 and 61. The fault was applied at time $t = 5$ s.

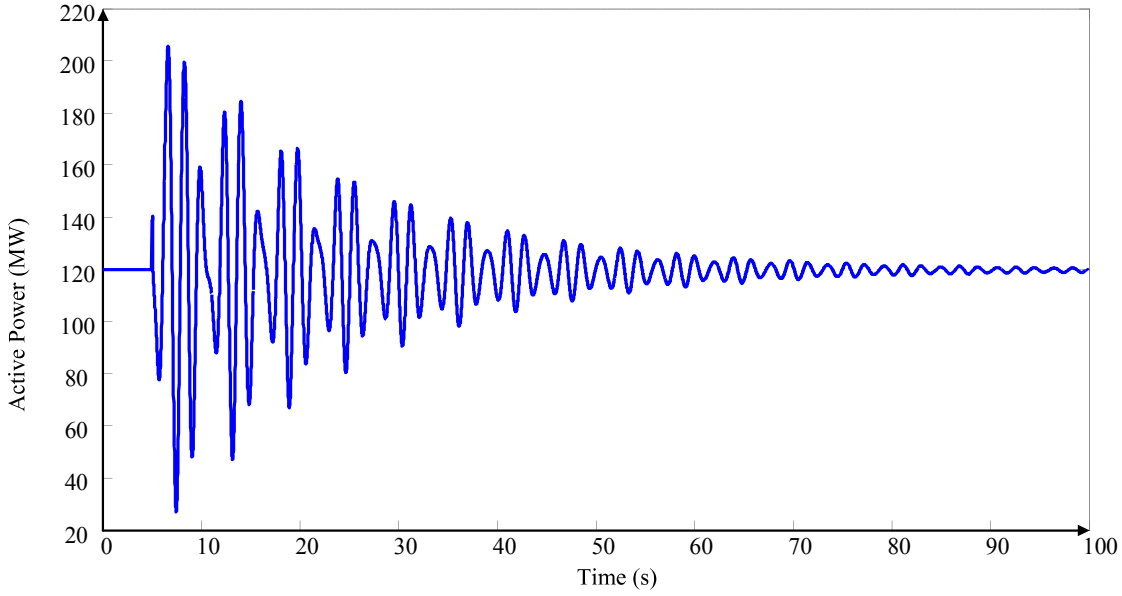

Figure 6.9: Active power flow along the line 60-61 subsequent to a contingency

The simulated signal was corrupted by adding measurement noise at 30 dB SNR generated using the MATLAB random number generator and 100 independent trials

were done to generate different random numbers. The event detection algorithm detected an onset of a ring-down oscillation at time, $t = 5.59$ s. Table 6.11 shows the true mode extraction capability of the algorithm over two data windows selected soon after and few seconds later initiating the algorithm. The three measures γ_1, γ_2 and γ_3 are same as those defined in Section 6.3.

Table 6.11: True mode extraction capability of the algorithm: Test system - 16 generator 68 bus

Data window	γ_1[a]	γ_2[b]	γ_3[c]
(6.0 - 14.0) s	81	19	0
(20.6 - 28.6) s	97	0	3

[a]No of trials in which only the true modes were extracted
[b]No of trials in which only one of the true modes was extracted
[c]No of trials in which true modes and fictitious modes were extracted

Table 6.12 shows the statistical significance of the mode parameter estimation with respect to the true mode parameters determined using the eigenvalue analysis over two data windows.

Table 6.12: Mode Parameter Estimations: 16-generator 68-test system

Data Window		(6.0 - 14.0) s		(20.6 - 28.6)s	
Mode No	Parameter	Mean Value	Std. Deviation	Mean Value	Std. Deviation
1	Fre. (Hz)	0.5205	0.0034	0.5216	0.0008
	Real Part of Eigenvalue	-0.0101	0.0122	-0.0482	0.0008
2	Fre. (Hz)	0.6989	0.0031	0.6994	0.0004
	Real Part of Eigenvalue	-0.0743	0.0673	-0.0699	0.0034

According to Table 6.11, the true mode extraction capability of the proposed oscillation monitoring algorithm is acceptable for online monitoring applications. As shown in Table 6.12, the damping estimations may significantly deviate when a data

window soon after the disturbance is processed using the improved Prony analysis. There are two possible reasons for this, a) nonlinearity of the power system response soon after the application of the disturbance [37], and b) inability of the Prony algorithm to accurately determine the mode damping when a poorly-damped mode is superimposed with a highly-damped mode. It was shown in Section 4.3.2 in Chapter 4, that the Prony algorithm correctly identifies the mode parameters even under the situations, where the input signal consists of both highly-damped and lightly-damped modes. Therefore, the reason b) above can be eliminated. Thus, it is recommended to discard the initial damping estimations of the algorithm before initiating any preventive control actions.

Test case 3: 50-generator 470-bus test system

The 470-bus test system [73], [29] used in Section 5.3.2 in Chapter 5 was also used to study the performance of the Shrinking Window Improved Prony algorithm. The small signal stability analysis was done using SSAT. The system has a poorly-damped inter-area mode between area 1 and area 2. The frequency and the damping ratio of the inter-area mode are 0.823 Hz and 2.55% respectively. Speed of the generator 16 highly participates in this inter-area mode.

Dynamic simulation of the system was done using TSAT software subsequent to a contingency of clearing a solid three-phase bus fault applied at bus bar 16 after 5 cycles of the fundamental frequency without any topology change in the network. The fault was applied at time, $t = 5$ s. Fig. 6.10 shows the active power injected by the generator 16 into the network.

The measured signal was corrupted by adding 20 dB measurement noise and 100 independent simulations were done to study the performance of the algorithm.

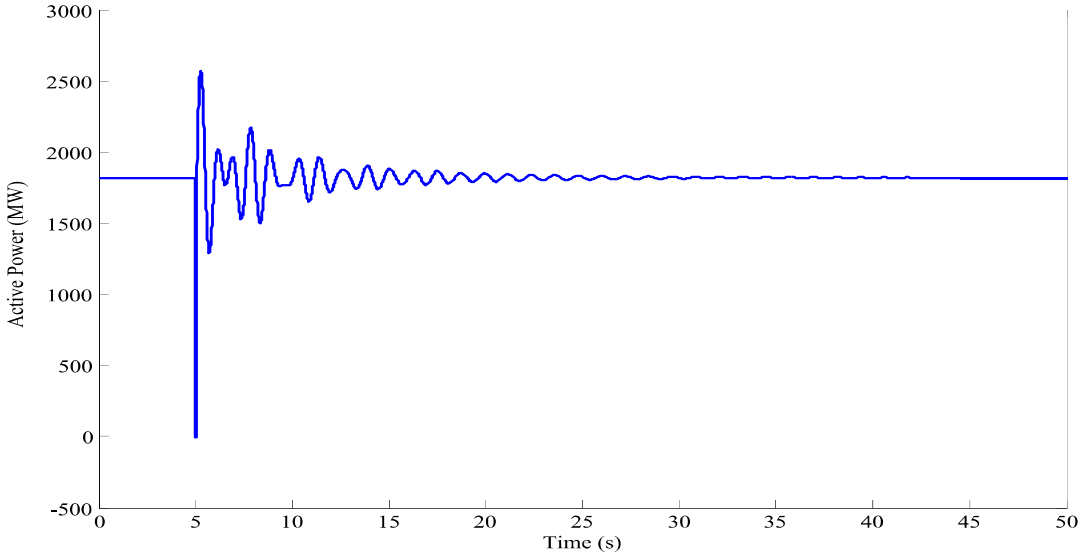

Figure 6.10: Active power output of generator 16 subsequent to a contingency

Assuming that there is no knowledge about the inter-area mode, the data window length was set as 10 s as explained in Section 6.2.3. The event detection logic identified an onset of a ring-down oscillation at time, $t = 5.33$ s. Table 6.13 shows the average values of the mode frequency and the real part of the eigenvalue considering the 100 independent simulations over two data windows selected just after and few seconds later initiating the Prony algorithm. The standard deviations were calculated with respect to the true mode parameters determined by the eigenvalue analysis.

Table 6.13: Mode Parameter Estimations: 50-generator 470-test system

Data Window		(5.92 - 15.92) s		(20.6 - 30.6)s	
Mode No	Parameter	Mean Value	Std. Deviation	Mean Value	Std. Deviation
1	Fre. (Hz)	0.8223	0.0005	0.8223	0.0005
	Real Part of Eigenvalue	-0.1528	0.0210	-0.1401	0.0082

Table 6.13 also highlights that the mode parameter estimations by the improved

Prony algorithm, especially the damping estimation deviate from the value obtained from the eigenvalue analysis when a data window soon after the disturbance is processed. Further, among the two data windows shown in Table 6.13, the improved Prony algorithm extracted another mode in the first data window. The average frequency and the damping ratio of this mode were 1.149 Hz and 5.4% respectively. The eigenvalue analysis also showed an oscillatory mode at frequency, 1.142 Hz and damping ratio, 5.32% respectively. It can be also seen from Fig. 6.10 that only a single mode is dominating over the second data window (20.6 - 30.6). Furthermore, among the 100 independent trials, the algorithm extracted only the true mode in 99 trials in the first data window and 92 trials in the second data window.

In all these cases, the analyses were done on a PC having Intel Core i7 processor with 8 GB RAM. The computational burden was acceptable to update the mode extraction results within every second in the online environment. This updating time would be sufficient to initiate preventive control actions.

6.4.2 Monitoring of sub-synchronous oscillatory modes

This section shows the applicability of the proposed oscillation monitoring algorithm for sub-synchronous mode identification. The Shrinking Window Improved Prony algorithm with following specifications was used on this regard. a) the main data window length was 0.5 s, b) two sub-windows inside the main data window was generated by reducing the length in steps of 0.01 s, c) the sampling rate was $\frac{1}{120}$ s, and d) the threshold used to extract the consistently appearing modes was 0.3.

Test case 4: A wind-integrated test system

Fig. 6.11 shows a single-line diagram of a wind-integrated 12 bus test system [83]. This is a modified version of the original 12 bus test system given in [87], such that a 200 MW wind plant is connected to bus 12 and the transmission line connecting the buses 6 and 4 is series compensated at the middle of the line [83]. The modeling of the test system to study sub-synchronous oscillations is explained in detail in [83].

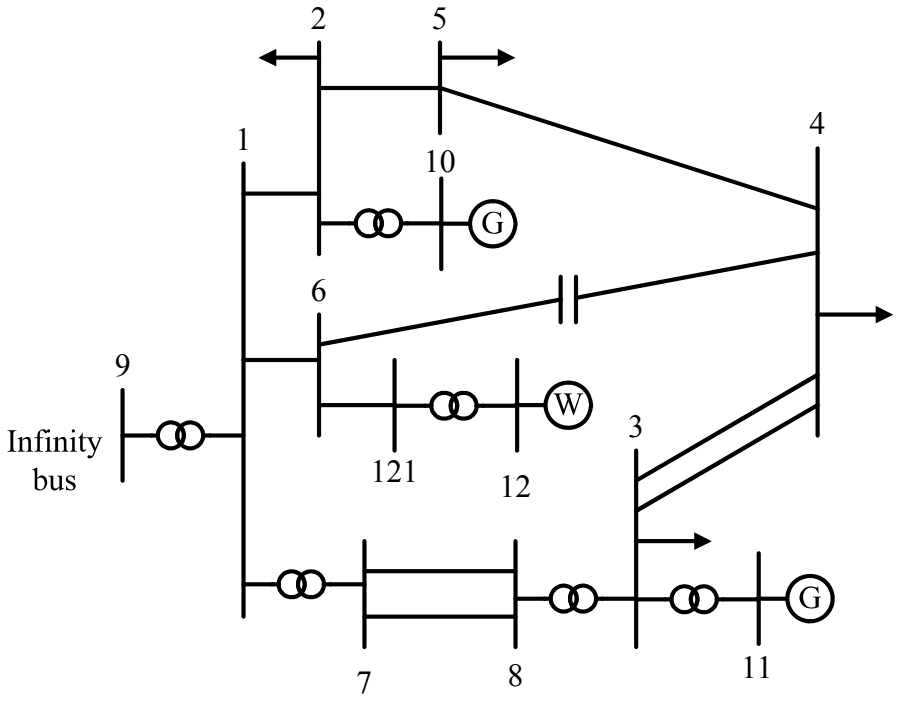

Figure 6.11: A single-line diagram of a wind-integrated 12 bus test system [83]

Fig. 6.12 shows the active power flow through the series compensated transmission line subsequent to a contingency of a solid three-phase fault in the line connecting the buses 1 and 6, very close to the bus 6, which was cleared after 100 ms by isolating the faulted line from the network. Reference [83] shows that the instability in this case is due to an unstable sub-synchronous mode around the frequency of 20.16 Hz.

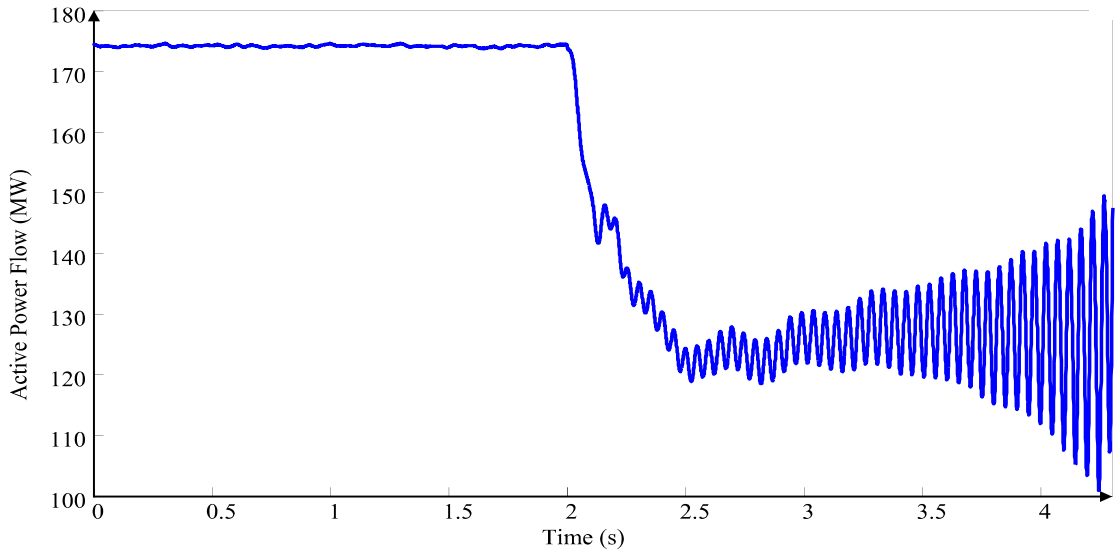

Figure 6.12: Active power flow through the series compensated line subsequent to a contingency [83]

First, the parameters of the modes present in the observed signal was determined using the built-in Prony tool available in TSAT software. Fig. 6.13 and Fig. 6.14 show the parameters of the dominant modes identified via this approach over two data windows. It is clearly seen from these figures that the conventional Prony algorithm generates large numbers of fictitious modes in addition to the true modes.

The same waveform was analyzed using the proposed oscillation monitoring algorithm. The event detection logic initiated the improved Prony algorithm at time, $t = 2.22$ s. Next the observed signal was sent through the parallel filter bank with cut off frequencies as given in Table 6.2. The output signals of the filters were analyzed using the Shrinking Window Improved Prony algorithm with the specifications mentioned at the beginning of this section. In this case, the improved Prony algorithm extracted modes only from the output signal of the bandpass filter. Table 6.14 shows the parameters of the dominant modes identified by the proposed algorithm and the built-in Prony tool in TSAT software (conventional Prony analysis) over three

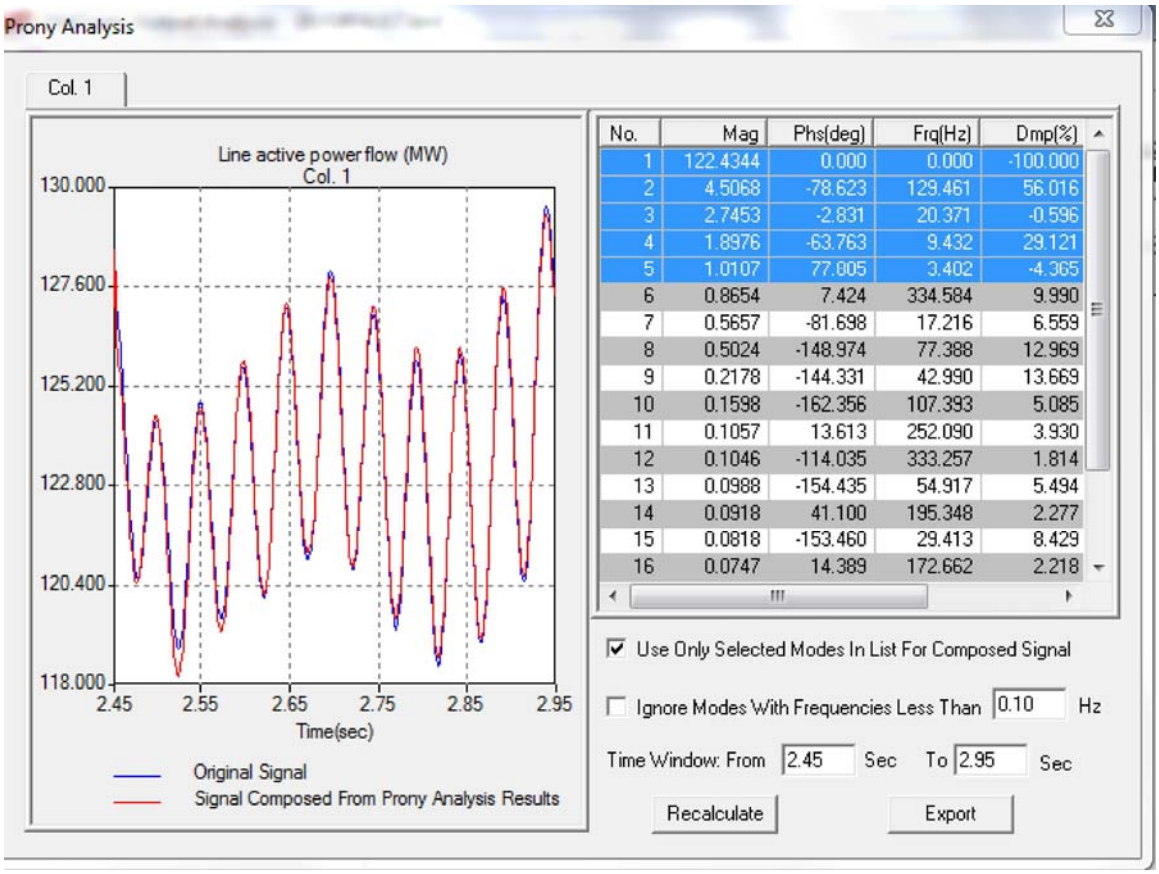

Figure 6.13: Mode identification using built-in Prony tool in TSAT: Data window - (2.45-2.95) s

different data windows.

Table 6.14: Mode Parameter Estimations: Wind-integrated 12 bus test system

Data Window	TSAT Prony tool		Improved Prony algorithm	
	Fre. (Hz)	Dam. Ratio (%)	Fre. (Hz)	Dam. Ratio (%)
(2.45 - 2.95) s	20.37	-0.596	20.42	-0.63
(3.02 - 3.52) s	20.38	-0.905	20.39	-0.93
(3.52 - 4.02) s	20.32	-1.056	20.33	-1.04

There are slight differences in the frequency and the damping ratio estimations of the dominant mode given in Table 6.14 in the two platforms. However, the improved Prony algorithm extracted only the dominant mode in all these cases, which highlights

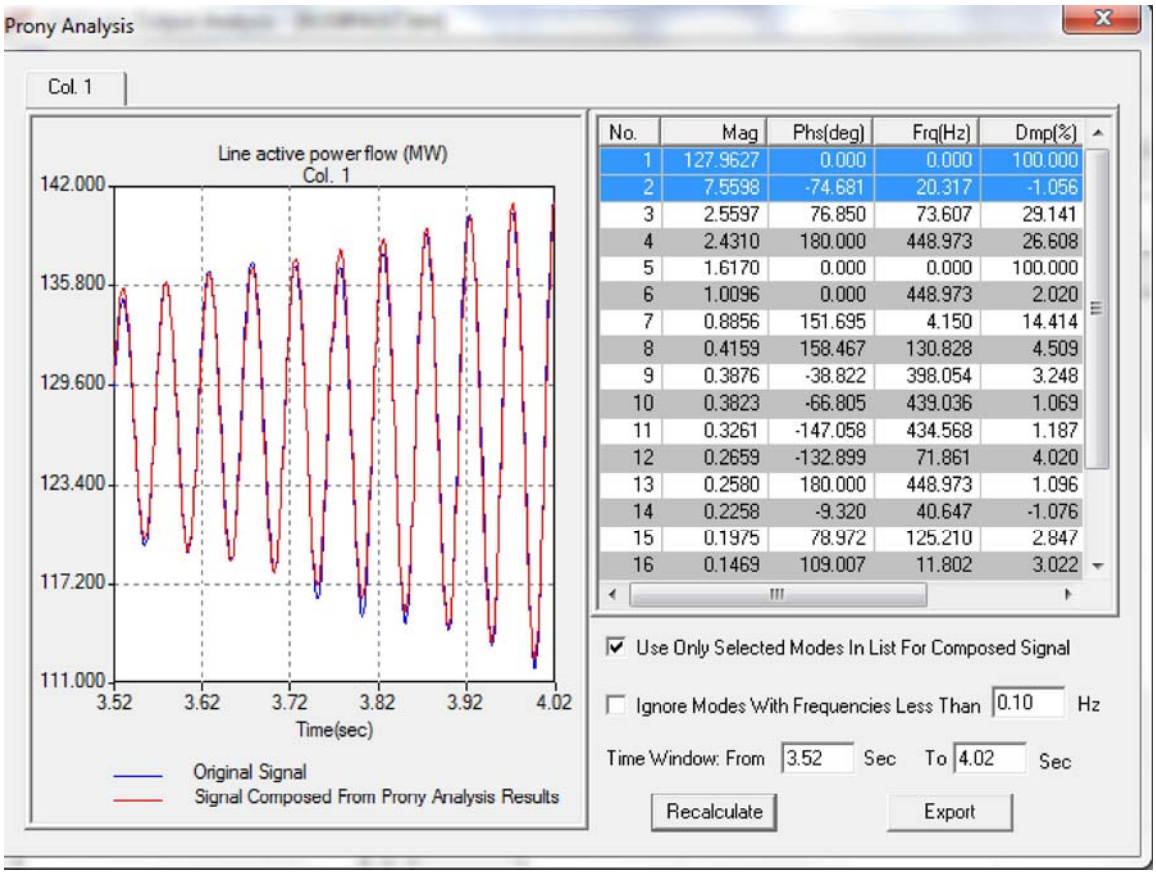

Figure 6.14: Mode identification using built-in Prony tool in TSAT: Data window - (3.52-4.02) s

the significance of the proposed oscillation monitoring algorithm. The conventional Prony analysis generated large numbers of fictitious modes.

In order to determine the sensitivity of the threshold on extracting the consistently appearing modes, the observed signal was corrupted by 30 dB measurement noise. The threshold value was changed in steps of 0.1 and the true modes were extracted using 100 independent trials. Threshold values of 0.2 and 0.3 provided an acceptable mode extraction accuracy.

Test case 5: An HVDC-integrated test system

Sub-synchronous oscillations can also present in HVDC-integrated systems. Fig. 6.15 shows the current flowing through a dc line subsequent to a pulse in magnitude 5% and duration 100 ms applied at the dc voltage reference in the rectifier end of a multi modular converter HVDC system.

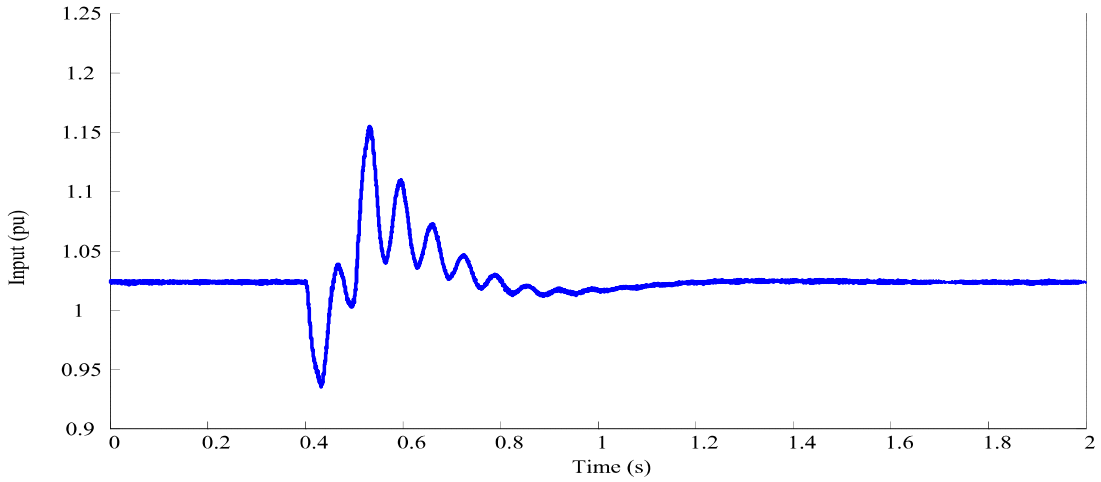

Figure 6.15: DC current subsequent to a pulse

The proposed oscillation monitoring algorithm was used to determine the frequencies and the damping ratios of the dominant modes present in this input signal. The event detection logic initiated the improved Prony algorithm at time, $t = 0.43$ s. Since there is no knowledge about the frequency of the dominant mode in this case, the signal was sent through the parallel filter bank with the pass-band edge frequencies as shown in Fig. 6.16. Output signals from each filter were individually analyzed using the improved Prony algorithm with the specifications mentioned at the beginning of this section.

The order of the bandpass filter 1 was 40. Thus, even though the Prony algorithm was initiated at time, $t = 0.43$ s, the computation started at $t = 0.76$ s ($= 0.43 + \{40 \times$

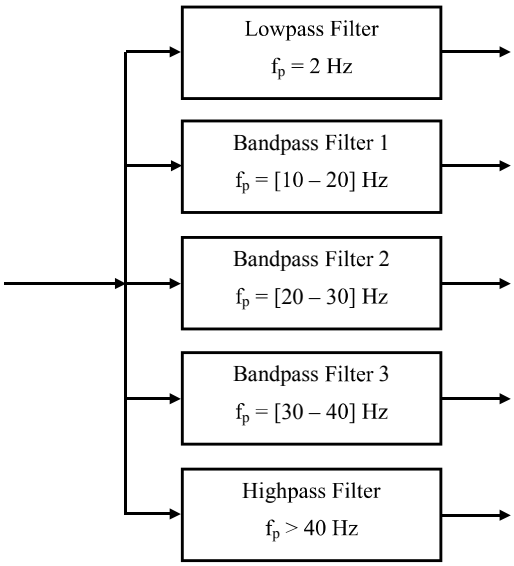

Figure 6.16: Filter bank specifications for HVDC system

$\frac{1}{120}$}). A dominant oscillatory mode with frequency, 15.43 Hz and damping ratio, 9.06 % was extracted from the output signal of the bandpass filter 1 over the data window, 0.76 - 1.26 s. None of the oscillatory modes was extracted from the output signals of the other filters. Fig. 6.17 shows the parameters of the modes identified using the conventional Prony analysis using TSAT software over the same window.

A sensitivity analysis was done assuming a higher PMU reporting rate of 240 fps. Now, the first data window over which the algorithm extracted a true mode was 0.59 - 1.09 s. The frequency and the damping ratio of the mode was determined as 15.42 Hz and 8.71 % respectively by the algorithm. A mode of 15.42 Hz with 8.8 % damping was determined by the built-in Prony tool in TSAT over the same data window. The differences in the mode parameters determined by the improved Prony algorithm and the built-in Prony tool in TSAT software are negligible. Note that the improved Prony algorithm averages the mode parameters determined by Prony models with varying orders while searching for consistently appearing modes. The

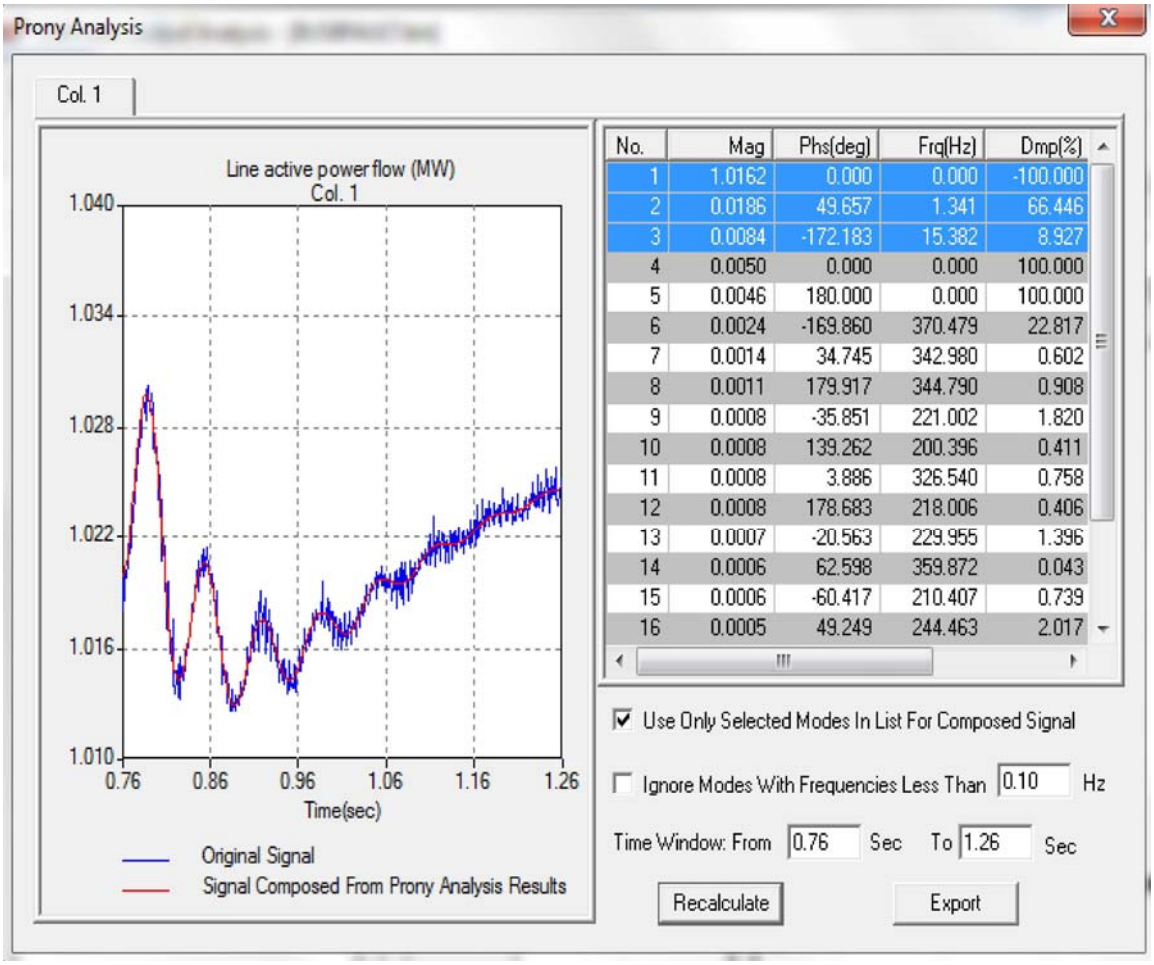

Figure 6.17: Mode identification using built-in Prony tool in TSAT: Data window - (0.76-1.26) s

main advantage of the proposed ascillation monitoring algorithm is that it extracted only the dominant modes present in the input signal unlike the conventional Prony algorithm.

6.5 Discussion

In this study, the performance of the proposed oscillation monitoring algorithm was investigated using simulated signals. However, the actual PMU measurements can

also have missing data points as well as abnormal data points. The problem of missing data points can be eliminated by replacing these data points using interpolation as proposed in [46] and [80]. The presence of an abnormal data point inside the Prony data window is indicated by a sudden spike in the ratio; $\frac{(|y(k)-y(k-1)|)}{\Delta t}$, where Δt is the sampling time. In this case, replacement of the abnormal data point $y(k)$ by $y(k-1)$ enhances the performance of the algorithm.

Furthermore, it is recommended to store the frequencies and the damping ratios of the true modes calculated over a predetermined number of data windows, say 3 windows and check the consistency of the parameters before indicating to the operator. This consistency check would avoid the possibility of giving false alarms in the online environment.

6.6 Chapter summary

The contribution of this chapter is that it has shown that the improved Prony algorithm presented in Chapter 4 can also be used to monitor power system oscillations in an online environment. Thus, if it is found that a poorly-damped mode has been excited, corrective control actions can be initiated to maintain the security of the system.

It has been shown in this chapter that the input signal needs to be fed through a parallel filter bank before analyzing via the improved Prony algorithm. This preprocessing allowed to extract both the low-frequency oscillations and the sub-synchronous oscillations present in the input signal. The performance of the proposed oscillation monitoring algorithm was tested using the simulated data of different power systems. The true mode extraction capability, the accurate determination of the mode parameters, less sensitivity of the mode parameter estimations to measurement noise, and

the acceptable computing time are the indicators of the applicability of the proposed oscillation monitoring algorithm to online monitoring of the power system oscillations.

The above contributions were published in References [88] and [89] during this PhD study.

Chapter 7

Conclusions and Contributions

7.1 General conclusions

This thesis presented two novel algorithms which can be used to determine the transient rotor angle stability and oscillatory rotor angle stability in power systems. The first algorithm was developed using the concept of Lyapunov exponents (LEs) and the second algorithm was an improved Prony algorithm. A hybrid algorithm consisting the LEs-based algorithm and the improved Prony algorithm was proposed in this thesis to be used in an online dynamic security assessment program. Furthermore, an oscillation monitoring algorithm was proposed using the improved Prony algorithm to be used in the online environment to monitor the power system oscillations. The suitability of the two novel algorithms for the aforementioned applications in power systems was shown using different case studies. The following paragraphs further elaborate the conclusions derived from each chapter of the thesis.

Chapter 2 systematically addressed the rotor angle stability problem in power systems starting from the fundamental concepts associated with the stability of a nonlinear dynamic system. It was pointed out the significance of valid assumptions

made to accurately assess the given stability problem in power systems. Appendix A illustrated the detailed mathematical model of 16-generator 68-bus test system followed by the discussion given in Chapter 2. It was further pointed out in this chapter that the interest is on the asymptotic stability of the equilibrium points of the post-fault power system subsequent to disturbances in power systems.

The rotor angle stability analysis scenarios subsequent to large-magnitude disturbances and small-magnitude disturbances were explained in detail in Chapter 2. The nonlinear behavior of the power system needs to be treated in order to assess the given stability problem subsequent to a large-magnitude disturbance. On the other hand it was pointed out in Chapter 2 and Appendix C that even though the method of linearization derives the stability conclusions in a small region around an equilibrium point, such an analysis is helpful to understand the causes affecting the stability problem.

Chapter 2 further presented a comprehensive literature review on the available methods to assess the transient rotor angle stability and oscillatory rotor angle stability giving due consideration to the applicability of each method into online dynamic security assessment and online oscillation monitoring in power systems. It was shown that the conventional time domain simulation method provides much information for dynamic security assessment studies. However, only a hybrid algorithm combining the time domain simulation with other algorithms is needed to make the approach applicable to online dynamic security assessment studies. Furthermore, it was also shown that the trend in power systems today is to use measurement-based approaches to monitor the power system low-frequency oscillations in the online environment. However, the online monitoring of sub-synchronous oscillations using synchronized data has not been widely discussed in the literature.

Chapter 3 showed that the concept of LEs can be used for rotor angle stability assessment subsequent to a large-magnitude disturbance in the power system. The LEs measures the exponential rates of divergence or convergence of nearby trajectories in the state space. It was shown that the asymptotically stable equilibrium point of the post-fault power system can be characterized by a negative Lyapunov spectrum, if the power system is stable subsequent to the disturbance. Otherwise, the largest LE becomes a positive number. Chapter 3 also showed the results of a comprehensive stability analysis based on this approach using a 3-generator 9-bus test system. It was shown that under a given fault scenario, the Lyapunov spectrum associated with the equilibrium point of the post-fault system is invariant from the fault clearing time up to the critical clearing time beyond which the system becomes unstable. Thus, the stability regions of the power system can be derived using the invariance property. However, the algorithm does not provide the indication on how close is the post-fault power system to instability.

The significant computational burden associated with computing the conventional LEs is an obstacle for rotor angle stability analysis in power systems. It was shown in Chapter 3 that the finite-time LEs calculated over a shorter data window accurately derives the rotor angle stability of the post-fault power system while minimizing the computational burden. It was shown using simulation results that the largest average exponential rate calculated over the short data window remains negative if the post-fault power system is stable and becomes a positive number otherwise. Thus, the largest average exponential rate becomes a security measure for the transient rotor angle stability of the power system making it appropriate for online dynamic security assessment studies.

If it is determined that the post-fault power system is stable subsequent to a

large-magnitude disturbance, the next objective is to determine the damping of the dominant oscillatory modes present in the ring-down oscillations. Even though the LEs measures the average exponential decaying rate of the trajectories, they cannot determine the damping ratio of the dominant modes, which is mandatory to determine the oscillatory stability of the power system. Chapter 4 of the thesis presented a modified Prony algorithm to assess the said stability problem. It was shown in this chapter that the major limitation of the conventional Prony algorithm is the difficulty of extracting the true modes present in the input signal among large number of fictitious modes produced by the algorithm. It was also shown that the true modes of the input signal consistently appear when the order of the Prony model was changed. Based on this observation, a Shrinking Window Improved Prony algorithm and a Multiple Sampling Time Improved Prony algorithm were developed in Chapter 4. The performances of the proposed algorithms were tested using the 3-generator 9-bus test system and validated the true mode extraction results against the true mode parameters determined via the eigenvalue analysis.

Chapter 5 presented a hybrid algorithm for online rotor angle security assessment in power systems. The hybrid algorithm combined the LEs-based algorithm and the Shrinking Window Improved Prony algorithm. The proposed hybrid algorithm first used the LEs-based algorithm to determine the large-disturbance rotor angle stability. The stable cases were then processed by the improved Prony algorithm to determine the oscillatory stability of the post-fault power system. A simple logic was introduced to rank the rotor angle trajectories before analyzing those by the improved Prony algorithm. The performance of the proposed hybrid algorithm was tested using a 16-generator 68 bus test system and a 50-generator 470-bus test system.

It was shown that the novel algorithm based on the concept of LEs can accu-

rately determine the first-swing rotor angle stability. Furthermore, the results were compared against the generalized equal area criterion. Both algorithms employed the simplified generator models to derive the stability conclusions. Unlike the generalized equal area criterion, the major limitation of the LEs-based algorithm is that it cannot identify a stability margin. However, the LEs-based computation is less complex than the generalized equal area criterion.

The LEs-based algorithm can also determine the oscillatory instability. However, the algorithm required a longer data window on this regard than the required length of the data window to conclude the first-swing stability. If the same data window was used under both scenarios (first-swing and oscillatory stability), the oscillatory unstable scenarios were concluded as stable by the LEs-based modified algorithm and the generalized equal area criterion. However, such cases were accurately recognized by the improved Prony algorithm. A dominant mode with negative damping ratio was extracted by the improved Prony algorithm under these scenarios concluding the oscillatory instability of the post-fault power system.

Chapter 5 also pointed out that the computational burden of the proposed hybrid algorithm is acceptable for online dynamic security assessment studies in power systems.

Chapter 6 of the thesis presented an online oscillation monitoring algorithm to process the data available from phasor measurement units. This oscillation monitoring algorithm can extract both low-frequency oscillations as well as sub-synchronous oscillations. The proposed algorithm first used an event detection logic to identify the onset of a ring-down oscillation in the power system. The input signal was then sent through a parallel filter bank to seperate various frequency components present in the input signal. Output signals of each filter were then analyzed by the improved

Prony algorithm to extract the dominant oscillatory modes.

The performance of the proposed oscillation monitoring algorithm was tested using synthetic signals and simulated signals of different test power systems. It was shown that the algorithm performs well even under noisy conditions. Furthermore, the mode parameter estimations by the algorithm were less sensitive to the different reporting rates of the phasor measurement unit recommended by the IEEE standard for synchrophasor measurements in power systems.

It was pointed out in this chapter that the measurements for oscillation monitoring in power system should be taken from the most observabale locations of the modes. Appendix C showed the steps of deriving the linearized model of a test power system around an equilibrium point and the procedure of performing the observability calculations using measurabale power system variables. Chapter 6 showed that the proposed algorithm can extract the low-frequency inter-area modes using the two-area four-generator test system, 16-generator 68-bus test system and the 50-generator 470-bus test system. Furthermore, the suitability of the algorithm for sub-synchronous mode identification was demonstrated using the simulation results of a wind-integrated power system and an HVDC-integrated power system.

The proposed oscillation monitoring algorithm, i) extracted only the dominant modes present in the input signal, ii) determined the true mode parameters accurately, iii) less sensitive to the measurement noise present in the input signal than the conventional Prony algorithm, and iv) derived the stability conclusions within an acceptable time for online applications.

The two novel algorithms developed in this thesis can be used for online dynamic security assessment studies as well as online oscillation monitoring studies in power systems.

7.2 Contributions

The main contributions of this thesis are:

- Proposed a novel algorithm using the concept of LEs to determine the large-disturbance rotor angle stability of the power system. A systematic stability analysis using this approach was performed.

- Improved the conventional Prony algorithm using a simple technique in order to extract the true dominant oscillatory modes present in ring-down oscillations in power systems.

- Developed a hybrid algorithm to perform the rotor angle security assessment in power systems. The hybrid algorithm determines whether the power system is transient rotor angle stable and oscillatory rotor angle stable subsequent to a contingency. The performance of the hybrid algorithm was evaluated using different test power system models and validated.

- Developed an oscillation monitoring algorithm to monitor the power system oscillations in the online environment. The oscillation monitoring algorithm was used to monitor the low-frequency inter-area oscillations as well as the sub-synchronous oscillations in power systems. The performance of the proposed algorithm was evaluated using different test power system models and validated.

- In addition to the above main contributions, an analytical program was developed in MATLAB to determine the small-signal stability of a 16-generator 68-bus test system and validated against SSAT, which is a commercially available software. The developed analytical program was used to determine the most

observable locations of the electromechanical modes from measurable power system variables.

These contributions have led to the following publications:

1. D. P. Wadduwage, C. Q. Wu, U. D. Annakkage, "Power system transient stability analysis via the concept of Lyapunov Exponents", *International Journal of Electric Power Systems Research*, Vol. 104, pp. 183-192, Nov. 2013 (Reference No. [61])

2. D. P. Wadduwage, U. D. Annakkage, C. Q. Wu, "A hybrid algorithm for rotor angle security assessment in power systems", *IET Journal of Engineering*, June, 2015 (Reference No. [74])

3. D. P. Wadduwage, U. D. Annakkage, K. Narendra, "Identification of dominant low-frequency modes in ring-down oscillations using multiple Prony models", *IET Transaction of Generation Transmission and Distribution*, Vol. 9,no. 15, pp. 2206-2214, Nov. 2015 (Reference No. [88])

4. D. P. Wadduwage, J. Geeganage, U. D. Annakkage, C. Q. Wu, "Investigation of the applicability of Lyapunov Exponents for transient stability assessment", *Electric Power and Energy Conference (EPEC)*, pp. 1-6, Aug. 2013 (Reference No. [62])

5. D. P. Wadduwage, U. D. Annakkage,K. Narendra "An oscillation monitoring algorithm to monitor power system oscillations using synchronized phasor measurements", *Cigre Lund Symposium*, 2015 (Reference No. [89])

7.3 Suggestions for future work

This thesis presented novel algorithms for rotor angle security assessment in power systems. The LEs-based algorithm for large-disturbance rotor angle stability assessment was tested using test systems having synchronous generators. However, the practical power systems have FACTS devices such as SVCs, STATCOMs, UPFC, etc as well as HVDC lines in addition to the synchronous generators. Thus, the applicability of the LEs-based algorithm to determine the power system transient stability under such circumstances can be investigated.

The suitability of the oscillation monitoring algorithm developed in this thesis for online applications was demonstrated using simulated signals. The compatibility of this algorithm for implementing on the Tesla data recorder of ERLPhase Technologies has been discussed with the company. However, this implementation could not do during the time period due to the time limitations. Therefore, I propose that the oscillation monitoring algorithm be implemented and tested in the field as the next step.

Appendix A

Modeling of a power system for transient stability assessment studies

This appendix provides the dynamic model of a 16 generator 68 bus test system [72] used for stability assessment studies.

A.1 Synchronous generator model

Differential equations

All the generators of the test system were modeled using the 6^{th} order model. This generator model represents the dynamic behavior of the generator rotor, filed winding, one damper winding along the d-axis and two damper windings along the q-axis [14]. Figure A.1 shows the d-axis and q-axis equivalent circuits of this generator model. Eq. (A.1) - Eq. (A.6) show the corresponding differential equations.

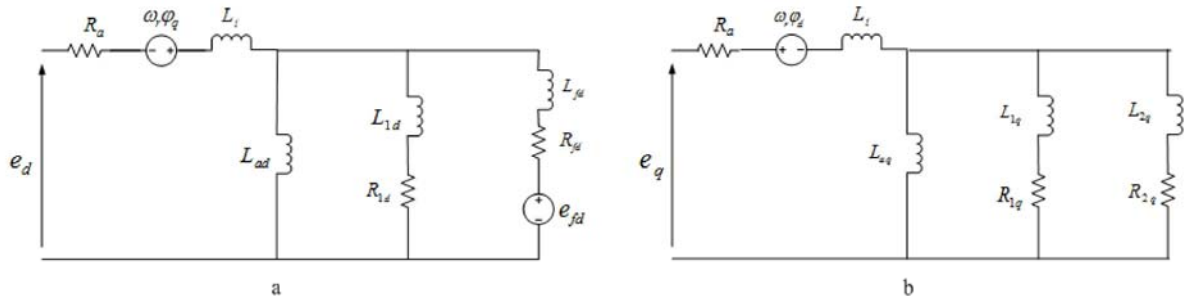

Figure A.1: a) d axis equivalent circuit b) q axis equivalent circuit

$$\Delta\dot{\omega}_r = \frac{1}{2H}\{\bar{T}_m - (\psi_{ad}i_q - \psi_{aq}i_d) - K_D\Delta\omega_r\} \tag{A.1}$$

$$\dot{\delta} = \omega_0\Delta\omega_r \tag{A.2}$$

$$\dot{\psi_{fd}} = \frac{\omega_0 R_{fd}}{L_{adu}}E_{fd} - \frac{\omega_0 R_{fd}}{L_{fd}}\psi_{fd} + \frac{\omega_0 R_{fd}}{L_{fd}}\{L''_{ads}(-i_d + \frac{\psi_{fd}}{L_{fd}} + \frac{\psi_{1d}}{L_{1d}})\} \tag{A.3}$$

$$\dot{\psi_{1d}} = \omega_0\{-\frac{R_{1d}}{L_{1d}}\psi_{1d} + \frac{R_{1d}}{L_{1d}}L''_{ads}(-i_d + \frac{\psi_{fd}}{L_{fd}} + \frac{\psi_{1d}}{L_{1d}})\} \tag{A.4}$$

$$\dot{\psi_{1q}} = \omega_0\{-\frac{R_{1q}}{L_{1q}}\psi_{1q} + \frac{R_{1q}}{L_{1q}}L''_{aqs}(-i_q + \frac{\psi_{1q}}{L_{1q}} + \frac{\psi_{2q}}{L_{2q}})\} \tag{A.5}$$

$$\dot{\psi_{2q}} = \omega_0\{-\frac{R_{2q}}{L_{2q}}\psi_{2q} + \frac{R_{2q}}{L_{2q}}L''_{aqs}(-i_q + \frac{\psi_{1q}}{L_{1q}} + \frac{\psi_{2q}}{L_{2q}})\} \tag{A.6}$$

where;

$$\psi_{ad} = L''_{ads}(-i_d + \frac{\psi_{fd}}{L_{fd}} + \frac{\psi_{1d}}{L_{1d}}) \tag{A.7}$$

$$\psi_{aq} = L''_{aqs}(-i_q + \frac{\psi_{1q}}{L_{1q}} + \frac{\psi_{2q}}{L_{2q}}) \tag{A.8}$$

$$L''_{ads} = \frac{1}{\frac{1}{L_{ads}} + \frac{1}{L_{fd}} + \frac{1}{L_{1d}}} \tag{A.9}$$

$$L''_{aqs} = \frac{1}{\frac{1}{L_{aqs}} + \frac{1}{L_{1q}} + \frac{1}{L_{2q}}} \tag{A.10}$$

Algebraic equations

The voltage and the current at the stator terminal of a synchronous generator is written using a set of algebraic equations.

$$e_q = -R_a i_q + \omega_r \psi_d = -R_a i_q - X_d^{''} i_d + E_q^{''} \tag{A.11}$$

$$e_d = -R_a i_d - \omega_r \psi_q = -R_a i_d + X_q^{''} i_q + E_d^{''} \tag{A.12}$$

where;

$$E_d^{''} = -\omega_r L_{aq}^{''} [\frac{\psi_{1q}}{L_{1q}} + \frac{\psi_{2q}}{L_{2q}}] \tag{A.13}$$

$$E_q^{''} = \omega_r L_{ad}^{''} [\frac{\psi_{fd}}{L_{fd}} + \frac{\psi_{1d}}{L_{1d}}] \tag{A.14}$$

If the subtransient saliency is neglected; $X_d^{''} \approx X_q^{''} = X^{''}$. Hence, (A.11) & (A.12) can be arranged in matrix form as:

$$\begin{bmatrix} e_q \\ e_d \end{bmatrix} = \begin{bmatrix} -R_a & -X^{''} \\ X^{''} & -R_a \end{bmatrix} \begin{bmatrix} i_q \\ i_d \end{bmatrix} + \begin{bmatrix} E_q^{''} \\ E_d^{''} \end{bmatrix} \tag{A.15}$$

$$\begin{bmatrix} i_q \\ i_d \end{bmatrix} = \frac{1}{d} \begin{bmatrix} -R_a & X^{''} \\ -X^{''} & -R_a \end{bmatrix} \begin{bmatrix} e_q \\ e_d \end{bmatrix} - \frac{1}{d} \begin{bmatrix} -R_a & X^{''} \\ -X^{''} & -R_a \end{bmatrix} \begin{bmatrix} E_q^{''} \\ E_d^{''} \end{bmatrix} \tag{A.16}$$

where, $d = R_a^2 + X^{''2}$

Thus, the stator voltage and the current of an individual generator is written with respect to its d and q axes. When deriving the mathematical model of a multi-machine power system, these equations are transformed into a common reference frame known as the "$R - I$" frame shown in Fig. A.2. The relationship between the quantities in

the $d-q$ frame and the $R-I$ frame is given by Eq. (A.17) and Eq. (A.18).

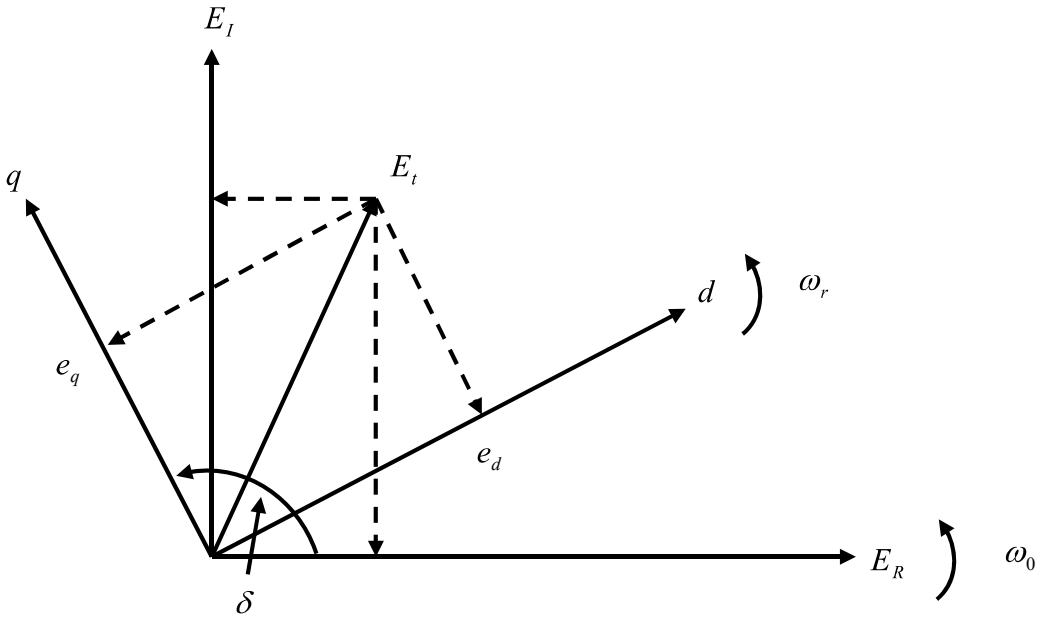

Figure A.2: Transformation from individual machine $d-q$ frame to common reference frame

$$\begin{bmatrix} e_q \\ e_d \end{bmatrix} = \begin{bmatrix} \cos\delta & \sin\delta \\ \sin\delta & -\cos\delta \end{bmatrix} \begin{bmatrix} E_R \\ E_I \end{bmatrix} \tag{A.17}$$

$$\begin{bmatrix} i_q \\ i_d \end{bmatrix} = \begin{bmatrix} \cos\delta & \sin\delta \\ \sin\delta & -\cos\delta \end{bmatrix} \begin{bmatrix} I_R \\ I_I \end{bmatrix} \tag{A.18}$$

Now, Eq. (A.16) can be transformed into $R-I$ frame as given in Eq. (A.19).

$$\begin{bmatrix} I_R \\ I_I \end{bmatrix} = \frac{1}{d} \begin{bmatrix} -R_a & -X'' \\ X'' & -R_a \end{bmatrix} \begin{bmatrix} E_R \\ E_I \end{bmatrix} - \frac{1}{d} \begin{bmatrix} (-R_a E''_q + X'' E''_d)\cos\delta - (X'' E''_q + R_a E''_d)\sin\delta \\ (-R_a E''_q + X'' E''_d)\sin\delta + (X'' E''_q + R_a E''_d)\cos\delta \end{bmatrix} \tag{A.19}$$

A.2 Power system stabilizer model

The generators 9, 13 and 16 were equipped with the power system stabilizer model shown in Fig. A.3. This can be modeled using the differential equations given in Eq. (C.21) - Eq. (C.23).

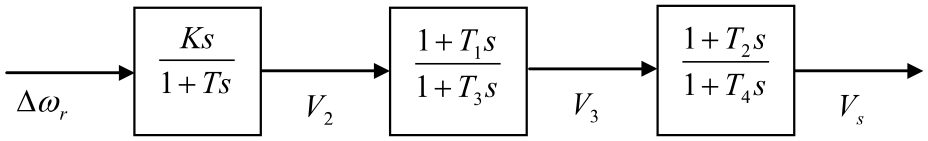

Figure A.3: Power system stabilizer model

$$\dot{V}_2 = \frac{1}{T}(-V_2 + K\frac{\Delta\dot{\omega}_r}{\omega_0}) \tag{A.20}$$

$$\dot{V}_3 = -\frac{1}{T_3}V_3 + \frac{1}{T_3}(1 - \frac{T_1}{T})V_2 + \frac{KT_1}{TT_3}\frac{\Delta\dot{\omega}_r}{\omega_0} \tag{A.21}$$

$$\dot{V}_s = -\frac{1}{T_4}V_s + \frac{1}{T_4}(1 - \frac{T_2}{T_3})V_3 + \frac{T_2}{T_3T_4}(1 - \frac{T_1}{T})V_2 + \frac{KT_1T_2}{TT_3T_4}\frac{\Delta\dot{\omega}_r}{\omega_0} \tag{A.22}$$

$\Delta\dot{\omega}_r$ in Eq. (C.21) - Eq. (C.23) can be substituted from Eq. (A.1).

A.3 Exciter model

Exciter model 1

All the synchronous generators of the test system except the generator 9 were equipped with the exciter model shown in Fig. A.4. This exciter can be modeled using the differential equations given in Eq. (A.23) - Eq. (A.24).

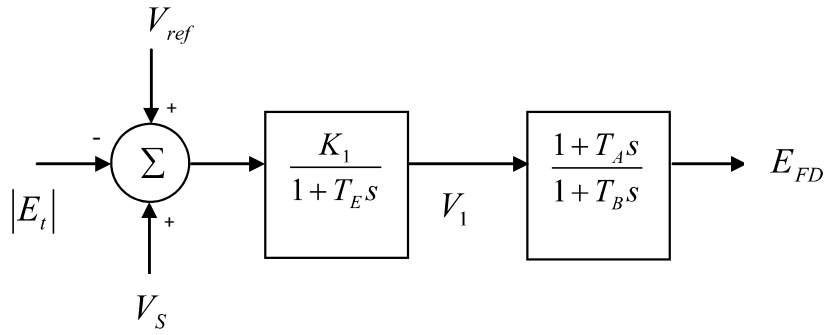

Figure A.4: Exciter model 1

$$\dot{V}_1 = \frac{1}{T_E}\{-V_1 + K_1(V_{ref} + V_s - |E_t|)\} \tag{A.23}$$

$$\dot{E}_{FD} = -\frac{1}{T_B}E_{FD} + \frac{1}{T_B}(1 - \frac{T_A}{T_E})V_1 + \frac{KT_A}{T_B T_E}V_s + \frac{KT_A}{T_B T_E}V_{ref} - \frac{KT_A}{T_B T_E}|E_t| \tag{A.24}$$

Exciter model 2

The generator 9 was equipped with the exciter shown in Fig. A.5, where the associated differential equations are given in Eq. (A.25) - (A.26).

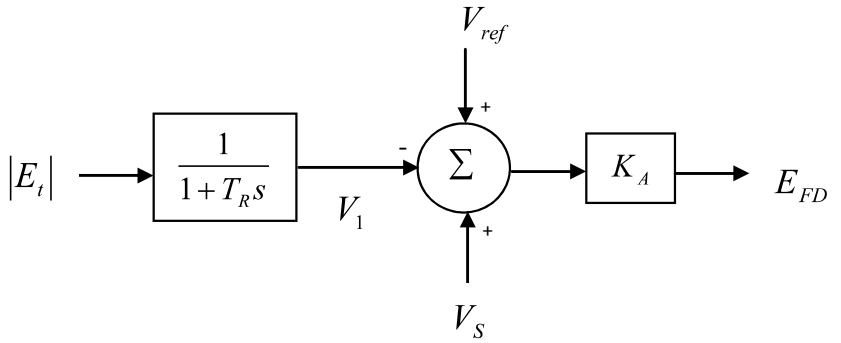

Figure A.5: Exciter model 2

$$\dot{V}_1 = \frac{1}{T_R}(-V_1 + |E_t|) \tag{A.25}$$

$$E_{FD} = K_A(V_{ref} + V_s - V_1) \tag{A.26}$$

where, $|E_t| = \sqrt{e_d^2 + e_q^2}$.

A.4 Load model

All the loads were modeled using the constant admittance load model, which allows to include the equivalent admittance of the load into the network admittance matrix.

Appendix B

Test system data

The objective of this appendix is to provide the data of different test systems used in this thesis for stability assessment studies. This includes the i) 3-generator 9-bus test system [18], ii) 2-area 4-generator test system [14], iii) 16-generator 68-bus test system [72], and iv) 50-generator 470-bus test system[73], [29].

B.1 3-generator 9-bus test system data

B.1.1 Steady state power flow data

Table B.1: Steady state power flow data

Bus No	Bus Type	Voltage (pu)	P_G (pu)	Q_G (pu)	$-P_L$ (pu)	$-Q_L$ (pu)
1	swing	1.04	0.716	0.27	–	–
2	P-V	$1.025\angle 9.3^0$	1.63	0.067	–	–
3	P-V	$1.025\angle 4.7^0$	0.85	-0.109	–	–
4	P-Q	$1.026\angle -2.2^0$	–	–	–	–
5	P-Q	$0.996\angle -4.0^0$	–	–	1.25	0.5
6	P-Q	$1.013\angle -3.7^0$	–	–	0.9	0.3
7	P-Q	$1.026\angle 3.7^0$	–	–	–	–
8	P-Q	$1.016\angle 0.7^0$	–	–	1.00	0.35
9	P-Q	$1.032\angle 2.0^0$	–	–	–	–

B.1.2 Generator dynamic data

Table B.2: Generator dynamic data

Generator No	H (s)	D/M	X_d^1
Generator 1	23.64	0.1	0.0608
Generator 2	6.40	0.2	0.1198
Generator 3	3.01	0.3	0.1813

B.2 2-area 4-generator test system data

The network data and the steady-state power flow data of this test system are available in page 813 of [14].

B.2.1 Dynamic data

All the generators of the test system were modeled using the sub-transient equivalent two axis model with one damper winding along the d-axis and two damper windings along the q-axis as shown in Fig. A.1. These data can be found in page 813 of [14]. Further, all the generators of the test system were modeled using the exciter and the power system stabilizer model shown in Fig. B.1. The gains and the time constants used were as follows:

$K_{STAB} = 1, T_W = 10, T_1 = 0.05, T_2 = 0.02, T_3 = 3, T_4 = 5.4, K_A = 100, T_R = 0.01, T_a = 0.05$.

Time constants are in seconds.

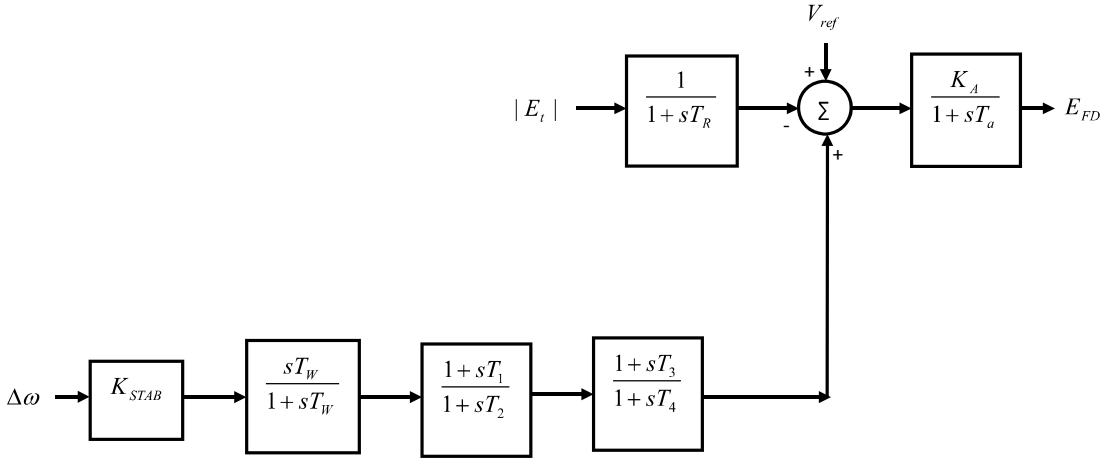

Figure B.1: Exciter and power system stabilizer model: 2-area 4-generator test system

All the generators of the test system were also accommodated with the turbine

governor model shown in Fig. B.2 with data given below:

$R = 0.04, T_1 = 0.1, T_2 = 1.25, T_3 = 5$

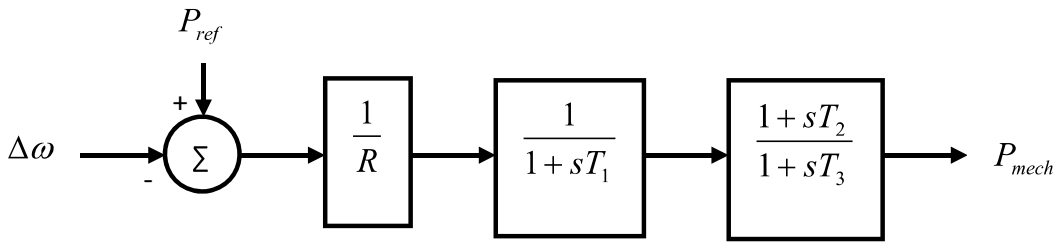

Figure B.2: Turbine governor model: 2-area 4-generator test system

B.3 16-generator 68-bus test system data

The network data and the steady-state power flow data of this tets system can be found in pages 171 - 175 of [72]. For the analysis presented in Chapter 5, generator 16 was treated as the swing bus and the generator 1 was treated as the swing bus for the oscillation monitoring studies presented in Chapter 6.

B.3.1 Dynamic data

All the generators of the test system were modeled using the 6^{th} order model as shown in Fig. A.1. These dynamic data can be found in pages 177 - 178 of [72]. The exciter and the power system stabilizer models used in the 16-generator 68-bus test system were shown in Fig. A.4, Fig. A.5, and Fig. A.3 in Appendix A. The time constants and the gains used were as follows:

Exciter model 1;

$K_1 = 200, T_E = 0.05, T_A = 1, T_B = 10$

Exciter model 2;

$K_A = 200, T_R = 0.01$

Power system stabilizer;

$K = 200, T = 10, T_1 = 0.05, T_2 = 3, T_3 = 0.02, T_4 = 5.4$

B.4 50-generator 470-bus test system data

The 50-generator 470-bus test system used in this thesis for stability assessment studies is same as the one used in [73] and [29].

The thermal generators and hydro generators were modeled using the 6^{th} order model and the 5^{th} order model respectively. Further, all the generators were modeled with the exciters.

Appendix C

Small-signal stability assessment of 16-generator 68-bus test system

The objectives of this appendix are: i) provides the detailed procedure of deriving a small signal stability assessment program of the 16-generator 68-bus test system, ii) validation of the analytical program written in MATLAB for small signal stability assessment with a commercially available software, SSAT, and iii) perform the observability calculations in order to identify the most observable locations of the modes from measurable power system variables.

C.1 Linearization of the dynamic model of 16-generator 68-bus test system

The generator, exciter and the power system stabilizer models used to model the 16-generator 68-bus test system for stability assessment studies were given in Appendix A. The following sections explain the procedure for deriving the linearized model of the generator with the exciter model given in Fig. A.4 and the power system stabilizer

model given in Fig. A.3 in Appendix A. The linearized models of the other generators with only the exciters can be derived from these equations by equating the coefficients of the state variables associated with the power system stabilizer dynamics to zero.

C.1.1 Linearization of synchronous machine dynamic equations

The dynamic behavior of a 6^{th} order synchronous generator is given by the set of first order differential equations Eq. (A.1) - Eq. (A.6) and the algebraic equations given in Eq. (A.16) in Appendix A. Eq. (A.18) gives the relationship between the synchronous generator current in the $d-q$ frame and the $R-I$ referrence frame. First, linearize Eq. (A.18) around an operating point to derive the following equation.

$$\begin{bmatrix} \Delta i_q \\ \Delta i_d \end{bmatrix} = \begin{bmatrix} (-I_R \sin\delta + I_I \cos\delta)\Delta\delta \\ (I_R \cos\delta + I_I \sin\delta)\Delta\delta \end{bmatrix} + \begin{bmatrix} \cos\delta & \sin\delta \\ \sin\delta & -\cos\delta \end{bmatrix} \begin{bmatrix} \Delta I_R \\ \Delta I_I \end{bmatrix} \tag{C.1}$$

Linearizing the synchronous generator equations given in (A.1) - Eq. (A.6) in Appendix A and substituting from Eq. (C.1), the linearized form of a synchronous generator dynamic equations can be derived as shown in following equations.

$$\begin{aligned} \Delta\dot{\omega} = & -\frac{K_D}{2H}\Delta\omega + \frac{1}{2H}\left\{(\psi_{ad} + L''_{aq} i_d) i_d + (\psi_{aq} + L''_{ad} i_q) i_q\right\}\Delta\delta \\ & - \frac{1}{2H}\frac{L''_{ads}}{L_{fd}} i_q \Delta\psi_{fd} - \frac{1}{2H}\frac{L''_{ads}}{L_{1d}} i_q \Delta\psi_{1d} + \frac{1}{2H}\frac{L''_{aqs}}{L_{1q}} i_q \Delta\psi_{1q} \\ & + \frac{1}{2H}\frac{L''_{aqs}}{L_{2q}} i_d \Delta\psi_{2q} + \frac{1}{2H}\Delta\bar{T}_m \\ & + \frac{1}{2H}\left\{-(\psi_{ad} + L''_{aq} i_d)\cos\delta + (\psi_{aq} + L''_{ad} i_q)\sin\delta\right\}\Delta I_R \\ & + \frac{1}{2H}\left\{-(\psi_{ad} + L''_{aq} i_d)\sin\delta - (\psi_{aq} + L''_{ad} i_q)\cos\delta\right\}\Delta I_I \end{aligned} \tag{C.2}$$

$$\Delta\dot{\delta} = \omega_0 \Delta\omega \tag{C.3}$$

$$\begin{aligned}\Delta\dot{\psi}_{fd} = &-\frac{\omega_0 R_{fd}}{L_{fd}} L''_{ads} i_q \Delta\delta + \frac{\omega_0 R_{fd}}{L_{fd}} \left[\frac{L''_{ads}}{L_{fd}} - 1\right] \Delta\psi_{fd} + \frac{\omega_0 R_{fd}}{L_{fd}} \frac{L''_{ads}}{L_{1d}} \Delta\psi_{1d} \\ &+ \frac{\omega_0 R_{fd}}{L_{adu}} \Delta E_{fd} - \frac{\omega_0 R_{fd}}{L_{fd}} L''_{ads} \sin\delta \Delta I_R + \frac{\omega_0 R_{fd}}{L_{fd}} L''_{ads} \cos\delta \Delta I_I\end{aligned} \tag{C.4}$$

$$\begin{aligned}\Delta\dot{\psi}_{1d} = &-\frac{\omega_0 R_{1d}}{L_{1d}} L''_{ads} i_q \Delta\delta + \frac{\omega_0 R_{1d}}{L_{1d}} \frac{L''_{ads}}{L_{fd}} \Delta\psi_{fd} + \frac{\omega_0 R_{1d}}{L_{1d}} \left[\frac{L''_{ads}}{L_{1d}} - 1\right] \Delta\psi_{1d} \\ &- \frac{\omega_0 R_{1d}}{L_{1d}} L''_{ads} \sin\delta \Delta I_R + \frac{\omega_0 R_{1d}}{L_{1d}} L''_{ads} \cos\delta \Delta I_R\end{aligned} \tag{C.5}$$

$$\begin{aligned}\Delta\dot{\psi}_{1q} = &-\frac{\omega_0 R_{1q}}{L_{1q}} L''_{aqs} i_d \Delta\delta + \frac{\omega_0 R_{1q}}{L_{1q}} \left[\frac{L''_{aqs}}{L_{1q}} - 1\right] \Delta\psi_{1q} + \frac{\omega_0 R_{1q}}{L_{1q}} \frac{L''_{aqs}}{L_{2q}} \Delta\psi_{2q} \\ &- \frac{\omega_0 R_{1q}}{L_{1q}} L''_{aqs} \cos\delta \Delta I_R - \frac{\omega_0 R_{1q}}{L_{1q}} L''_{aqs} \sin\delta \Delta I_R\end{aligned} \tag{C.6}$$

$$\begin{aligned}\Delta\dot{\psi}_{2q} = &\frac{\omega_0 R_{2q}}{L_{2q}} L''_{aqs} i_d \Delta\delta + \frac{\omega_0 R_{2q}}{L_{2q}} \frac{L''_{aqs}}{L_{1q}} \Delta\psi_{1q} - \frac{\omega_0 R_{2q}}{L_{2q}} \left[\frac{L''_{aqs}}{L_{2q}} - 1\right] \Delta\psi_{2q} \\ &- \frac{\omega_0 R_{2q}}{L_{2q}} L''_{aqs} \cos\delta \Delta I_R - \frac{\omega_0 R_{2q}}{L_{2q}} L''_{aqs} \sin\delta \Delta I_R\end{aligned} \tag{C.7}$$

Eq. (C.2) - Eq. (C.7) give the linearized form of the synchronous generator dynamic equations in the following form.

$$\Delta\dot{X}_1 = A_1 \Delta X_1 + B_1 \Delta U_1 + E_1 \Delta I \tag{C.8}$$

Linearizing Eq. (A.19) around an operating point gives the change in machine current injections in the $R-I$ reference frame.

$$\begin{bmatrix}\Delta I_R\\ \Delta I_I\end{bmatrix} = \frac{1}{d}\begin{bmatrix}-R_a & -X''\\ X'' & -R_a\end{bmatrix}\begin{bmatrix}\Delta E_R\\ \Delta E_I\end{bmatrix} + \begin{bmatrix}m_1\Delta\delta + m_2\Delta\psi_{fd} + m_3\Delta\psi_{1d} + m_4\Delta\psi_{1q} + m_5\Delta\psi_{2q}\\ n_1\Delta\delta + n_2\Delta\psi_{fd} + n_3\Delta\psi_{1d} + n_4\Delta\psi_{1q} + n_5\Delta\psi_{2q}\end{bmatrix} \tag{C.9}$$

where;

$$m_1 = -\frac{1}{d}\{(R_aE_q'' - X''E_d'')\sin\delta - (R_aE_d'' + X''E_q'')\cos\delta\} \tag{C.10}$$

$$m_2 = \frac{1}{d}(R_a\cos\delta + X''\sin\delta)\frac{L_{ads}''}{L_{fd}} \tag{C.11}$$

$$m_3 = \frac{1}{d}(R_a\cos\delta + X''\sin\delta)\frac{L_{ads}''}{L_{1d}} \tag{C.12}$$

$$m_4 = -\frac{1}{d}(R_a\sin\delta - X''\cos\delta)\frac{L_{aqs}''}{L_{1q}} \tag{C.13}$$

$$m_5 = -\frac{1}{d}(R_a\sin\delta - X''\cos\delta)\frac{L_{aqs}''}{L_{2q}} \tag{C.14}$$

$$n_1 = -\frac{1}{d}\{(R_aE_q'' + X''E_d'')\cos\delta - (R_aE_d'' + X''E_q'')\sin\delta\} \tag{C.15}$$

$$n_2 = \frac{1}{d}(R_a\sin\delta - X''\cos\delta)\frac{L_{ads}''}{L_{fd}} \tag{C.16}$$

$$n_3 = \frac{1}{d}(R_a\sin\delta - X''\cos\delta)\frac{L_{ads}''}{L_{1d}} \tag{C.17}$$

$$n_4 = \frac{1}{d}(R_a\cos\delta + X''\sin\delta)\frac{L_{aqs}''}{L_{1q}} \tag{C.18}$$

$$n_5 = \frac{1}{d}(R_a\cos\delta + X''\sin\delta)\frac{L_{aqs}''}{L_{2q}} \tag{C.19}$$

Thus, Eq. (C.9) is in the following form.

$$\Delta I = C_1\Delta X_1 + D_1\Delta V \tag{C.20}$$

Accordingly, each synchronous generator contributes to the overall state vector of the system by adding six state variables; $[\Delta\omega, \Delta\delta, \Delta\psi_{fd}, \Delta\psi_{1d}, \Delta\psi_{1q}, \Delta\psi_{2q}]$.

C.1.2 Linearizing exciter and power system stabilizer dynamic equations

While deriving the linearized equations of the exciter and the power system stabilizer models shown in Fig. A.4 and Fig. A.3, the models were rearranged as shown in Fig. C.1. The purpose of this rearrangement is to compare the results of analytical program written in MATLAB with the results of SSAT, which identifies the system state variables as shown in C.1.

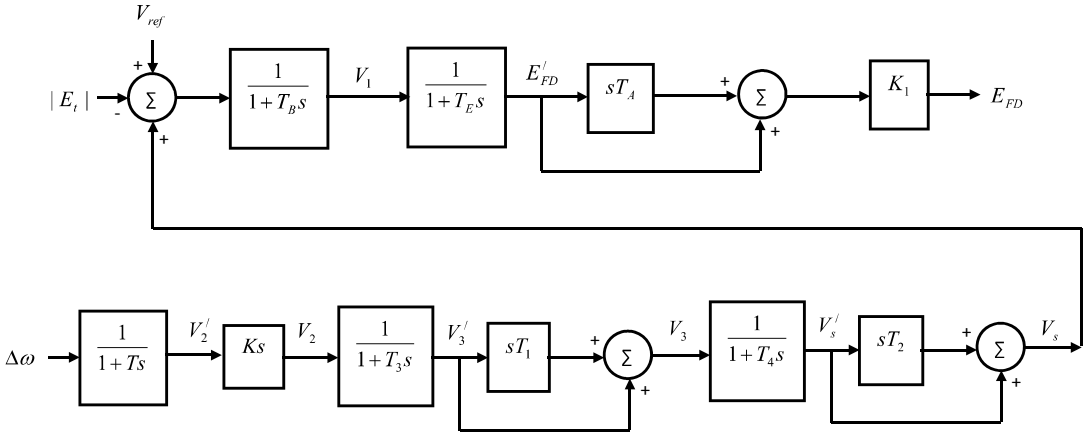

Figure C.1: Alternate arrangement of exciter and PSS

Considering the small changes associated with small signal stability studies, the linearized equations of the block 1 of the power system stabilizer is;

$$\Delta\dot{V}_2^{'} = \frac{1}{T}\frac{\Delta\omega}{\omega_0} - \frac{1}{T}\Delta V_2^{'} \tag{C.21}$$

$$\Delta V_2 = \frac{K}{T}\frac{\Delta\omega}{\omega_0} - \frac{K}{T}V_2^{'} \tag{C.22}$$

The linearized equations associated with the blocks 2 and 3 of the power system stabilizer can be derived as shown in (C.23) - (C.24).

$$\Delta\dot{V}_3^{'} = \frac{K}{TT_3}\frac{\Delta\omega}{\omega_0} - \frac{K}{TT_3}V_2^{'} - \frac{1}{T_3}V_3^{'} \tag{C.23}$$

$$\Delta V_3 = \frac{KT_1}{TT_3}\frac{\Delta\omega}{\omega_0} - \frac{KT_1}{TT_3}\Delta V_2^{'} + \left(1 - \frac{T_1}{T_3}\right)\Delta V_3^{'} \tag{C.24}$$

$$\Delta\dot{V}_s^{'} = \frac{KT_1}{TT_3T_4}\frac{\Delta\omega}{\omega_0} - \frac{KT_1}{TT_3T_4}\Delta V_2^{'} + \frac{1}{T_4}\left(1 - \frac{T1}{T_3}\right)\Delta V_3^{'} - \frac{1}{T_4}\Delta V_s^{'} \tag{C.25}$$

$$\Delta V_s = \frac{KT_1T_2}{TT_3T_4}\frac{\Delta\omega}{\omega_0} - \frac{KT_1T_2}{TT_3T_4}\Delta V_2^{'} + \frac{T_2}{T_4}\left(1 - \frac{T1}{T_3}\right)\Delta V_3^{'} + \left(1 - \frac{T_2}{T_3}\right)\Delta V_s^{'} \tag{C.26}$$

Therefore, the power system stabilizer used for the study adds three more state variables; $[\Delta V_2^{'}, \Delta V_3^{'}, \Delta V_s^{'}]$ in to the individual generator state space model.

The linearized equations associated with the exciter block 1 can be derived as shown in (C.27).

$$\begin{aligned}\Delta\dot{V}_1 = {} & \frac{KT_1T_2}{TT_3T_4T_B}\frac{\Delta\omega}{\omega_0} - \frac{KT_1T_2}{TT_3T_4T_B}\Delta V_2^{'} + \frac{T_2}{T_4T_B}\left(1 - \frac{T_1}{T_3}\right)\Delta V_3^{'} \\ & + \frac{1}{T_B}\left(1 - \frac{T_2}{T_4}\right)\Delta V_s^{'} - \frac{1}{T_B}\Delta V_1 - \frac{1}{T_B}\Delta|E_t| + \frac{1}{T_B}\Delta V_{ref}\end{aligned} \tag{C.27}$$

$|E_t| = \sqrt{e_d^2 + e_q^2}$. Thus, it can be proven that, $\Delta|E_t|$ is given by Equation C.28

$$\begin{aligned}\Delta|E_t| = {} & \frac{e_d}{|E_t|}\{(-R_a I_R \cos\delta - R_a I_I \sin\delta - X^{''} I_R \sin\delta + X^{''} I_I \cos\delta)\Delta\delta \\ & - \frac{L^{''}_{aqs}}{L_{1q}}\Delta\psi_{1q} - \frac{L^{''}_{aqs}}{L_{2q}}\Delta\psi_{2q} + (-R_a \sin\delta + X^{''}\cos\delta)\Delta I_R \\ & + (R_a \cos\delta + X^{''}\sin\delta)\Delta I_I\} \\ & \frac{e_q}{|E_t|}\{(-X^{''} I_R \cos\delta - X^{''} I_I \sin\delta + R_a I_R \sin\delta - R_a I_I \cos\delta)\Delta\delta \\ & + \frac{L^{''}_{ads}}{L_{fd}}\Delta\psi_{fd} + \frac{L^{''}_{ads}}{L_{1d}}\Delta\psi_{1d} + (-X^{''}\sin\delta - R_a\cos\delta)\Delta I_R \\ & + (X^{''}\cos\delta - R_a \sin\delta)\Delta I_I\}\end{aligned} \tag{C.28}$$

The linearized equation of the exciter block 2 can be derived as;

$$\begin{aligned}\Delta\dot{E}^{'}_{fd} = {} & \frac{KT_1T_2T_A}{TT_3T_4T_BT_E}\frac{\Delta\omega}{\omega_0} - \frac{KT_1T_2T_A}{TT_3T_4T_BT_E}\Delta V_2^{'} + \frac{T_AT_2}{T_4T_BT_E}\left(1 - \frac{T_1}{T_3}\right)\Delta V_3^{'} \\ & + \frac{T_A}{T_BT_E}\left(1 - \frac{T_2}{T_4}\right)\Delta V_s^{'} - \frac{T_A}{T_BT_E}\Delta V_1 - \frac{1}{T_B}\Delta|E_t| + \frac{1}{T_B}\Delta V_{ref}\end{aligned} \tag{C.29}$$

$$\Delta E_{fd} = K\Delta E^{'}_{fd} \tag{C.30}$$

Therefore, the considered exciter model adds two more state variables in to the individual generator state-space representation.

C.1.3 Linearized representation of a generator with an exciter and a power system stabilizer

Overall linearized representation of a synchronous generator with the exciter and the power system stabilizer models can be developed as described in this section. All together, the dynamic behavior can be described using 11 state variables;

$[\Delta\omega, \Delta\delta, \Delta\psi_{fd}, \Delta\psi_{1d}, \Delta\psi_{1q}, \Delta\psi_{2q}, \Delta V_2^{'}, \Delta V_3^{'}, \Delta V_s^{'}, \Delta V_1, \Delta E_{fd}^{'}]$.

$$\begin{bmatrix} \Delta\dot{\omega} \\ \Delta\dot{\delta} \\ \Delta\dot{\psi_{fd}} \\ \Delta\dot{\psi_{1d}} \\ \Delta\dot{\psi_{1q}} \\ \Delta\dot{\psi_{2q}} \\ \Delta\dot{V}_2^{'} \\ \Delta\dot{V}_3^{'} \\ \Delta\dot{V}_s^{'} \\ \Delta\dot{V}_1 \\ \Delta\dot{E}_{fd}^{'} \end{bmatrix} = \begin{bmatrix} a_{11} & a_{12} & \cdots & a_{1,11} \\ a_{21} & a_{22} & \cdots & a_{2,11} \\ \vdots & \vdots & \ddots & \vdots \\ a_{11,1} & a_{11,2} & \cdots & a_{11,11} \end{bmatrix} \begin{bmatrix} \Delta\omega \\ \Delta\delta \\ \Delta\psi_{fd} \\ \Delta\psi_{1d} \\ \Delta\psi_{1q} \\ \Delta\psi_{2q} \\ \Delta V_2^{'} \\ \Delta V_3^{'} \\ \Delta V_s^{'} \\ \Delta V_1 \\ \Delta E_{fd}^{'} \end{bmatrix} + \begin{bmatrix} b_{11} & b_{12} \\ b_{21} & b_{22} \\ \vdots & \vdots \\ b_{11,1} & b11,2 \end{bmatrix} \begin{bmatrix} \Delta\bar{T}_m \\ \Delta V_{ref} \end{bmatrix} + \begin{bmatrix} e_{11} & e_{12} \\ e_{21} & e_{22} \\ \vdots & \vdots \\ e_{11,1} & e_{11,2} \end{bmatrix} \begin{bmatrix} \Delta I_R \\ \Delta I_I \end{bmatrix} \tag{C.31}$$

Equation (C.32) gives the linearized equations for generator current injections in to the network, i.e.

$$\begin{bmatrix} \Delta I_R \\ \Delta I_I \end{bmatrix} = \begin{bmatrix} c_{11} & c_{12} \cdots & c_{1,11} \\ c_{21} & c_{22} \cdots & c_{2,11} \end{bmatrix} \begin{bmatrix} \Delta\dot{\omega} & \Delta\dot{\delta} & \cdots & \Delta\dot{E}'_{fd} \end{bmatrix}^T + \begin{bmatrix} d_{11} & d_{12} \\ d_{21} & d_{22} \end{bmatrix} \begin{bmatrix} \Delta E_R \\ \Delta E_I \end{bmatrix} \tag{C.32}$$

Equation (C.31) and Equation (C.32) can be combined to determine the individual generator state-space representation in the general form.

$$\Delta\dot{X}_d = A_d\Delta X + B_d\Delta U + E_d\Delta I_d \tag{C.33}$$

$$\Delta I_d = C_d\Delta X + D_d\Delta V \tag{C.34}$$

$$\Delta\dot{X}_d = (A_d + E_dC_d)\Delta X_d + B_d\Delta U + E_dD_d\Delta V \tag{C.35}$$

$$\Delta\dot{X}_d = A_m\Delta X_d + B_m\Delta U + E_m\Delta V \tag{C.36}$$

Equation (C.36) and Equation (C.34) can be used derive the overall state-space representation of the 16 generators of the test system as;

$$\Delta\dot{X} = A\Delta X + B\Delta U + E\Delta V \tag{C.37}$$

$$\Delta I = C\Delta X + D\Delta V \tag{C.38}$$

where; $\begin{bmatrix}\Delta X\end{bmatrix} = \begin{bmatrix}\begin{bmatrix}\Delta X_{d1}\end{bmatrix} & \begin{bmatrix}\Delta X_{d2}\end{bmatrix} & \cdots \begin{bmatrix}\Delta X_{d16}\end{bmatrix}\end{bmatrix}^T$ and A_m, B_m, E_m, C_d and D_d of individual generators become the corresponding diagonal blocks to form the complete A, B, E, C and D matrices.

C.1.4 Overall system state space representation

The stator terminal is the interface between each synchronous generator and the outside transmission network. For small signal stability assessment of the power system, the transmission network is represented as a set of linear equations. The test system has 68 buses including 6 generators connected to buses, 1-16.

$$\begin{bmatrix} I_1 \\ I_2 \\ \vdots \\ I_{68} \end{bmatrix} = \begin{bmatrix} Y_{11} & Y_{12} & \cdots & Y_{1,68} \\ Y_{21} & Y_{22} & \cdots & Y_{2,68} \\ \vdots & \vdots & \cdots & \vdots \\ Y_{68,1} & Y_{68,2} & \cdots & Y_{68,68} \end{bmatrix} \begin{bmatrix} V_1 \\ V_2 \\ \vdots \\ V_{68} \end{bmatrix} \tag{C.39}$$

Equation (C.39) can be rearranged as;

$$\begin{bmatrix} \begin{bmatrix} \Delta I_D \\ \Delta I_L \end{bmatrix} \end{bmatrix} = \begin{bmatrix} \begin{bmatrix} Y_{11} \\ Y_{21} \end{bmatrix} & \begin{bmatrix} Y_{12} \\ Y_{22} \end{bmatrix} \end{bmatrix} \begin{bmatrix} \begin{bmatrix} \Delta V_D \\ \Delta V_L \end{bmatrix} \end{bmatrix} \tag{C.40}$$

where, the subscripts D and L corresponds to generators and loads respectively. Since, $\Delta I_L = 0$, the relationship between the synchronous generator stator voltages and currents can be expressed using the equivalent network admittance matrix as;

$$\begin{bmatrix} \Delta I_D \end{bmatrix} = \begin{bmatrix} Y_{eq} \end{bmatrix} \begin{bmatrix} \Delta V_D \end{bmatrix} \tag{C.41}$$

where, $\begin{bmatrix} Y_{eq} \end{bmatrix} = \begin{bmatrix} Y_{11} \end{bmatrix} - \begin{bmatrix} Y_{12} \end{bmatrix} \begin{bmatrix} Y_{22} \end{bmatrix}^{-1} \begin{bmatrix} Y_{21} \end{bmatrix}$

Combining Equation (C.41) with Equation (C.38) ; $\Delta V = (Y_{eq} - D)^{-1} C \Delta X$ and substituting in to Equation (C.37) derives the overall system state space representation as;

$$\Delta\dot{X} = A_{sys}\Delta X + B\Delta U \tag{C.42}$$

$$A_{sys} = A + E(Y_{eq} - D)^{-1}C \tag{C.43}$$

C.2 Validation of analytical program results with SSAT

The complete small signal stability program of the 16 generator 68 bus system with the previously discussed generator, exciter and PSS models were written in MATLAB and validated with SSAT, a commercially available software used to perform small signal stability assessment. The motivation behind this validation was to make sure that the analytical program gives correct eigen values and hence the actual electromechanical oscillatory modes at the current operating point since these are needed to perform the mode observability calculations.

The generators, 9, 13 and 16 were accommodated with both an exciter and a PSS. As discussed in the previous section, generators 13 & 16 contribute to the overall state-space representation by adding 11 state variables, whereas generator 9 adds 10 state variables. A generator with only an exciter gives 8 state variables. In order to validate the analytical program results, A_m and C_m matrices of the generators 1, 9 and 16 are considered. Tables C.1, C.2, C.3 and Table C.4 show the results of nonzero elements of these comparisons.

Table C.1: Comparison of individual generator A matrices: Part I

Gen No	Tool	$a_{1,1}$	$a_{1,2}$	$a_{1,3}$	$a_{1,4}$	$a_{1,5}$	$a_{1,6}$
G1	MATLAB	−0.05	−204.65	18.89	11.50	−107.80	−35.65
	SSAT	−0.05	−204.65	18.89	11.50	−107.80	−35.65
G9	MATLAB	−0.20	−129.95	−48.51	−45.08	−47.29	−17.58
	SSAT	−0.20	−129.95	−48.51	−45.08	−47.29	−17.58
G16	MATLAB	−0.11	−155.03	−33.20	−41.94	−89.89	−34.33
	SSAT	−0.11	−155.03	−33.20	−41.94	−89.89	−34.33
		$a_{2,1}$					
G1	MATLAB	1					
	SSAT	1					
G9	MATLAB	1					
	SSAT	1					
G16	MATLAB	1					
	SSAT	1					
		$a_{3,2}$	$a_{3,3}$	$a_{3,4}$	$a_{3,8}$		
G1	MATLAB	0.05	−0.34	0.07	24.86		
	SSAT	0.05	−0.34	0.07	24.86		
		$a_{3,1}$	$a_{3,2}$	$a_{3,3}$	$a_{3,4}$	$a_{3,7}$	$a_{3,8}$
G9	MATLAB	3.58	−0.39	−0.95	0.40	−49.12	1351.6
	SSAT	3.58	−0.39	−0.95	0.40	−49.15	−1351.56
		$a_{3,2}$	$a_{3,3}$	$a_{3,4}$	$a_{3,11}$		
G16	MATLAB	−0.18	−0.92	0.53	28.34		
	SSAT	−0.18	−0.92	0.53	28.34		
		$a_{4,2}$	$a_{4,3}$	$a_{4,4}$			
G1	MATLAB	2.92	7.89	−24.8			
	SSAT	2.92	7.89	−24.8			
G9	MATLAB	−10.17	11.25	−25.33			
	SSAT	-10.17	11.25	−25.33			

Table C.2: Comparison of individual generator A matrices: Part II

Gen No	Tool	$a_{5,2}$	$a_{5,5}$	$a_{5,6}$
G1	MATLAB	−1.25	−1.72	0.23
	SSAT	−1.25	−1.72	0.23
G9	MATLAB	−0.87	−2.47	0.72
	SSAT	−0.87	−2.47	0.72
G16	MATLAB	−2.24	−4.99	2.02
	SSAT	−2.24	−4.99	2.02
		$a_{6,2}$	$a_{6,5}$	$a_{6,6}$
G1	MATLAB	−18.18	10.37	−32
	SSAT	−18.18	10.37	−32
G9	MATLAB	−7.50	16.72	−31.75
	SSAT	−7.50	16.74	−31.75
G16	MATLAB	−8.45	19.92	−31.17
	SSAT	−8.45	19.92	−31.17
		$a_{7,1}$	$a_{7,7}$	$a_{7,8}$
G1	MATLAB	0	−0.1	0
	SSAT	0	−0.1	0
G9	MATLAB	0	−100	0
	SSAT	0	−100	0
G16	MATLAB	0.0003	−0.1	0
	SSAT	0.0003	0.1	0
		$a_{8,1}$	$a_{8,7}$	$a_{8,8}$
G1	MATLAB	0	18	−20
	SSAT	0	18	−20
G9	MATLAB	0.0003	0	−0.1
	SSAT	0.0003	0	−0.1
G16	MATLAB	2.65	−1000	50
	SSAT	2.65	−1000	−50

Table C.3: Comparison of individual generator A matrices: Part III

Gen No	Tool	$a_{9,1}$	$a_{9,7}$	$a_{9,8}$	$a_{9,9}$		
G9	MATLAB	2.65	0	−1000	−50		
	SSAT	2.65	0	−1000	−50		
G16	MATLAB	0.02	−9.26	−0.28	−0.18		
	SSAT	0.02	−9.26	−0.28	−0.18		
		$a_{10,1}$	$a_{10,7}$	$a_{10,8}$	$a_{10,9}$	$a_{10,10}$	
G9	MATLAB	0.02	0	−9.26	−0.28	−0.182	
	SSAT	0.02	0	−9.26	−0.28	−0.18	
G16	MATLAB	0.007	−2.75	−0.08	0.045	−0.1	
	SSAT	0.007	−2.75	−0.08	0.045	−0.1	
		$a_{11,1}$	$a_{11,7}$	$a_{11,8}$	$a_{11,9}$	$a_{11,10}$	$a_{11,11}$
G16	MATLAB	0.15	−55	−1.65	0.9	18	−20
	SSAT	0.15	−55	−1.65	0.9	18	−20

Table C.4: Comparison of individual generator C matrices

Gen No	Tool	$c_{1,2}$	$c_{1,3}$	$c_{1,4}$	$c_{1,5}$	$c_{1,6}$
G1	MATLAB	43.6365	−4.0287	−2.4523	22.9865	7.6024
	SSAT	43.6362	−4.0288	−2.4523	22.9865	7.6024
G9	MATLAB	19.4509	10.1409	9.4237	4.0798	1.5169
	SSAT	19.4511	10.1409	9.4237	4.0801	1.5171
G16	MATLAB	222.9147	150.2513	189.7911	51.5473	19.6863
	SSAT	222.9147	150.2511	189.7909	51.5487	19.6869
		$c_{2,2}$	$c_{2,3}$	$c_{2,4}$	$c_{2,5}$	$c_{2,6}$
G1	MATLAB	−3.2689	−20.9285	−12.7391	−4.4249	−1.4635
	SSAT	−3.2689	−20.9285	−12.7391	−4.4249	−1.4635
G9	MATLAB	14.8659	−2.9095	−2.7037	14.22	5.2872
	SSAT	14.8660	−2.9097	−2.7039	14.2199	5.2872
G16	MATLAB	298.1536	−31.5857	−39.8977	245.2079	93.6469
	SSAT	298.1551	−31.5865	−39.8988	245.2076	93.6468

Tables C.1, C.2, C.3 and Table C.4 show only the non-zero elements of the matrices. It is seen that the analytical program results are in good agreement with the SSAT results. In addition to these non-zero elements, the corresponding zero elements are exactly matching in the both environments. These comparisons conclude the accuracy of the small signal stability analysis program written in MATLAB for the test system and its validity to be used for observability calculations.

C.3 Identification of electromechanical modes of the 16 generator 68 bus system

In small signal stability analysis of the power system, the type of the oscillatory mode can be determined by using the concept of mode shape and this can be further verified by looking at the participation factors. If $\begin{bmatrix} Z \end{bmatrix} = \begin{bmatrix} z_1 & z_2 & \cdots & z_n \end{bmatrix}^T$, where $z_1, z_2, \cdots, z_n$ are directly related with the individual modes of an n^{th} order system, then the relationship between the vector of state variables; $\begin{bmatrix} \Delta X \end{bmatrix} = \begin{bmatrix} x_1 & x_2 & \cdots & x_n \end{bmatrix}^T$ and $\begin{bmatrix} Z \end{bmatrix}$ can be written as follows;

$$\begin{bmatrix} \Delta X \end{bmatrix} = \begin{bmatrix} \Phi_1 & \Phi_2 & \cdots \Phi_n \end{bmatrix} \begin{bmatrix} Z \end{bmatrix} \tag{C.44}$$

where, $\Phi_1, \Phi_2, \cdots, \Phi_n$ are the right eigen vectors associated with n eigen values of an n^{th} order system. Therefore, it is seen that the magnitudes and angles of the elements in i^{th} right eigen vector corresponds to the relative activity of the state variables when the i^{th} mode is excited and the phase displacement of the state variables respectively. The right eigen vectors are therefore termed as mode shapes and the type of the oscillatory modes can be identified by using this principle.

Electromechanical modes of a power system are initiated since the generators in the system are always trying to remain in synchronism, i.e. generators try to keep the balance between the input mechanical torque and the air-gap electromagnetic torque. Any mismatch between these two would either accelerate or decelerate the generator rotor. Therefore, the state variable corresponds to the generator speed deviation from the synchronous speed ($\Delta\omega$) can be used to identify the electromechanical oscillatory modes and their types, i.e. whether the mode is a local plant mode, inter-plant mode or an inter-area mode, from the complex eigen values of the entire state matrix. By

observing the phase displacements of the generator speeds with respect to all the complex eigen values of the entire state matrix would help to identify the actual electromechanical modes of the system.

Table C.5 shows the electromechanical oscillatory modes of the 16 generator 68 bus system at the given operating conditions determined using both MATLAB and SSAT. It has all together 15 electromechanical oscillatory modes.

Modes 12, 13, 14 and 15 are the interarea modes of the system which corresponding respectively the oscillatory mode of generator 14 in the area 3 against the generator 15 in the area 4, group of generators in the area 1 against the generator 13 in the area 2, the generator 14 in the area 3 against the generator 16 in the area 5 and the generators in the areas 1 & 2 against the generators in the areas 3, 4 & 5. Out of these modes, the mode 13 & 14 are two interarea modes of the system with poor damping ratios. Usually, an electromechanical oscillatory mode with a damping ratio of less than 3% is assumed to be a poorly damped mode [14]. At the current operating point, the system is steady state stable, i.e. all its eigen values lie in the left half of the complex plain. However, the system has two poorly damped interarea modes at the current operating point.

Table C.5: Electromechanical modes of 16 generator 68 system at the given operating point

Mode No	MATLAB		SSAT	
	Fre (Hz)	Dam Ra (%)	Fre (Hz)	Dam Ra (%)
1	1.7785	5.0046	1.7785	5.01
2	1.5113	5.8526	1.5113	5.85
3	1.5397	8.441	1.5397	8.44
4	1.4993	9.0422	1.4993	9.04
5	1.3482	7.1341	1.3482	7.13
6	1.2579	6.494	1.2579	6.49
7	1.1896	14.9327	1.1896	14.93
8	1.1995	5.0086	1.1995	5.01
9	1.1731	5.769	1.1731	5.77
10	1.1242	4.1277	1.1238	4.13
11	1.0161	3.2592	1.0161	3.26
12	0.7929	4.4302	0.793	4.44
13	0.6988	1.533	0.6986	1.53
14	0.5224	1.7429	0.5225	1.74
15	0.4143	12.854	0.4143	12.89

C.4 Observability calculations of the 16 generator 68 bus system

As discussed in section C.1.4, the state-space representation of the power system for small signal stability studies can be determined as;

$$\Delta\dot{X} = A\Delta X + B\Delta U \tag{C.45}$$

$$\Delta Y = M\Delta X + N\Delta U \tag{C.46}$$

where, Y is a vector of measurable output variables.

Substituting from Equation C.44, $\Delta Y = M\Phi Z + N\Delta U = M^{'}Z + N\Delta U$, where, $M^{'} = M\Phi$. Since Z is a vector corresponding to the individual modes of the overall system, if i^{th} column of $M^{'} = 0$, then the i^{th} mode cannot be observed in the output. Therefore, each column of $M^{'}$ determines whether the modes are contributed to form the outputs of the system. $M^{'}$ is then known as the mode observability matrix. By performing observability calculations on measurable power system variables, it is possible to determine the optimal observable locations of the modes. This section describes the observability calculations of the 16 generator 68 bus system using generator active power injection and active power flow in selected transmission lines as measurable power system variables.

Observable variable: generator real power output

Assuming the terminal voltage and the current injected by the generator connected at the k^{th} generator bus are $\bar{V}_k = V_{Rk} + jV_{ik}$ and $\bar{I}_k = I_{Rk} + jI_{Ik}$ respectively, the complex power (S_k) and hence the active power (P_k) injected by the generator can

be determined using Equation (C.47).

$$S_k = \bar{V}_k \bar{I}_k^* = (V_{Rk} + jV_{Ik})(I_{Rk} + jI_{Ik})^* \tag{C.47}$$

$$P_k = V_{Rk}I_{Rk} + V_{Ik}I_{Ik} \tag{C.48}$$

For small perturbations in the small signal stability studies, linearization of Equation (C.48), derives the Equation (C.50).

$$\Delta P_k = \begin{bmatrix} V_{Rk} & V_{Ik} \end{bmatrix} \begin{bmatrix} \Delta I_{Rk} \\ \Delta I_{Ik} \end{bmatrix} + \begin{bmatrix} I_{Rk} & I_{Ik} \end{bmatrix} \begin{bmatrix} \Delta V_{Rk} \\ \Delta V_{Ik} \end{bmatrix} \tag{C.49}$$

$$\tag{C.50}$$

Substituting from the derived equations for the change in generator terminal voltage; $\Delta V = (Y_{eq} - D)^{-1}C\Delta X$ and change generator terminal current; $\Delta I = Y_{eq}\Delta V$; the observability matrix of generator real power output can be derived as given in (C.51).

$$\Delta P_k = \left\{ \begin{bmatrix} V_{Rk} & V_{Ik} \end{bmatrix} Y_{eq}(Y_{eq} - D)^{-1}C + \begin{bmatrix} I_{Rk} & I_{Ik} \end{bmatrix} (Y_{eq} - D)^{-1}C \right\} \Delta X \tag{C.51}$$

Observable variable: real power flow in transmission lines

Consider the branch connecting the two nodes m and n in a power system as shown in Figure C.2.

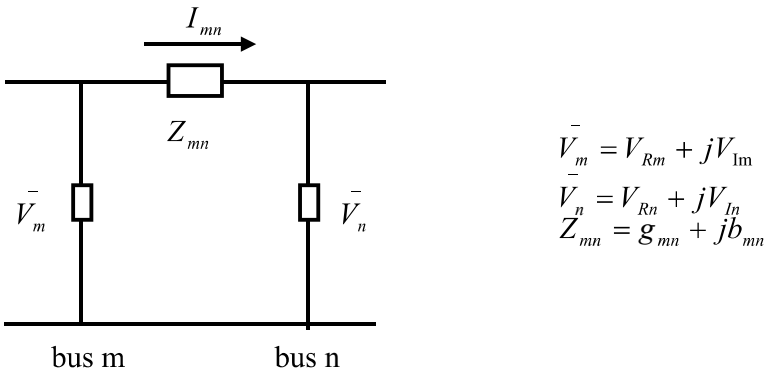

Figure C.2: Arrangement of a network branch

Referring the figure;

$$I_{mn} = [(V_{Rm}-V_{Rn})g_{mn}-(V_{Im}-V_{In})b_{mn}]+j[(V_{Rm}-V_{Rn})b_{mn}+(V_{Im}-V_{In})g_{mn}] \quad \text{(C.52)}$$

Complex power flow in the line from node m to node n is given by Equation (C.53) and the real part of this gives the real power flow in the line between these two nodes.

$$S_{mn} = (V_{Rm} + jV_{Im})I_{mn} \quad \text{(C.53)}$$

$$P_{mn} = (V_{Rm}-V_{Rn})V_{Rm}g_{mn}-(V_{Im}-V_{In})V_{Rm}b_{mn}+(V_{Rm}-V_{Rn})V_{Im}b_{mn}+(V_{Im}-V_{In})V_{Im}g_{mn} \quad \text{(C.54)}$$

Linearizing Equation (C.54) around an operating point for the small perturbations considered during the small-signal stability assessment, the change in branch real power flow (ΔP_{mn}) can be derived as given in (C.55).

$$\Delta P_{mn} = \begin{bmatrix} a & b \end{bmatrix} \begin{bmatrix} \Delta V_{Rm} \\ \Delta V_{Im} \end{bmatrix} + \begin{bmatrix} c & d \end{bmatrix} \begin{bmatrix} \Delta V_{Rn} \\ \Delta V_{In} \end{bmatrix} \quad \text{(C.55)}$$

where;

$$a = g_{mn}(2V_{Rm} - V_{Rn}) + b_{mn}V_{In} \quad \text{(C.56)}$$

$$b = g_{mn}(2V_{Im} - V_{In}) - b_{mn}V_{Rn} \quad \text{(C.57)}$$

$$c = -g_{mn}V_{Rm} - b_{mn}V_{Im} \quad \text{(C.58)}$$

$$d = b_{mn}V_{Rm} - g_{mn}V_{Im} \quad \text{(C.59)}$$

Substituting accurately for $\begin{bmatrix} \Delta V_{Rm} \\ \Delta V_{Im} \end{bmatrix}$ and $\begin{bmatrix} \Delta V_{Rn} \\ \Delta V_{In} \end{bmatrix}$ with necessary formulations from the network admittance matrix, the matrix for the observable variable (ΔP_{mn}) can be represented in the required form.

Using the above derivations, the observability matrices of the 16 generator 68 bus system were determined for the generator real power output and the real power flow in selected transmission lines. The rationale behind the selection of these two variables is that, the electromechanical modes are observable in the network power flows since these modes themselves originate due to change in network power flows. Furthermore, these quantities are measurable from the PMU measurements. Tables C.6 and C.7 show the observability indices of the interarea modes.

Observable varibale: generator real power output

Table C.6: Observability indices: generator real power output

Measurable Quantity	Obsevability Index			
	Mode 12	Mode 13	Mode 14	Mode 15
Gen. 1 real power output	0.0265	0.117	0.1202	0.14
Gen. 2 real power output	0.0328	0.1337	0.0969	0.1084
Gen. 3 real power output	0.0466	0.1844	0.1215	0.1318
Gen. 4 real power output	0.0673	0.2672	0.1234	0.1148
Gen. 5 real power output	0.072	0.2664	0.118	0.1092
Gen. 6 real power output	0.085	0.3251	0.1512	0.1417
Gen. 7 real power output	0.0585	0.2326	0.1106	0.1045
Gen. 8 real power output	0.0135	0.0829	0.0758	0.0831
Gen. 9 real power output	0.0437	0.1345	0.1119	0.1273
Gen. 10 real power output	0.0299	0.0245	0.0495	0.0824
Gen. 11 real power output	0.015	0.0397	0.0258	0.0727
Gen. 12 real power output	0.1078	0.4688	0.0956	0.2907
Gen. 13 real power output	1.0288	**3.4463**	0.4958	**1.5902**
Gen. 14 real power output	3.8852	0.0662	2.6021	0.4217
Gen. 15 real power output	**6.2155**	0.1057	0.326	0.4399
Gen. 16 real power output	2.7736	0.0905	**3.7519**	0.2861

Based on the above calculations, following conclusions can be made.

- Mode 12 is highly observable in generator 15 real power output

- Mode 13 is highly observable in generator 13 real power output
- Mode 14 is highly observable in generator 16 real power output
- Mode 15 is highly observable in generator 13 real power output

Observable varibale: real power flow along network branches

Table C.7: Observability indices: branch real power flow

Measurable Quantity	Obsevability Index			
	Mode 12	Mode 13	Mode 14	Mode 15
Real power flow in the line 53 to 54	0.1106	0.49	0.2571	0.2593
Real power flow in the line 53 to 27	0.0236	0.1083	0.0532	0.0509
Real power flow in the line 60 to 61	0.0409	**0.6056**	0.3035	0.1695
Real power flow in the line 41 to 42	**3.547**	0.0653	**2.0621**	0.1645
Real power flow in the line 41 to 40	0.395	0.055	0.5763	**0.5035**
Real power flow in the line 18 to 49	0.0935	0.0111	0.6214	0.3139

Based on these calculations, following conclusions can be made.

- Mode 12 is highly observable in real power flow in the line 41 to 42
- Mode 13 is highly observable in real power flow in the line 60 to 61
- Mode 14 is highly observable in real power flow in the line 41 to 42
- Mode 15 is highly observable in real power flow in the line 41 to 40

Furthermore, it is also observed that mode 13 is the highly observable mode in the real power flow in the major tie lines connecting the area 1 and area 2. Based on the

observability calculations performed, the following conclusions are made regarding the most observable locations of the four interarea modes.

- Mode 12 is highly observable in the generator 15 real power output
- Mode 13 is highly observable in the real power flow along the line 60–61
- Mode 14 is highly observable in the generator 16 real power output
- Mode 15 is highly observable in the real power flow along the line 18–49

C.5 Concluding remarks

This appendix described the steps involved in deriving the small-signal stability program of the 16-generator 68-bus test system. The results of the small-signal stability analytical program written in MATLAB have been validated against a commercially available software package, SSAT. It has been shown that the system is steady-state stable at the current operating point. However, it has poorly damped interarea modes which might cause small-signal instability.

The identified interarea modes of the test system have been further processed to determine the most observable locations of these modes in the network from the measurable power system variables. It has been proposed to receive the data from PMUs installed at such locations to have a comparatively higher observability of the modes under interest.

References

[1] NERC Planning Standards, "Definition of adequate level of reliability", [Online] Available:http://www.nerc.com/docs/pc/Definition-of-ALR-approved-at-Dec-07-OC-PC-mtgs.pdf, Dec. 2007.

[2] L. H. Fink and K. Carisen, "Operating under stress and strain", in *IEEE spectrum*, Mar. 1978, pp. 48–53.

[3] T. E. DyLiacco, "The adaptive reliability control system", *IEEE Trans. Power App. Syst.*, vol. PAS-86, no. 5, pp. 517–531, May 1978.

[4] P. Kundur, J. Paserba, V. Ajjarapu, G. Andersson, A. Bose, C. Canizares, N. Hatziargyriou, D. Hill, A. Stankovic, C. Taylor, T. V. Custem, and V. Vittal, "Definition and classification of power system stability", *IEEE Trans. Power Syst.*, vol. 19, no. 2, pp. 1387 – 1401, May 2004.

[5] H. K. Khalil, *Nonlinear Systems*, 2nd ed., Prentice Hall, NJ, 1996.

[6] F. F. Wu, K. Moslehi, and A. Bosel, "Power system control centers: Past, present, and future", *IEEE Proceedings*, vol. 93, no. 11, pp. 1890–1908, Nov. 2005.

[7] "IEEE standard for synchrophasor measurements for power systems", IEEE Std. C37.118.1, Dec. 2011.

[8] Y. Mansour, E. Vaahedi, A. Y. Chang, B. R. Corns, B. W. Garrett, K. Demaree, T. Athay, and K. Cheung, "B. C. Hydro's on-line transient stability assessment (TSA) model development, analysis and post-processing", *IEEE Trans. Power Syst.*, vol. 10, no. 1, pp. 241–253, Feb. 1995.

[9] J. Tong and L. Wang, "Design of a DSA tool for real time system operation", in *Int. Conf. Power Syst. Tech.*, Oct. 2006, pp. 1–5.

[10] N. Balu, T. Bertram, A. Bose, V. Brandwajn, G. Cauley, D. Curtice, A. Fouad, L. Fink, M. G. Lauby, B. F. Wollenberg, and J. N. Wrubel, "On-line power system security analysis", *IEEE Proceedings*, vol. 80, no. 2, pp. 262–279, Feb. 1992.

[11] J. E. Daggle, "Postmortem analysis of power grid blackouts-the role of measurement systems", *IEEE Power and Energy Mag.*, vol. 4, no. 5, pp. 30–35, 2006.

[12] A. M. Lyapunov, *Stability of Motion*, English Translation, Academic Press Inc., 1967.

[13] M. Pavella, D. Ernst, and D. Ruiz-Vega, *Transient stability of power systems: A unified approach to assessment and control*, Kluwer, 2000.

[14] P. Kundur, *Power System Stability and Control*, McGraw-Hill Inc., New York, 1993.

[15] U. D. Annakkage, N. K. C. Nair, Y. Liang, A. M. Gole, V. Dinavahi, B. Gustavsen, T. Noda, H. Ghasemi, A. Monti, M. Matar, R. Iravani, and J. A. Martinez, "Dynamic system equivalents: A survey of available techniques", *IEEE. Trans. Power. Syst.*, vol. 27, no. 1, pp. 411–420, Jan. 2012.

[16] B. Stott, "Power system dynamic response calculation", *Proc. of IEEE*, vol. 67, no. 2, pp. 219–240, Feb. 1979.

[17] Power Tec Lab, BC, Canada, *Transient Security Assessment Tool (TSAT) User Manual*, 2009.

[18] P. W. Sauer and M. A. Pai, *Power System Dynamics and Stability*, Prentice Hall, NewJersey, 1998.

[19] A. Rahimi and G. Schaffer, "Power system transient stability indexes for on-line analysis of worst-case dynamic contingencies", *IEEE Trans. Power Syst.*, vol. PWRS-2, no. 3, pp. 660–666, Aug. 1987.

[20] Y. Xue, Th. V. Custem, and M. R. Pavella, "A simple direct method for fast transient stability assessment of large power systems", *IEEE Trans. Power Syst.*, vol. 3, no. 2, pp. 400–412, May 1988.

[21] Y. Xue, Th. V. Custem, and M. R. Pavella, "Extended equal area criterion justifications, generalizations, applications", *IEEE Trans. Power Syst.*, vol. 4, no. 1, pp. 44–52, May 1989.

[22] Fouad A. A. and V. Vittal, *Power system transient stability analysis using the transient energy function method*, Prentice-Hall, New Jersey, 1992.

[23] H-D Chiang, *Direct methods for stability analysis of power systems: Theoretical foundation, BCU methodologies and applications*, John Wiley, 2010.

[24] I. Kamwa, S. R. Samantaray, and G. Joos, "Development of rule-based classifiers for rapid stability assessment of wide-area post-disturbance records", *IEEE Trans. Power Syst.*, vol. 1, no. 24, pp. 258–270, Feb. 2009.

[25] N. Amjady and S. A. Banihashemi, "Transient stability prediction of power systems by a new synchronism status index and hybrid classifier", *IET Trans. Gener. Transm. Distrib.*, vol. 4, no. 4, pp. 509–518, Feb. 2010.

[26] Q. Gao and S. M. Rovnyak, "Decision trees using synchronized phasor measurements for wide-area response-based control", *IEEE Trns. Power Syst.*, vol. 26, no. 2, pp. 855–861, May 2011.

[27] Y. Xu, Z. Y. Dong, J. H. Zhao, P. Zhang, and K. P. Wong, "A reliable intelligent system for real-time dynamic security assessment of power systems", *IEEE Trns. Power Syst.*, vol. 27, no. 3, pp. 1253–1263, Aug 2012.

[28] F. R. Gomez, A. D. Rajapakse, U. D. Annakkage, and I. T. Fernando, "Support vector machine-based algorithm for post-fault transient stability status prediction using synchronized measurements", *IEEE Trns. Power Syst.*, vol. 26, no. 3, pp. 1474–1483, Aug 2011.

[29] B. Jayasekara and U. D. Annakkage, "Derivation of an accurate polynomial representation of the transient stability boundary", *IEEE Trans. Power App. Syst.*, vol. 21, no. 4, pp. 1856–1863, Nov. 2006.

[30] J. Lv, M. Pawlak, and U. D. Annakkage, "Prediction of the transient stability boundary using the lasso", *IEEE Trns. Power Syst.*, vol. 28, no. 1, pp. 282–288, Feb. 2013.

[31] J. Geeganage, U. D. Annakkage, B. A. Archer, and T. Weekes, "Application of energy based power system features for dynamic security assessment", *IEEE Trns. Power Syst.*, vol. 30, no. 4, pp. 1957–1965, 2015.

[32] W. H. Press, B. P. Flannery, S. A. Teukolsky, and W. T. Vetterling, *Numerical recipes in C: The art of scientific computing*, 3rd ed., Cambridge Uni. Press, 2007.

[33] R. T. Byerly, R. J. Bennon, and D. E. Sherman, "Eigenvalue analysis of synchronizing power flow oscillations in large electric power systems", *IEEE Trans. Power Appar. and Syst.*, vol. PAS-101, no. 1, pp. 235–243, Jan. 1982.

[34] Y. Saad, "Variations of Arnoldis' method for computing eigenelements of large unsymmetric matrices", *Linear algebra and its applications*, vol. 34, pp. 184–198, Jun. 1981.

[35] Power Tec Lab, BC, Canada, *Small Signal Analysis Tool (SSAT) User Manual*, 2009.

[36] J. Thambirajaj, E. Barocio, and N. F. Thornhill, "Comparative review of methods for stability monitoring in electrical power systems and vibrating structures", *IET Trans. Gener. Transm. and Distrib.*, vol. 4, no. 10, pp. 1086–1103, 2010.

[37] J. F. Hauer, C. J. Demeure, and L. L. Scharf, "Initial results in prony analysis of power system response signals", *IEEE Trans. Power Syst.*, vol. 5, no. 1, pp. 80 – 89, Feb. 1990.

[38] T. K. Sarkar and O. Pereira, "Using the Matrix Pencil method to estimate the parameters of a sum of complex exponentials", *IEEE Antennas Propag. Mag.*, vol. 37, no. 1, pp. 47–55, Feb. 1995.

[39] M. L. Crow and A. Singh, "The Matrix Pencil for power system modal extraction", *IEEE Trans. Power Syst.*, vol. 20, no. 1, pp. 47–55, Feb. 2005.

[40] I. Kamwa, R. Grondin andJ. Dickinson, and S. Fortin, "A minimal realization approach to reduced-order modelling and modal analysis for power system response signals", *IEEE Trans. Power Syst.*, vol. 8, no. 3, pp. 1020–1029, Aug. 1993.

[41] J. J. S. Gasca and J. H. Chow, "Computation of power system low-order models from time domain simulations using a Hankel matrix", *IEEE Trans. Power Syst.*, vol. 12, no. 4, pp. 1461–1467, Nov. 1997.

[42] J. C. H. Peng and N. K. C. Nair, "Comparative assessment of Kalman filter and Prony methods for power system oscillation monitoring", in *Proc. IEEE Power Eng. Soc. General Meeting*, 2009, pp. 1–8.

[43] P. Korba, "Real-time monitoring of electromechanical oscillations in power systems:first findings", *IET Trans. Gener. Transm. and Distrib.*, vol. 1, no. 1, pp. 80–88, Jan. 2007.

[44] J. C. H. Peng and N. K. C. Nair, "Enhancing Kalman filter for tracking ringdown electromechanical oscillations", *IEEE Trans. Power Syst.*, vol. 27, no. 2, pp. 1042–1050, May 2012.

[45] K. P. Poon and K. C. Lee, "Analysis of transient stability swings in large interconnected power systems by Fourier transform", *IEEE Trans. Power Syst.*, vol. 3, no. 4, pp. 1573–1580, Nov. 1988.

[46] Z. Tashman, H. Khalilinia, and V. Venkatasubramanian, "Multi-dimensional Fourier ringdown analysis for power systems using synchrophasors", *IEEE Trans. Power Syst.*, vol. 29, no. 2, pp. 731–741, Mar. 2014.

[47] D. J. R. Ostojic, "Spectral monitoring of power system dynamic performances", *IEEE Trans. Power Syst.*, vol. 8, no. 2, pp. 445–450, May 1993.

[48] M. Bronzini, S. Bruno, M. De Benedictics, and M. La Scala, "Power system model identification via Wavelet analysis", in *Proc. IEEE Power Tech*, Jul 2007, pp. 2041–2046.

[49] N. E. Huang, Z. Shen, S. R. Long, M. C. Wu, H. H. Shih, Q. Zheng, N-C Yen, C. C. Tung, and H. H. Liu, "The empirical mode decomposition and the Hilbert spectrum for nonlinear and nonstationary time series analysis", in *In Proc. R. Soc. Lond. A*, 1998, pp. 903–995.

[50] A. R. Messina, V. Vittal, D. R. Vega, and G. E. Harper, "Interpretation and visualization of wide area PMU measurements using Hilbert analysis", *IEEE Trans. Power Syst.*, vol. 21, no. 4, pp. 1763–1771, Nov. 2006.

[51] I. Kamwa, A. K. Pradhan, and G. Joos, "Robust detection and analysis of power system oscillations using the Teager-Kaiser energy operator", *IEEE Trans. Power Syst.*, vol. 26, no. 1, pp. 323–333, Feb. 2011.

[52] A. Wolf, J. B. Swift, H. L. Swinney, and J. A. Vastano, "Determining lyapunov exponents from a time series", *Physica 16D*, pp. 285–317, 1985.

[53] W. Kinsner, "Characterizing chaos through lyapunov metrics", *IEEE Trans. Syst. Man Cybern. C, Appl. Rev.*, vol. 36, no. 2, pp. 141–151, Mar. 2006.

[54] V. I. Oseledec, "A multiplicative ergodic theorem: Lyapunov characteristic numbers for dynamical systems", *Trans. Mosc. Math. Soc.*, vol. 19, pp. 197–231, 1968.

[55] J. M. Nese, "Quantifying local predictability in phase space", *Physica D*, vol. 35, pp. 237–250, 1989.

[56] F. Lekien and S. D. Ross, "The computation of finite-time Lyapunov exponents on unstructured meshes and for non-euclidean manifolds", *Chaos*, vol. 20, pp. 1–20, 2010.

[57] S. Dasgupta, *Theoretical foundations for finite-time transient stability and sensitivity analysis of power systems*, PhD thesis, Iowa State University, 2014.

[58] C. W. Liu, J. S. Thorp, J. Liu, R. J. Thomas, and H. D. Chiang, "Detection of transiently chaotic swings in power systems using real-time phasor measurements", *IEEE Trans. Power Syst.*, vol. 9, no. 3, pp. 1285–1292, Aug. 1994.

[59] S. Dasgupta, M. Paramasivam, U. Vaidya, and V. Ajjarapu, "Real-time monitoring of short-term voltage stability using pmu data", *IEEE Trans. Power Syst.*, vol. 28, no. 4, pp. 3702–3711, Nov. 2013.

[60] J. Yan, C. C. Liu, and U. Vaidya, "PMU-based monitoring of rotor angle dynamics", *IEEE Trans. Power Syst.*, vol. 26, no. 4, pp. 2125–2133, Nov. 2011.

[61] D. P. Wadduwage, C. Q. Wu, and U. D. Annakkage, "Power system transient stability analysis via the concept of Lyapunov Exponents", *Int. J. Electric Power Syst. Res.*, vol. 104, pp. 183–192, Nov. 2013.

[62] D. P. Wadduwage, J. Geeganage, U. D. Annakkage, and C. Q. Wu, "Investigation of the applicability of Lyapunov Exponents for transient stability assessment", in *Proc. IEEE Electric Power and Energy Conf.*, Aug. 2013, pp. 1–6.

[63] J. F. Hauer, "Application of prony analysis to the determination of modal content and equivalent models for measured power system response", *IEEE Trans. Power Syst.*, vol. 6, no. 3, pp. 1062–1068, Aug. 1993.

[64] D. J. Trudnowski, "Order reduction of large-scale linear oscillatory system models", *IEEE Trans. Power Syst.*, vol. 9, no. 1, pp. 451–458, Feb. 1994.

[65] J. C. H. Peng and N. K.C. Nair, "Adaptive sampling scheme for monitoring oscillations using Prony analysis", *IET Trans. Gener. Transm. and Distrib.*, vol. 3, no. 12, pp. 1052 – 1060, 2009.

[66] A. Vien, *Practical numerical issues in industrial identification*, PhD thesis, Univ. of Alberta, 1994.

[67] N. Zhou, J. W. Pierre, and D. Trudnowski, "A stepwise regression method for estimating dominant electromechanical modes", *IEEE Trans. Power Syst.*, vol. 27, no. 2, pp. 451–458, May 2012.

[68] D. J. Trudnowski, J. M. Johnson, and J. F. Hauer, "Making Prony analysis more accurate using multiple signals", *IEEE Trans. Power Syst.*, vol. 14, no. 1, pp. 226–231, Nov. 1999.

[69] J. Quintero, L. Guoping, and V. M. Venkatasubramaniam, "An oscillation monitoring system for real-time detection of small-signal instability in large electric power systems", in *Proc. IEEE Power Eng. Soc. General Meeting*, Jun 2007, pp. 1–8.

[70] D. J. Trudnowski, "Order reduction of large-scale linear oscillatory system models", *IEEE Trans. Power Syst.*, vol. 9, no. 1, pp. 451–458, Feb. 1994.

[71] R. Kumaresan and D. W. Tufts, "Estimating the parameters of exponentially damped sinusoids and pole-zero modeling in noise", *IEEE Trans. Acoust., Speech, Signal process.*, vol. ASSP-30, no. 6, pp. 833–840, Dec. 1982.

[72] B. Chaudhuri and B. Pal, *Robust control in power systems*, Springer, New York, 2005.

[73] K. Y. B. D. S. Jayasekara, *Determination of transient stability boundary in functional form with applications in optimal power flow and security control*, PhD thesis, Univ. of Manitoba, 2006.

[74] D. P. Wadduwage and U. D. Annakkage, "A hybrid algorithm for rotor angle security assessment in power systems", *IET J. of Engineering*, June 2015.

[75] M. Kelin, G. J. Rogers, and P. Kundur, "A fundamental study of inter-area oscillations in power systems", *IEEE Trans. Power Syst.*, vol. 6, no. 3, pp. 914–921, Aug. 1991.

[76] D. N. Kosterev, C. W. Taylor, and W. A. Mittelstadt, "Model validation for the August 10, 1996 WSCC system outage", *IEEE Trans. Power Syst.*, vol. 14, no. 3, pp. 967–979, Aug. 1999.

[77] P. Saraf and G. K. Venayagamoorthy, "Online oscillation monitoring of synchronous generators using parallel-Prony analysis", in *Proc. 5^{th} IEEE PES Innovative Smart Grid Technologies Conference*, Feb 2014, pp. 19–22.

[78] IEEE subsynchronous resonance working group, "Reader's guide to subsynchronous resonance", *IEEE Trans. Power Syst.*, vol. 7, no. 1, pp. 150–155, Feb. 1992.

[79] R. G. Farmer, A. L. Schwalb, and E. Katz, "Navajo project report on subsynchronous resonance analysis and solutions", *IEEE Trans. Power App. Syst.*, vol. PAS-96, no. 4, pp. 1226–1232, Aug. 1977.

[80] N. Zhou, J. W. Pierre, D. J. Trudnowski, and R. T. Guttromson, "Robust RLS method for online estimation of power system electromechanical modes", *IEEE Trans. Power Syst.*, vol. 22, no. 3, pp. 1240–1249, Aug. 2007.

[81] N. Zhou, Z. Huang, F. Tuffner, J. Pierre, and S. Jin, "Automatic implementation of Prony analysis for electromechanical mode identification from phasor measurements", in *Proc. IEEE Power Eng. Soc. General Meeting*, Jul. 2010, pp. 1–8.

[82] C. Karawita, *HVDC interaction studies using small signal stability assessment*, PhD thesis, Univ. of Manitoba, 2009.

[83] D. H. R. Suriyaarachchi, U. D. Annakkage, and C. Karawita, "A procedure to study sub-synchronous interactions in wind integrated power systems", *IEEE Trans. Power Syst.*, vol. 28, no. 1, pp. 377–384, Feb. 2013.

[84] J. G. Proakis and D. G. Manolakisl, *Digital signal processing: principles, algorithms and applications*, 4th ed., Prentice Hall, NJ, 2007.

[85] G. Rogers, *Power system oscillations*, Kluwer, New York, 2000.

[86] RTDS Technologies, Winnipeg, MB, Canada, *Real Time Digital Simulator for the power industry User Manual*.

[87] S. Jiang, U. D. Annakkage, and A. M. Gole, "A platform for validation of FACTS models", *IEEE Trans. Power Del.*, vol. 21, no. 1, pp. 484–491, Jan. 2006.

[88] D. P. Wadduwage, U. D. Annakkage, and K. Narendra, "Identification of dominant low-frequency modes in ring-down oscillations using multiple prony models", *IET Trans. Gener. Transm. and Distrib.*, vol. 9, no. 15, pp. 2206–2214, Nov. 2015.

[89] D. P. Wadduwage, U. D. Annakkage, and K. Narendra, "An oscillation monitoring algorithm to monitor power system oscillations using synchronized phasor measurements", in *Proc. Cigre Lund symp.*, May 2015.